Universidade de Aveiro
2020

Artur Neves e Sousa

Técnicas de Transmissão para Altas Taxas em Fibra Óptica e Meios Alternativos

Transmission Techniques for High Rates in Optical Fiber and Alternative Media

Universidade de Aveiro
Ano de 2020

Departamento de Engenharia Electrónica,
Telecomunicações e Informática

Artur Neves e Sousa

Técnicas de Transmissão para Altas Taxas em Fibra Óptica e Meios Alternativos

Transmission Techniques for High Rates in Optical Fiber and Alternative Media

Universidade de Aveiro
Ano de 2020

Departamento de Engenharia Electrónica, Telecomunicações e Informática

Artur Neves e Sousa

Técnicas de Transmissão para Altas Taxas em Fibra Óptica e Meios Alternativos

Transmission Techniques for High Rates in Optical Fiber and Alternative Media

Tese apresentada à Universidade de Aveiro para cumprimento dos requisitos necessários à obtenção do grau de Doutor em Engenharia Electrotécnica / Telecomunicações, realizada sob a orientação científica do Doutor António Luís Jesus Teixeira, Professor Catedrático do Departamento de Engenharia Electrónica, Telecomunicações e Informática da Universidade de Aveiro, e do Doutor Mário José Neves Lima, Professor Auxiliar do Departamento de Engenharia Electrónica, Telecomunicações e Informática da Universidade de Aveiro.

o júri / the jury

Presidente / President

Prof. Doutor Artur da Rosa Pires
Professor Catedrático no Departamento de Ciências Sociais, Políticas e do Território da Universidade de Aveiro

Vogais / Examiners Committee

Prof. Doutora Maria do Carmo Raposo de Medeiros
Professora Associada na Faculdade de Ciências e Tecnologia da Universidade de Coimbra

Prof. Doutor Manuel Alberto Reis de Oliveira Violas
Professor Auxiliar no Departamento de Electrónica, Telecomunicações e Informática da Universidade de Aveiro

Prof. Doutor Pedro Renato Tavares de Pinho
Professor Adjunto no Instituto Superior de Engenharia de Lisboa

Prof. Doutor Rogério Pais Dionísio
Professor Adjunto no Instituto Politécnico de Castelo Branco

Prof. Doutor António Luís Jesus Teixeira
Professor Catedrático no Departamento de Engenharia Electrónica, Telecomunicações e Informática da Universidade de Aveiro

Agradecimentos

As imposições inerentes ao meu percurso académico no ISEP e o interesse em aprofundar os conhecimentos no âmbito das comunicações ópticas, motivaram os estudos que culminaram na escrita desta Tese conducente a obtenção do grau de Doutor (PhD). Desta forma e em primeiro lugar, endereço os maiores agradecimentos ao meu orientador, Prof. Dr. António Luís Jesus Teixeira e ao co-orientador, Prof. Dr. Mário José Neves de Lima por me terem aceite e orientado como aluno de doutoramento ao longo destes anos. Agradeço-lhes a oportunidade de ter usufruído das instalações e do corpo de investigadores do Instituto de Telecomunicações (Universidade de Aveiro), que em muito contribuíram para o sucesso dos meus trabalhos.

Ao longo destes anos, muitos foram os colegas dentro do Instituto de Telecomunicações com os quais convivi, troquei ideias, trabalhei em conjunto ou, simplesmente, passei bons momentos. Agradeço ao Ali Shahpari e ao Isiaka Alimi pela participação generosa e activa nos meus trabalhos. Agradeço ao Ricardo Ferreira, Fernando Guiomar, Abel Lorences-Riesgo e a Cátia Pinho pelo trabalho conjunto e disponibilidade de tempo que tiveram comigo.

Agradeço ao Prof. Dr. Paulo P. Monteiro pelo apoio manifestado e por me permitir participar em projectos por ele orientados.

Agradeço a todos os restantes elementos do IT, com quem convivi e que contribuíram, pelas mais variadas formas, para que os meus objectivos fossem concretizados.

Agradeço aos colegas do Instituto Superior de Engenharia do Porto, que ao longo destes anos manifestaram o seu apoio ao meu doutoramento.

O meu especial agradecimento à minha família que ao longo destes anos suportou os constrangimentos pessoais, emocionais e de disponibilidade que uma tarefa desta envergadura acarreta.

A todos, o meu sincero, Obrigado!

Palavras-Chave

Transmissão óptica, Redes ópticas passivas, Convergência, Transmissão óptica em espaço livre, Fibras ópticas em plástico, Redes de Acesso ópticas de próxima geração, Multiplexagem de comprimento de onda, Comunicações Coerentes.

Resumo

O aumento dos serviços prestados pelas operadoras de rede móvel, assim como do tráfego nas redes-sem-fios (WiFi) têm explorado intensamente o espectro de radiofrequência (RF) disponível. A rede fixa de telecomunicações que conecta as antenas rádio, pontos de acesso WiFi ou outras tecnologias (ex. Wimax), suporta novos serviços que exigem maiores taxas de transmissão e conexões, como por exemplo a computação na nuvem, HDTV, Internet das Coisas (IoT) ou a comunicações de Máquina-a-Máquina (M2M). A fibra óptica monomodo em silício (SMF) tem sido a escolhida como o meio de transporte de dados na rede fixa, uma vez que disponibiliza maiores larguras de banda e taxas de transmissão.

Num contexto desejável de rede óptica ubíqua e transparente, subsistem variados estrangulamentos na estrutura da rede, sejam devido às características da SMF, sejam económicos numa perspectiva de custo/retorno. Além disso, as actuais redes de acesso, baseadas em cabos de SMF ou em ligações RF, estão sujeitas a interrupções e, portanto, devem poder contemplar caminhos de transmissão alternativos.
Por outro lado, o aumento esperado no tráfego de informações no futuro próximo leva ao estabelecimento de novos protocolos de alocação espectral para a SMF. O padrão ITU-T G.989 surge, assim, para promover as redes de próxima geração (NG-PON2) que procuram explorar o espectro disponível em SMFs através de redes WDM (*Wavelength Division Multiplexing*) ponto-multiponto, bem como através de redes em UDWDM (*Ultra-Dense* WDM) numa configuração ponto a ponto, endereçado ao utilizador final.

Neste contexto, a fibra óptica plástica (POF) surge como um meio de transmissão alternativo à SMF e promissor na rede de curto alcance. A implementação da POF estende-se à rede de acesso das operadoras de telecomunicações, à rede de telecomunicações residencial/predial, aos veículos de transporte ou no rápido restabelecimento das comunicações em redes ópticas propensas a acidentes. A transmissão óptica de espaço livre (FSO) também é um meio promissor de comunicação e uma alternativa nas conexões em RF ou SMF de curto alcance. As conexões FSO podem ser aplicadas à rede de acesso do operador de telecomunicações, às conexões em reserva entre as antenas dos operadores móveis, à conexão entre os edifícios de uma instituição, às comunicações sem fio ponto-multiponto ou no rápido restabelecimento de um cabo óptico interrompido acidentalmente.

Assim, os meios de transmissão POF e FSO serão aqui estudados, explorando-se novos limites espectrais e capacidades de transmissão envolvendo os protocolos de redes GPON e NG-PON2. Serão exploradas a recepção coerente e a recuperação de dados através de receptores definidos por software, para o processamento de sinais digitais em tempo real.

Keywords

Optical transmission, Passive Optical networks, Convergence, Free-Space Optical Transmission, Plastic optical fibers, Next-generation optical access networks, Wavelength division multiplexing, Coherent communications.

Abstract

The increase in services provided by mobile network operators, as well as traffic over wireless networks (WiFi), has intensely exploited the available radio frequency (RF) spectrum. The fixed telecommunications network that connects radio antennas, Wi-Fi access points, or other technologies (eg, Wimax) supports new services that require higher transmission rates and connections, such as cloud computing, HDTV, Internet of Things (IoT) or Machine-to-Machine (M2M) communication. Silicon single-mode fiber optic (SMF) has been chosen as a means of transporting data on the fixed network as it offers higher bandwidths and transmission rates.

In a desirable ubiquitous and transparent optical network context, there are still several bottlenecks in the network structure, whether due to the characteristics of SMF or economical from a cost/return perspective. Besides, current access networks based on SMF cable or RF connections are subject to interruptions and should therefore be able to provide alternative transmission paths.
On the other hand, the expected increase in information traffic in the near future leads to the establishment of new spectral allocation protocols for SMF. The ITU-T G.989 standard thus emerges to promote next-generation (NG-PON2) networks that seek to exploit the spectrum available in SMFs through point-to-multipoint Wavelength Division Multiplexing (WDM) networks as well as in UDWDM (Ultra-Dense WDM) in a point to point configuration, addressed to the end-user.

In this context, plastic optical fiber (POF) appears as an alternative transmission medium to the SMF and promising in the short-range network. The implementation of the POF extends to the telecommunications operators' access network, the residential / building telecommunications network, transport vehicles or the rapid re-establishment of communications in accident-prone optical networks. Free Space Optical Transmission (FSO) is also a promising means of communication and alternative for short-range RF or SMF connections. FSO connections can be applied to the telecom operator's access network, standby connections between GSM antennas, the connection between an institution's buildings, point-to-multipoint wireless communications, or the quick re-establishment of a cable optical device accidentally interrupted.

Thus, the POF and FSO transmission media will be studied here, exploring new spectral limits and transmission capabilities involving GPON and NG-PON2 network protocols. Coherent reception and data retrieval through software-defined receivers for real-time digital signal processing will be explored.

Ao meu Filho *André Luís Sousa*

Em memória ao meu Pai *Artur Mendes Sousa*

Contents

List of Figures

List of Tables

List of Acronyms

Notation		Description
5G	-	Fifth Generation (cellular network technology)
ΓΓ	-	Gamma-Gamma distribution
ADC	-	Analog-to-Digital Converter
APON	-	Asynchronous (Transfer Mode on) Passive Optical Network
ATM	-	Asynchronous Transfer Mode
AWG	-	Arbitrary Waveform Generator
AWGN	-	Additive White Gaussian Noise
B2B	-	Back-to-Back
BC	-	Beam Combiner
BD	-	Balanced Detectors
BP	-	Balanced Photodiodes
BER	-	Bit-Error Rate
BPON	-	Broadband Passive Optical Network
BPSK	-	Binary Phase-Shift Keying
CATV	-	Community Access Television System
CMA	-	Constant Modulus Algorithm
CNR	-	Carrier-to-Noise-Ratio
CoI-A/B	-	Pair of collimators to adapt two different optical media
CoRx	-	Coherent Receiver
C-RAN	-	Cloud-Radio Access Network
DD	-	Direct Detection
DFB	-	Distributed Feedback Laser
DL	-	Delay Line
DOP	-	Degree of Polarization
DP	-	Dual-Polarization
DP-QPSK	-	Dual-Polarization Quadrature Phase-Shift Keying
DPL	-	Data Packet Loss
DSP	-	Digital Signal Processing
DWDM	-	Dense Wavelength-Division Multiplexing

ECL - External Cavity Laser
EDFA - Erbium-Doped Fiber Amplifier
EGC - Equal Gain Combining
EMI - Electro-Magnetic Interference
EPON - Ethernet Passive Optical Network
ExB - Extender Box

FEC - Forward Error Correction (code)
FIR - Finite Impulse Response Filter
FITH - Fiber-Into-The-Home
FPGA - Field-Programmable Gate Array
FSAN - Full Service Access Network (Industrial & Commercial iniciative)
FSO - Free-Space Optics
FTTB - Fiber-To-The-Building
FTTH - Fiber-To-The-Home

GD - Group Delay
GEM - Gigabit Passive Optical Network Encapsulated Method
GI - Graded-Index
GI-POF - Graded-Index Plastic Optical Fiber
GOF - Glass (Silica) Optical Fiber
GPON - Gigabit Passive Optical Network
GTC - Gigabit Passive Optical Network with Transmission Convergence

HD-FEC - Hard-Decision Forward Error Correction

IEEE - Institute of Electrical and Electronics Engineers
IFFT - Inverse Fast Fourier Transform
IGTA - The “IXIA © Generator and Traffic Analyzer
ILMZ - Integrated Laser Mach-Zehnder
IM - Intensity-Modulation
InFSO - FSO Internal Path
IoT - Internet of Things
IP - Internet Protocol
IPTV - TV over Internet Protocol
IQM - I/Q (Quadrature) Modulator
IQ-MZM - Mach-Zehnder Modulator (In-phase and Quadrature Inputs)
IR - InfraRed
ITU-T - International Telecommunication Union (for Telecommunication)

LAN - Local Access Network
LD - Laser Diode
LED - Light Emitter Diode
LN - Log-Normal (statistical) distribution
LO - Local Oscillator
LOS - Line-Of-Sight

M2M - Machine-to-Machine intercomunication
MAN - Metropolitan Access Network
MBH - Mobile Backhaul
MC-POF - Multi-Core Index-Step Plastic Optical Fiber
MIMO - Multiple-Input and Multiple-Output
MMF - MultiMode Fiber
MPE - Maximum Permissible Exposure
MRC - Maximum Ratio Combining

NA - Numerical Aperture
NGN - Next-Generation Networks
NG-PON - Next-Generation Passive Optical Networks
NG-PON2 - (A 40-Gigabit-capable) Next-Generation Passive Optical Networks

ODN - Optical Distribution Network
OFDM - Orthogonal Frequency Division Multiplexing
OLT - Optical Line Terminal
OMI - Optical Modulation Index
ONU - Optical Network Unit
OOK - On-Off Keying
OSA - Optical Spectrum Analyser
OTT - Over-The-Top TV
OutFSO - FSO External Path
OWC - Optical Wireless Communication

PAN - Personal Area Network
PBC - Polarization Beam Combiner
PC - Polarization Controllers
PD - PhotoDiode
PD-CoRx - Coherent Receiver with Polarization Diversity
PDM - Polarization-Division Multiplexing

PER	-	Packet Error Rate
PF-POF	-	Perfluorinated Graded-Index Polymer Optical Fiber
PIN	-	Diode with P+Intrinsic+N type semiconductor regions
PMMA	-	Poly(Methyl MethAcrylate), also known as acrylic
POF	-	Polymer (Plastic) Optical Fiber
PolDemux	-	Polarization Demultiplexing
Pol-X	-	Polarization through the X axis of the core profile.
Pol-Y	-	Polarization through the Y axis of the core profile.
PON	-	Passive Optical Network
POTS	-	Plain Old Telephone Service
PRBS	-	Pseudo-Random Binary Sequence
PtP	-	Point-to-Point
PtP-WDM	-	Point-to-Point Wavelength-Division Multiplexing
QPSK	-	Quadrature Phase-Shift Keying
RC	-	Raised-Cosine Filter
RF	-	Radio-Frequency
RF-Video	-	Radio-Frequency Video Overlay
RFID	-	Radio-Frequency Identification
RoF	-	Radio over Fiber
RoFSO	-	Radio-on-FSO
SE	-	Spectral Efficiency
SI	-	Step-index
SISO	-	Single-Input and Single-Output
SMF	-	Single-Mode Fiber
SNR	-	Signal to Noise Ratio
SOA	-	Semiconductor Optical Amplifiers
SONET		Synchronous Optical Networking
SRS	-	Stimulated Raman Scattering
SSMF	-	Standard Single Mode Fiber
TDM	-	Time Division Multiplexing
TDMA	-	Time Division Multiple Access
TIA	-	Transimpedance Amplifiers
TWDM	-	Time and Wavelength Division Multiplexing
UDWDM	-	Ultra-Dense Wavelength-Division Multiplexing

UV	-	Ultra-Violet
V	-	Normalized Frequency
V-Blast	-	Vertical-Bell Laboratories Layered Space-Time
VL	-	Visible Light
VLC	-	Visible Light Communication
VOA	-	Variable Optical Attenuator
VoIP	-	Voice over Internet Protocol
WAN	-	Wide Access Network
WDM	-	Wavelength-Division Multiplexing
XG-PON	-	Extended Gigabit Passive Optical Network
XG-PON2	-	10-Gigabit-capable Symmetric XG-PON
XGS-PON	-	10-Gigabit-capable Symmetric XG-PON
XPM	-	Cross-Phase Modulation

List of Symbols

Notation		Description
r	-	Electrical signal received in the receive aperture
η_e	-	Effective photoelectric conversion ratio of the receiver
$\mathbf{n}$	-	Additive White Gaussian noise (AWGN)
N_0	-	Noise Power Spectral Density
σ_n^2	-	Variance of the Additive White Gaussian noise
σ_s^2	-	Standard deviation variance of the pointing error displacement at the receiver
σ_x^2	-	Log-amplitude variance
h	-	Channel irradiance
h_l	-	Deterministic path loss
h_a	-	Random attenuation (Atmospheric turbulence-induced fading)
h_p	-	Random attenuation (due to geometric spread and pointing errors)
$f_{h_a}(h_a)$	-	Probability density functions of the random variable h_a
$f_{h_p}(h_p)$	-	Probability density functions of the random variable h_p
$h_l(\lambda, z)$	-	Loss as function of propagation path of length z at wavelength λ
$P(\lambda, 0)$	-	Emitted signal power at distance z = 0
$P(\lambda, z)$	-	Emitted signal power at distance z
$\sigma(\lambda)$	-	Attenuation path
V	-	Visibility (km)
q	-	Parameter that is a function of the particle size distribution in the atmosphere
$w_{z_{eq}}$	-	Equivalent beamwidth
α	-	Radial displacement of the geometric spread, from the detector origin.
erf $(\cdot)$	-	Error function
k	-	Optical wave number
σ_I^2	-	Log-irradiance variance
L	-	Distance
C_n^2	-	Refractive-index structure parameter that is altitude-dependent
$K_v(\cdot)$	-	Modified Bessel function of the second kind of order v
$\Gamma(\cdot)$	-	Gamma function
α	-	Effective numbers of large-scale eddies of the scattering process
β	-	Effective numbers of small-scale eddies of the scattering process
D	-	Diameter of the receiver aperture
σ_R^2	-	Rytov variance

σ_N^2	-	Atmospheric related scintillation index (normalized variance of the irradiance)
$\langle \cdot \rangle$	-	Average over the scintillation
$G_{p,q}^{m,n}[\cdot]$	-	Meijer's G-function
M	-	Number of lasers in a MIMO FSO system
N	-	Number of photodetectors in a MIMO FSO system
I_M	-	$M \times M$ Identity matrix
$(\cdot)^\dagger$	-	Hermitian transpose
γ_{inst}	-	Instantaneous electrical SNR
C_{erg}	-	MIMO FSO link ergodic capacity
$E(\cdot)$	-	Expectation operator
$f_{\gamma_{inst}}(\gamma_{inst})$	-	Probability density function (pdf) of γ_{inst}

Chapter 1

Introduction

The growth in data traffic, fuelled by the so-called “Information Society” and market competition, has led telecom operators to offer new and faster services to customers. Thus, single-mode silicon fiber optic networks, due to their higher bandwidth and lower attenuation, have replaced copper-based telecommunications networks. The know-how gained from single-mode optical fiber (SMF) and the wide range of SMF-interface optical equipment available on the market paved the way for SMFs from the core of the telecommunications network to the access network. Currently, telecom operators provide SMF gigabit access to homes in a topology called Fiber-to-the-Home (FTTH). SMF has become the paradigm of optical networks but is not the most desired solution in scenarios where mechanical flexibility, traction robustness, handling by non-technical personnel, rapid re-establishment of connections, or provision of services to very low subscriber density regions is important.

However, it should be noted that in specific scenarios, alternative optical transmission media with singular characteristics, such as polymer optical fiber (POF) or optical transmission in free space (FSO), may be alternative to standard optical fibers in silica. Thus, it is understandable that the installation of these alternative media will help strengthen the concept and interconnection of optical networks.

On the other hand, the desired optical transparency (no optical-electrical-optical conversion), within a network with heterogeneous optical transmission

media, raises questions that are not always answered in the literature. These problems may be related to the interfaces between the optical media, the feasibility of transmitting high data rates within the same optical window, or the dual-polarization and multi-wavelength bidirectional traffic behavior. Besides, POFs exhibit high and much differentiated attenuation in the infrared bands, while the atmospheric FSO channel is subject to turbulence, which can generate phase dispersion in the optical beam.

On the other hand, and to meet the expected increase in data traffic, recommendations for next-generation optical networks rely on wavelength-division multiplexing (WDM) point-to-multipoint networks and WDM networks with high-density point-to-point carriers.

In this context, involving POF and FSO transmission media and next generation WDM networks, some issues are addressed and can be investigated, serving as a basis for the formulation of the theme of this work.

1.1 From copper to fiber optics

Phones, after the telegraph, were at the origin of the great development that telecommunication networks, essentially based on copper cables, had throughout the twentieth century to this day. These networks grew and were hierarchically structured, in planning strongly conditioned by administrative or geographical boundaries, population density or demand for services. Thus, the Local Area (Access) Network connects, through local subscriber lines, the terminal equipment directly to the Local Exchange Center in its geographical area of influence, as show in Figure 1.1. These Local Exchange Centers connect to each other and to a Primary (Tandem) Transit Center through the so-called Junction Network. A defined set of Primary Transit Centers interconnects to a Secondary Transit Center through the Primary Long-Distance Network (Trunks). Secondary Transit Centers, as well as the International Gateway Exchange (Trunk) Center, are interconnected through a network also known as Long-Distance [1].

The data transport network follows a hierarchical structure, somewhat similar to the voice network described above and shown in Figure 1.1, being the Local Network called Local Access Network (LAN), the Junction Network called MAN (Metropolitan Access Network) and the Long-Distance network as WAN (Wide Access Network) [1].

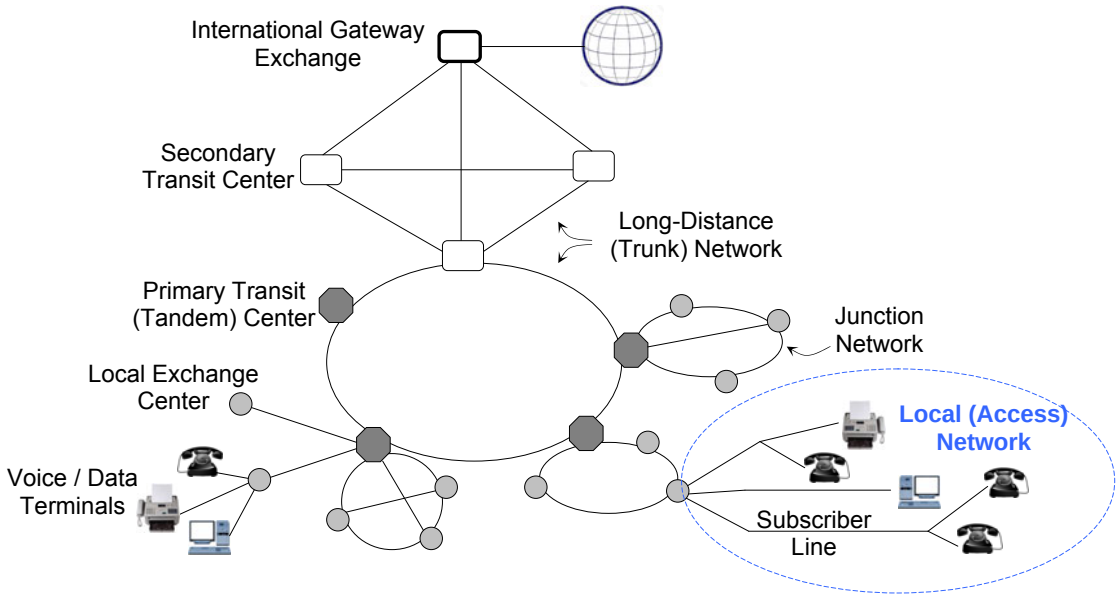

Figure 1.1: Common hierarchical structure of a public telecommunications network

The high distance and consequent attenuation in copper networks require the installation of amplifiers and regenerators every 2 km. In the 1970's, the installation of silicon fiber optic cables was initiated between telephone exchanges, with advantages such as electromagnetic noise immunity, much lower attenuation, higher bandwidth, as well as lighter, smaller diameter cables. Therefore, these passive optical networks (PON), essentially composed of SMF cables, are initially used in direct connections with segregated access between the Telecommunications Centers.

1.2 Optical Networks

PONs are optical networks that, besides fiber, use passive components such as splitters and combiners, which insert losses. As such, these networks containing splitters and splices are of relatively short reach up to about 20 km, being used by telecommunications operators in the access network of metropolitan areas in a point-to-multipoint topology for providing internet, voice over IP (VoIP) or digital TV. Other applications include backhaul connections from mobile stations or Wi-Fi access points. There are currently two technology standards for PONs, promoted in particular by the Institute of Electrical and Electronic Engineers (IEEE) and the International Telecommunication Union (ITU-T). The Ethernet-PON (EPON) and Gigabit-PON (GPON) versions are respectively the most widely deployed. As part of the work presented here, the conceptual development, laboratory implementation or published documents involve networks already standardized by ITU-T recommendations or under study. Therefore, some of the networks promoted by ITU-T and referred to in the works developed here are presented below.

ITU-T - Recommendation G.983 - APON, BPON

The first PON was defined in the mid-1990's through the Full-Service Access Network (FSAN) initiative, driven by an industrial and commercial alliance interested in providing services (Ethernet, data over IP, VoIP and Video) to residential customers and small and medium-sized enterprises. Thus, the Asynchronous-PON (APON) standard was created based on the Asynchronous Transfer Mode (ATM) transmission protocol, used for long-distance packet transmission and essentially for commercial applications. The initial APON standard, using a single fiber operating at 1.3 μm upstream and 1.55 μm downstream, did not include commercially important RF video overlay service for residential customers. In 1998, ITU-T adopts the APON standard as the international standard through recommendation G.983. In 2001, ITU-T G.983.3 recommendation establishes an enhanced version of APON to support more

broadband services, including high-speed Ethernet and video distribution, renaming the ATM-PON standard as Broadband PON (BPON). A typical BPON sends data at 622 megabits per second (Mbit/s) (or 155 Mbit/s) downstream at 1490 ± 10 nm and 155 Mbit/s upstream at 1390 ± 50 nm, providing also a video overlay service at 1555 ± 5 nm. [2 - 5]

ITU-T - Recommendation G.984 - GPON

The growth of Ethernet networks and Internet Protocol (IP) withdrew the ATM standard, the expectation of becoming the universal protocol of networks, in the transport of different applications. Gigabit-capable PON (GPON) networks, standardized from 2003 by ITU-T G.984 series recommendations, are an evolution of BPON networks in terms of speed and service flexibility, integrating emerging protocols and higher data rates. In a single fiber system, GPONs are bidirectional point-to-multipoint optical networks using downstream wavelengths of 1490 ± 10 nm and 1310 ± 50 nm upstream. The 1555 ± 5 nm optical range is often used here to broadcast sub-carrier modulated RF−based video overlay transmission [5, 6]. GPON provides a total downstream rate of 2.488 Gbit/s in broadcast mode to all Optical Network Units (ONU) and 1.244 Gbit/s upstream to the Optical Line Terminal (OLT). For upstream transmission, ONUs access the network using the Time Division Multiple Access (TDMA) protocol, in which a specific time interval is assigned to the requesting ONU, to send its data to the OLT, as shown in Figure 1.2.

The FTTH access network through GPON can share a physical line for up to 64 subscribers within a physical reach of up to 20 km. In a GPON with Transmission Convergence (GTC), the information string is organized into frames. These are composed of cells with ATM protocol and by a GPON's own frame format, called GPON Encapsulated Method (GEM), through which it is possible to encapsulate voice information protocols, POTS (Plain Old Telephone Service), TDM (Time Division Multiplexing) or Ethernet (Video, VoIP, Data, TV over IP (IPTV)), as shown in the diagram in Figure 1.3 [6].

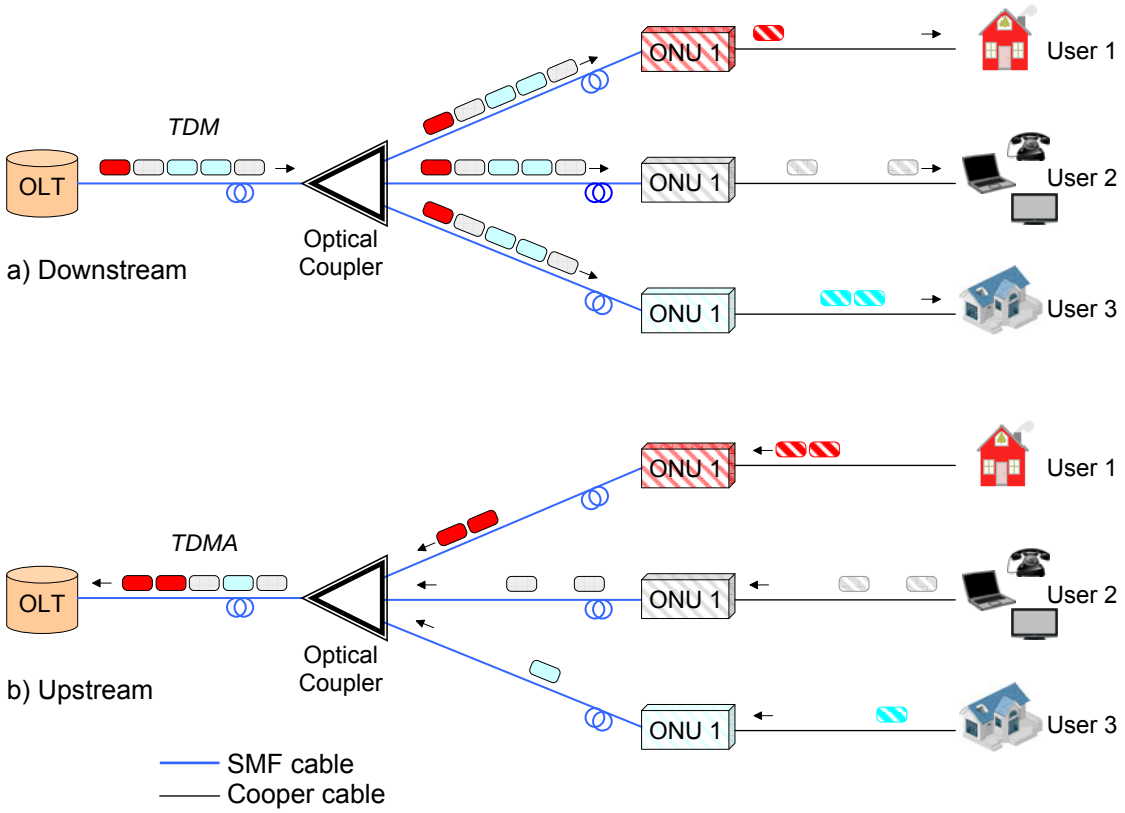

Figure 1.2: GPON transmission architecture. A downstream broadcast transmission occurs in a), where the ONUs filters the data for themselves, according to the identifier header in the GPON frames of the input string. In b) GPON frames send upstream by ONUs, are concatenated through the TDMA protocol.

To reserve wavelength bands for access to next-generation additional services, overlaid by WDM in GPON networks, the 2007 ITU-T G.984.5 recommendation was published, redefining the GPON wavelength plane. With the aim of maximize the capacity of future optical distribution networks (ODN), this recommendation introduces upstream the Reduced and Narrow wavelength range, as described in Table 1.1.

GPON Wavelength Plan (Single fiber system)

Downstream	Upstream	
1480 - 1500 nm	Regular Band Option:	1260 - 1360 nm
	Reduced Band Option:	1290 - 1330 nm
	Narrow Band Option:	1300 - 1320 nm

Table 1.1: GPON wavelength plan for the single fiber system as proposed by the 2007 ITU-T G.984.5 Recommendation [7]

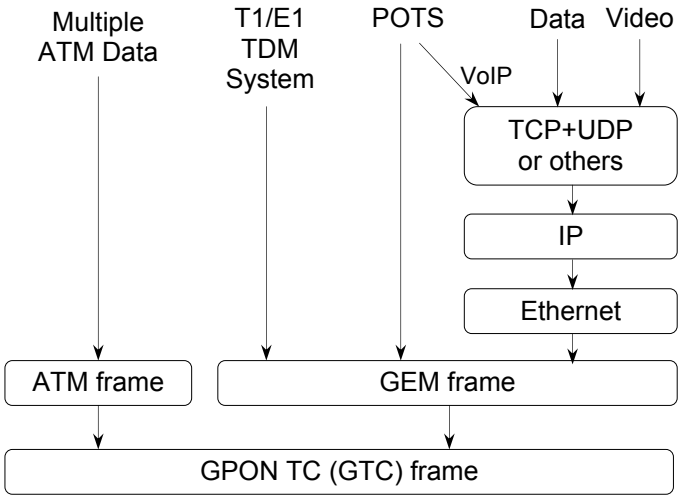

Figure 1.3: Protocol structure for the GPON Transmission Convergence (GTC) layer, composed of GEM and ATM frames

ITU-T - Recommendation G.987 - XG-PON1 and
ITU-T - Recommendation G.9807.1 - XGS-PON

The emergence of IP-based services such as over-the-top (OTT) TV (Netflix, Amazon Prime or YouTube) or video streaming underscores the need to increase data rates to meet the emerging high-definition entertainment market. To meet this purpose, ITU-T began to develop standards that reflected an evolution beyond that established by GPON networks, which has become known generically for next-generation networks (NG-PON). The NG-PON concept comprises the development of NG-PON1, based on medium-term upgrades and

maintenance of the established ODN for BPON and GPON, as well as the development of NG-PON2 as a solution that allows the evolution of new PONs and the redefinition of ODN from that defined in BPON and GPON [9, 25].

The NG-PON1 began to be developed through the 2010 ITU-T G.987 Recommendation series, which established an enhanced (eXtended) version of GPON named as XG-PON "as a 10-Gigabit capable PON in at least one direction".

In the above Recommendation, an asymmetric transmission network is established allowing 10 Gbit/s downstream at 1577 ± 2.5 nm and 2.5 Gbit/s upstream at 1270 ± 10 nm, and identified as XG-PON1, as show in Figure 1.4. The wavelength range of RF Video overlay services is the same as defined in ITU-T G.983.3. This XG-PON1 service is not GPON standard compliant, requiring different ONUs. However, it does allow WDM coexistence with existing GPON networks that follow the 2007 G.984.5 recommendation for upstream transmission band [7 – 9, 25]. Recommendation [9] also announced a network identified as XG-PON2 and capable of 10 gigabits downstream and upstream, but referencing its characterization for later recommendations.

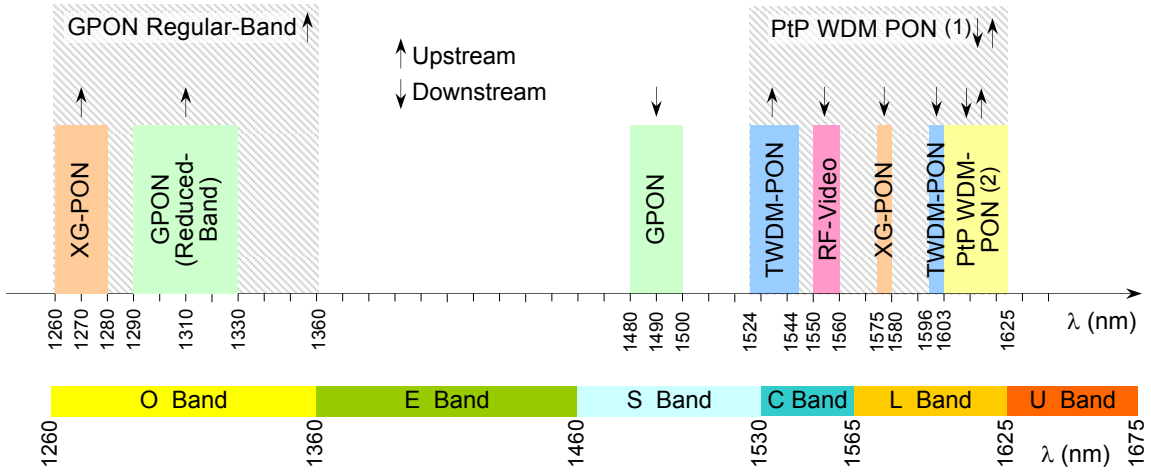

Figure 1.4: Wavelength plan to the GPON (G.984.5), XG-PON, TWDM-PON (NG-PON2) with Upstream Wideband Option, and PtP WDM-PON (NG-PON2) with (1) Extended Spectrum and (2) Shared Spectrum

In 2016, the concept of the XG-PON2 is developed through the ITU-T G.9807.1 recommendation series, which defines the characteristics of a 10-Gigabit-capable Symmetric Passive Optical Network (XGS-PON). A striking feature of the XGS-PON is its operating wavelengths, which assume two options. A Basic wavelength set consisting of the reuse of standard XG-PON1 wavelengths and an Optional wavelength set consisting of the reuse of standard GPON wavelengths. It is thus possible in XGS-PON, the coexistence of the Basic set with the Optional set of transmission wavelengths [24].

ITU-T - Recommendation G.989 - NG-PON2

The XG-PON standard still arouses little attention from the operators, presents few equipment suppliers and little compatibility between equipment from different manufacturers [11]. Currently, GPON meets the bandwidth requirements of residential customers. However, 5G technology is on the horizon, multimedia content is growing over IP, smaller cells need faster backhaul and businesses are consuming more traffic. Operators want to relax the bandwidth potential that PONs offer and realize financial returns by providing new services.

However, the increase in transmission rates above that established by the XG-PON standard is not economically and technologically convenient when placed on a single downstream/upstream wavelength pair. In fact, OLTs would have to provide high transmission TDM traffic and ONUs would have much higher bandwidth than needed for the end-user data rate. In addition, ONUs would have to deal with a high upstream TDMA signaling rate. Furthermore, to be attractive to telecom operators, any new transmission protocol must work on the existing ODN, which represents 70% of the investment made in PONs [11], as it should allow through WDM, coexistence with other legacy systems to monetize invested capital [12].

In this context, ITU-T Recommendation G.989.1 of 2013 [13] introduced the next-generation PON networks (NG-PON2). This recommendation defined a 40-Gigabit-capable PON, with an aggregate downstream reference rate of 40 Gbit/s

(4×10 Gbit/s), through a time and wavelength division multiplexing (TWDM) PON architecture of multiple TWDM channels. A TWDM channel refers to the pair consisting of a downstream wavelength and an upstream wavelength, which provide point-to-multipoint connectivity using, respectively, time division multiplexing (TDM) and multiple access mechanisms (TDMA). These channels can be up to 4 or 8 (in the future) pairs of wavelengths, allowing for a gradual growth pattern in the number of channels, such as “pay as you grow”, depending on the bandwidth required.

This standard allows for a symmetrical or asymmetric rate of 2.5 Gbit/s or 10 Gbit/s downstream by broadcast and/or upstream via TDMA signaling, and a passive range of up to 40 km. The TWDM-PON establishes a wavelength plane [14] as described in Table 1.2 that allows shared coexistence with the spectra of the G-PON, XG-PON, Radio-Frequency video (RF-Video) overlay, and Point-to-Point wavelength division multiplexing PON (PtP WDM-PON) systems, as shown in Figure 1.4.

TWDM-PON (NG-PON2)

Downstream	Upstream	
1596 - 1603 nm	Wide Band Option:	1524 - 1544 nm
	Reduced Band Option:	1528 - 1540 nm
	Narrow Band Option:	1532 - 1540 nm

Table 1.2: Wavelength range to the TWDM-PON on NG-PON2 [14]

1.2.1 WDM-PON

Optical fibers have an extremely high theoretical bandwidth. However, in commercial terms, speeds of only a few gigabits per second per optical channel are achieved. This data rate limitation is a consequence of the restricted speed of optoelectronic circuits at fiber optic terminals, as well as the associated electronic equipment, resulting in what is known as "electronic bottleneck", which makes it difficult to exploit the enormous bandwidth of a fiber using a single high

capacity optical channel [21]. This problem can be reduced by dividing the desired data rate on the fiber by various wavelengths in a process called Wavelength Division Multiplexing (WDM).

Looking at today's TDMA-based and next-generation PONs, there is a power budget that limits both the PON split ratio and the range/distance between OLT and ONU, as the use of 1:N passive power splitters leads to severe insertion losses, thus limiting the lengths attainable by the link [20].

TWDM-PON networks, defined by the NG-PON2 standard [13], have sought to overcome limitations in the availability of multiple gigabits per subscriber by offering an aggregate network capacity of 40 Gbit/s by exploiting the network time and wavelength domains. However, based on current trends in network access capacity growth, it is estimated that an aggregate capacity of over 100 Gbit/s is required by 2020 and 250 Gbit/s by 2025 [17].

Given these challenges and considering next-generation networks, ITU-T G.989.2 (NG-PON2) Recommendation [14] also specifies the characteristics of a PtP WDM-PON. The PtP WDM system is made up of tunable point-to-point wavelength overlay channels, which can optionally coexist with TWDM system channels. Each channel in the PtP WDM system is composed of a downstream wavelength and an upstream wavelength, thus enabling bidirectional data transmission between OLT and ONU. PtP WDM-PON uses the same wavelength range for Upstream/Downstream and has two range options, namely, Extended Spectrum at 1524-1625 nm and Shared Spectrum at 1603-1625 nm, as shown in Figure 1.4. Note that isolation requirements for TWDM-PON and/or other legacy systems (RF-Video, XG-PON) must be considered when determining the expanded spectrum wavelengths to be used by the PtP WDM-PON.

Dense WDM (DWDM)

Dense WDM (DWDM) is a wavelength division multiplexing system governed by ITU-T Recommendation G.694.1, which is typically characterized by narrow inter-channel spacing, ranging from 12.5 GHz to 100 GHz. In general, systems employing DWDM require stability in the wavelength values, whereby appropriate laser control systems are employed [15].

DWDM was first installed on long-haul fiber paths as the preferred equipment-saving solution. In a peer-to-peer topology, these long-distance communications can be hundreds of kilometers between transmitter and receiver and use high speeds in the range from 10 to 40 Gbit/s, in addition to being characterized by high aggregate bandwidth [22].

Subsequently, with the introduction of fiber optics in the metropolitan market, DWDM technology establishes a competitive advantage over the Synchronous Optical Networking (SONET) protocol in MANs, enabling faster and more efficient transmission of various types of services. In this context, with DWDM, providing a new service can be as simple as activating another light wave [23].

The great advantage of DWDM technology lies in exploiting the huge fiber transmission capacity. Investment in optical networks, in addition to being preserved, can be optimized to a minimum of 32 times as fiber capacity can grow as demand increases by upgrading terminal equipment or adding new wavelengths to existing fiber. In the latter case, the physical optical network is reused and the cost of additional capacity is exclusively for terminal equipment. Moreover, being physical layer architecture, DWDM is a transparent technology because it can support different transmission protocols, such as TDM, ATM, or Gigabit Ethernet, with different interfaces on the same physical layer. DWDM also enables fast and simple dynamic provisioning of network connections to provide high bandwidth services in a matter of days [23].

Ultra-Dense WDM (UDWDM)

The expected increase in traffic over the next 10 years involving 5G networks, video on demand, exchange of information from machine to machine (M2M), and Internet of Things (IoT) will make the TWDM-PON standard inappropriate. The limitations of bandwidth involving the electronic circuits responsible for TDMA signaling at ONU and the prediction that the required capacity in 2025 will reach 250 Gbit/s [16, 17], are some of the reasons that led the researchers to explore multi-wavelength networks with dense spacing, which can reach 2.5 GHz and where each wavelength is restricted to a single user.

Ultra-Dense Wavelength Division Multiplex (UDWDM) is a developing WDM system, which is characterized by providing a wavelength and a narrow optical band to each individual user. As an optical access network, the UDWDM is considered a potential future solution given its spectral efficiency, the ability to aggregate hundreds of channels (wavelengths) in a compact way, as well as allowing a very close separation between channels, for example 3 GHz [18]. As an example of a UDWDM system, it was demonstrated in [19] the transmission of 16 spaced wavelengths of 3.125 GHz, each with 1.244 Gbit/s in Quadrature Phase-Shift Keying (QPSK), in coexistence with the G/XG-PON standards and RF-video overlay.

1.3 Motivation and Objectives

Mobile and short-range wireless networks, as well as end-user access networks, seek to exploit greater bandwidth to ensure necessarily higher transmission rates. The copper transmission medium has been relegated by the installation of PONs and for an increasing number of current consumers, making optical fiber directly available to them through FTTH and Fiber-Into-The-Home (FITH) network configurations. Indeed, the availability of an optical connection opens the user to a whole new range of services.

POFs are guided transmission media with potential use in FITH networks or short-range data transmission. The perfluorinated index-graded POF (PF-POF) is currently the one with the best attenuation characteristic in data transmission. However, this attenuation varies beyond 100 dB/km in the C-band. Furthermore, in the current manufacturing process, the amorphous polymer structure of the PF-POF still exhibits impurities which may compromise the refractive index. These problems are not characterized by next-generation networks, such as those defined in [14]. As such, one of the objectives of this work is the design and implementation of high speed, bidirectional and double polarized point-to-point WDM transmission, with subsequent analysis of its viability.

Free-space optical transmission (FSO), established in the atmospheric environment through point-to-point and in line-of-sight connections, has aroused interest due to its deregulation, low cost, and high bandwidth. However, the free-space optical beam is subject to fluctuations in wind and temperature, expressed randomly along the propagation path, as well as by other atmospheric events. These fluctuations cause random variations in the refractive index and consequently the wavelengths of the beam along the channel, severely degrading the wavefront of the optical beam carrying the signal and increasing the attenuation. Another objective of this study is to analyze the effects of the fluctuation of the refractive index of a FSO channel when performing a GPON+CATV transmission and when performing the next generation PtP WDM transmission with reduced spacing between channels.

1.4 Thesis Organization

This thesis is organized into six chapters, according to established research proposals. Thus, it is sought here to summarize the theoretical studies, the research works and the implementations realized in the laboratory or in the field.

In order to contextualize the theme of this thesis, the motivations that gave rise to this work are presented in Chapter 1, which involves alternative media of optical transmission, namely Polymeric Optical Fibers (POFs) and the channel in atmospheric free space. As these transmission media have their applications mostly in the Access Network, the optical networks standardized by the ITU-T and the next-generation WDM access networks are also presented.

The characteristics of POF, as one of the alternative media of transmission, are discussed in Chapter 2 as well as their behavior in an orthogonal and bi-directional transmission.

Wireless optical communications are described and classified in Chapter 3, as well as some RF transmission configurations through the FSO. We also present the FSO configuration implemented externally, and used in several works throughout this investigation.

The FSO channel is characterized by several simulation models, which are differentiated by their input parameters and by the turbulence intensity considered. Chapter 4 describes two of these models and the simulations performed for a 1 km link at a rate of 10 Gbit/s, considering the different atmospheric turbulence conditions in the Bit-Error Rate (BER) performance.

The results obtained experimentally by a coherent long-reach and gigabit-capable UDWDM-PON system as by the presence of a FSO section on the transmission link is described in Chapter 5. Also presented are the results of a GPON system implemented during this investigation involving the combined transmission of data traffic and Community Access Television System (CATV) optical signal through a bidirectional connection consisting of two FSO sections and 20 km SMF.

The conclusions of the research developed are presented in Chapter 6, as well as some considerations about the possible developments that later can be followed in this investigation.

1.5 List of Publications

The original works published in journals or presented at conferences during the research carried out in the course of this Thesis are presented below.

1.5.1 Journal Articles

[J1] A. Shahpari, R. Ferreira, V. Ribeiro, **A. Sousa**, S. Ziaie, A. Tavares, Z. Vujicic, F.P. Guiomar, J.D. Reis, A.N. Pinto, A. Teixeira; “Coherent ultra dense wavelength division multiplexing passive optical networks”; *Opt. Fiber Technol.*, 26, Part A, (2015) 100–107, DOI: 10.1016/j.yofte.2015.07.001, [Online]. http://www.sciencedirect.com/science/article/pii/S1068520015000863

[J2] **Artur Sousa**, Ali Shahpari, Vítor Ribeiro, Mário Lima, António Teixeira, “Gigabit passive optical networks and CATV over hybrid bidirectional free space optics

+20 km single mode fiber", *Microw. Opt. Technol. Lett.*, 57 (12) (2015) 2867–2871. DOI: 10.1002/mop.29456, [Online]. http://dx.doi.org/10.1002/mop.29456

[J3] Isiaka Alimi, Ali Shahpari, Vítor Ribeiro, **Artur Sousa**, Paulo Monteiro, António Teixeira, "Channel characterization and empirical model for ergodic capacity of free-space optical communication link", *Opt. Commun.*, 390 (2017), pp. 123-129, DOI: 10.1016/j.optcom.2017.01.001, [Online]. http://www.sciencedirect.com/science/article/pii/S0030401817300019

[J4] **Artur N. Sousa**, Isiaka A. Alimi, Ricardo M. Ferreira, Mário Lima, Paulo P. Monteiro, António L. Teixeira, "Real-time dual-polarization transmission based on hybrid optical wireless communications", *Optical Fiber Technology*, Volume 40, Pages 114-117, 2018, DOI: 10.1016/j.yofte.2017.11.011, [Online]. http://www.sciencedirect.com/science/article/pii/S1068520017302900

[J5] **Artur N. e Sousa**, Ricardo Ferreira, Isiaka Alimi, Ali Shahpari, Mário Lima, António Teixeira, "Bidirectional SMF and PF-POF Transmission of 400 Gbps Nyquist Shaped on DP-QPSK Systems", *Microw. Opt. Technol. Lett.*, vol. 61, Issue 16, pp 256-260, 2019, DOI:10.1002/mop.31512, [Online]. https://onlinelibrary.wiley.com/doi/abs/10.1002/mop.31512

[J6] Abel Lorences-Riesgo, Fernando P. Guiomar, **Artur N. Sousa**, António L. Teixeira, Nelson J. Muga, Maria C. R. Medeiros, Paulo P. Monteiro, "200 G Outdoor Free-Space-Optics Link Using a Single-Photodiode Receiver", *Journal of Lightwave Technology,* Vol. 38, Issue 2, pp. 394-400, Jan. 2020, DOI: 10.1109/JLT.2019.2952930, [Online]. https://ieeexplore.ieee.org/document/8896066

1.5.2 International Conferences

[C1] Ali Shahpari, **Artur N. Sousa**, Ricardo Ferreira, Mário Lima, António Teixeira, "Free space optical communications for ultra high-capacity PON system", *Proc. SPIE 9286, Second International Conference on Applications of Optics and Photonics (AOP)*, 92861Y, August 2014; DOI: 10.1117/12.2063776; [Online]. https://doi.org/10.1117/12.2063776

[C2] Ali Shahpari, Ricardo Ferreira, Vítor Ribeiro, Zoran Vujicic, Ana Tavares, Somayeh Ziaie, **Artur Sousa**, Fernando Guiomar, Mário Lima, Armando Pinto, António Teixeira, "Free space optics hybrid PTMP advanced modulation bidirectional PON", *The European Conference on Optical Communication (ECOC)*, Cannes, Sept. 2014, pp. 1-3. DOI: 10.1109/ECOC.2014.6964074, [Online]. https://ieeexplore.ieee.org/document/6964074

[C3] A. Shahpari, R. Ferreira, **A. Sousa**, V. Ribeiro, J. D. Reis, M. Lima, A. Teixeira "Optimization Criteria for Coherent PONs with Video Overlay and Hybrid ODN", *Optical Fiber Communications Conference and Exhibition (OFC)*, Los Angeles-CA, March 2015, pp. 1-3. DOI: 10.1364/OFC.2015.Th3I.2, [Online]. https://ieeexplore.ieee.org/document/7121728

[C4] J. Heidarialamdarloo, **A. N. Sousa**, E. F. J. Silva, R. S. Oliveira, R. M. Ferreira, A. Shahpari, R. N. Nogueira, J. C. W. A. Costa and A. J. Teixeira, "Digitized Radio Over Plastic Optical Fiber for In-Home Network Applications", *26th International Conference on Plastic Optical Fibres, POF 2017 - Proceedings*, Aveiro, Portugal, 13-15 September 2017, Code131577, ISBN: 978-989-97345-2-4, [Online]. https://ria.ua.pt/bitstream/10773/18859/1/proceedings_POF2017.pdf

[C5] Abel Lorences-Riesgo, Fernando P. Guiomar, **Artur N. Sousa**, António L. Teixeira, Nelson J. Muga, Paulo P. Monteiro, "200 Gbit/s Free-Space Optics Transmission Using a Kramers-Kronig Receiver", *2019 Optical Fiber Communication Conference and Exhibition (OFC)*, San Diego-CA, March 2019, Paper: W4A.3, DOI: 10.1364/OFC.2019.W4A.3; [Online]. https://www.osapublishing.org/abstract.cfm?URI=OFC-2019-W4A.3

[C6] F. P. Guiomar, A. Lorences-Riesgo, D. Ranza, F. Rocco, **A. N. Sousa**, A. Carena, A. L. Teixeira, M. C. R. Medeiros, P. P. Monteiro, "High-Capacity and Rain-Resilient Free-Space Optics Link Enabled by Time-Adaptive Probabilistic Shaping", *45th European Conference on Optical Communication (ECOC)*, Dublin, September 2019, pp. 1-4, DOI: 10.1049/cp.2019.0864, [Online]. https://ieeexplore.ieee.org/document/9125592

1.5.3 Book Chapters

[B1] António Teixeira, Ali Shahpari, Vítor Ribeiro, Ricardo Ferreira, **Artur Sousa**, Somayeh Ziaie, Jacklyn Reis, Giorgia Parca, Silvia Dibartolo, Vincenzo Attanasio, Stefano Penna, Giorgio Maria Tosi Beleffi, "FSO for High Capacity Optical Metro and Access Networks", *in: Murat Uysal e al. (Ed.), Optical wireless communications - An emerging technology*, Springer, Cham, 2016, Ch. 23, pp. 511-526. DOI: 10.1007/978-3-319-30201-0_23, [Online]. https://link.springer.com/book/10.1007/978-3-319-30201-0

[B2] I. Alimi, A. Shahpari, **A. Sousa**, R. Ferreira, P. Monteiro, A. Teixeira, "Challenges and opportunities of optical wireless communication technologies", *in: P. Pinho (Ed.), Optical Communication Technology, InTech*, Rijeka, 2017, Ch. 02, pp. 5-44. DOI:10.5772/intechopen.69113, [Online]. http://dx.doi.org/10.5772/intechopen.69113

1.5.4 Other Contribution:

[C7] Cátia Pinho, Berta Neto, Tiago M. Morgado, **Artur Sousa**, André Albuquerque, Mário Lima, António Teixeira, "Spatial light modulator based flexible coupling platform for applications in SDM and PIC", *ECIO 2018 - 20th European Conference on Integrated Optics* – Valencia, Spain, Vol., pp. 238 - 240, May 2018, [Online]. https://www.researchgate.net/publication/327319035_Spatial_light_modulator_based_flexible_coupling_platform_for_applications_in_SDM_and_PIC

References

[1] João J. O. Pires, "Sistemas e Redes de Telecomunicações (1st Chapter)", *DEEC, Instituto Superior Técnico*, 2006

[2] Broadband optical access systems based on Passive Optical Networks (PON), ITU-T Recommendation G.983.1, *International Telecommunication Union*, October 1998

[3] A broadband optical access system with increased service capability by wavelength allocation, ITU-T Recommendation G.983.3, *International Telecommunication Union*, March 2001

[4] Cedric Lam, "Passive Optical Networks - Principles and Practice", *Elsevier*, 2007, ISBN 978-0-12-373853-0

[5] Henrique J. A. da Silva, "Optical Access Networks", *Instituto de Telecomunicações*, March 2005

[6] Gigabit-capable Passive Optical Networks (GPON): Transmission convergence layer specification, ITU-T Recommendation G.984.3, *International Telecommunication Union*, February 2004.

[7] Gigabit-capable Passive Optical Networks (G-PON): Enhancement band, ITU-T Recommendation G.984.5, *International Telecommunication Union*, September 2007.

[8] Michael Emmendorfer, "Comparing IEEE EPON & FSAN/ITU-T GPON Family Of Technologies", *ARRIS Enterprises*, 2014

[9] 10-Gigabit-capable passive optical network (XG-PON) systems: Definitions, abbreviations, and acronyms, ITU-T Recommendation G.987, *International Telecommunication Union*, January 2010

[10] 40-Gigabit-capable passive optical networks (NG-PON2): Definitions, abbreviations and acronyms, ITU-T Recommendation G.989, *International Telecommunication Union*, October 2015

[11] Evolution of FTTH Networks for NG-PON2, *Altice Labs*, 2013, [Online]. https://www.alticelabs.com/content/WP-Evolution-of-FTTH-Networks-for-NG-PON2.pdf

[12] TWDM-PON: Taking Fiber to New Wavelengths, *Alcatel-Lucent*, 2015, [Online]. http://www.fiber-optical-networking.com/tag/dwdm-pon

[13] 40-Gigabit-capable passive optical networks (NG-PON2): General requirements, ITU-T Recommendation G.989.1, *International Telecommunication Union*, March 2013

[14] 40-Gigabit-capable passive optical networks 2 (NG-PON2): Physical media dependent (PMD) layer specification, ITU-T Recommendation G.989.2, *International Telecommunication Union*, December 2014

[15] Spectral grids for WDM applications: DWDM frequency grid, ITU-T Recommendation G.694.1, *International Telecommunication Union*, February 2012

[16] Cisco Visual Networking Index: Forecast and Trends, 2017–2022, *Cisco White paper*, [Online]. https://www.cisco.com/c/en/us/solutions/collateral/service-provider/visual-networking-index-vni/white-paper-c11-741490.html

[17] M. Sezer Erkılınç, et all, "Comparison of Low Complexity Coherent Receivers for UDWDM-PONs (λ-to-the-user)", *Journal of Lightwave Technology*, vol. 36, Issue 16, pp. 3453-3464, March 2018, DOI: 10.1109/JLT.2018.2835376, [Online]. https://www.osapublishing.org/jlt/viewmedia.cfm?uri=jlt-36-16-3453&seq=0

[18] H. Rohde, S. Smolorz, S. Wey, E. Gottwald, "Coherent optical access networks," *Proc. Optical Fiber Communication Conf. (OFC)*, Los Angeles, CA, pp. 1-3, March 2011, DOI: 10.1364/OFC.2011.OTuB1, [Online]. https://www.researchgate.net/publication/230743761_Coherent_Optical_Access_Networks

[19] H. Rohde, E. Gottwald, A. Teixeira, J. Reis, A. Shahpari, K. Pulverer, J. S. Wey, "Coherent Ultra Dense WDM Technology for Next Generation Optical Metro and Access Networks," *Journal of Lightwave Technology*, vol. 32, no. 10, pp. 2041-2052, May 2014, DOI: 10.1109/JLT.2014.2316369, [Online]. http://www.hit.bme.hu/~jakab/edu/litr/Access/PON/Ultradense_WDM_ngPON2014_06786334.pdf

[20] Klaus Grobe, Jörg-Peter Elbers, "PON in Adolescence: From TDMA to WDM-PON", *IEEE Communications Magazine*, vol. 46, no. 1, pp. 26–34, January 2008, DOI: 10.1109/MCOM.2008.4427227, [Online]. https://www.academia.edu/19408071/PON_in_adolescence_from_TDMA_to_WDM-PON

[21] Mohan Gurusamy, C. Siva Ram Murthy, "WDM Technology and Issues in WDM Optical Networks", *Prentice Hall.*, 1st edition, November 2001, ISBN-13: 978-0-13-060637-2

[22] Lakshmi D L, P C Srikanth, Sanjaya kumar C, "DWDM in Transmission System, a Review", *International Journal of Engineering Research in Electronics and Communication Engineering (IJERECE)*, vol. 4, issue 12, pp. 117-120, December 2017, ISSN-2394-6849

[23] "Introduction to DWDM Technology", *Cisco Systems, Inc.*, 2000, [Online]. https://www.cisco.com/c/dam/global/de_at/assets/docs/dwdm.pdf

[24] 10-Gigabit-capable symmetric passive optical network (XGS-PON): Optical line systems for local and access networks, ITU-T Recommendation G.9807.1, *International Telecommunication Union*, June 2016

[25] 10-Gigabit-capable passive optical network (XG-PON): General requirements, ITU-T Recommendation G.987.1, *International Telecommunication Union*, March 2016

Chapter 2

Plastic Optical Fibers - POF

2.1 Introduction

The terminal portion of a fiber optic glass distribution network near the houses/offices, referred to as FTTH, is usually less protected and therefore more subject to sudden mechanical movements, fortuitous interventions and handling by unskilled people. These problems regarding silicon optical fibers are also addressed when studying the installation of optical networks inside the housing / offices (FITH).

When talking about fiber optic networks, the majority of the actors involved in the area, even some experts, are paying attention to the fibers in silicon, disregarding of the existence of plastic optical fibers (in polymer) that also allow the transmission of an optical signal, these having distinct physical and spectral characteristics of the optical glass fibers obviously with advantages and disadvantages.

Polymer fibers, although presenting a relatively high attenuation these days, are an optical device with good handling, installation, with an easy connectorization and cost characteristics that make them attractive for intensive use over short distances. This chapter presents the evolution of POFs and describes their constituent materials, as well as some important parameters in

the characterization of optical fibers, the most frequent types of POFs, their most relevant characteristics and current application areas.

2.2 Fiber Optic Composition

Optical fibers are made of uniformly extending longitudinal dielectric materials having a transverse profile, generally formed by one or more cylindrical and concentric layers, which constitute the core and where light is conducted, surrounded by a cladding, for the purpose of confining the light inside.

The highly transparent raw materials predominantly used in core construction are silica ("glass") and polymers ("plastics"). A feature of the core is the value of its refractive index, which can be constant or radially variable and even modified by the addition of impurities (dopants).

It is observed that the silica is very stable and with low manufacturing cost. In the case of polymers, the most commercially available material is Poly-Methyl MethAcrylate (PMMA), Polystyrene (PS), Polycarbonate (PC) and fluorinated polymers (substitution of CH-bonds with fluorinated CF bonds).

Among the materials used in the production of plastic fibers, the best values for attenuation, IR bandwidth and production capacity are those based on perfluorinated graded-index polymers (PF-POF). The best attenuation results are those reported by Asahi Glass Company with the perfluorinated polymer called *CYTOP*® [1].

2.3 Optical Fiber Light Propagation

Light propagation in any medium will always be slower than vacuum propagation. The refractive index (*n*) of a medium measures how fast the light propagates in a vacuum relative to the medium, where *n* is a dimensionless

value. A medium is said to be more refractive the higher the value of its index *n*. Some examples of refractive indexes for fiber optic cores are given in Table 2.1.

Medium	Refractive Index (*n*)
Glass Optical Fiber (GOF);	1.469
POF in PMMA	1.492
PF-POF (from *CYTOP*®).	1.356

Table 2.1: Refractive indexes *n*, for some silicon and polymer fiber optic (POF) cores.

Following Figure 2.1, let's consider medium *A* with refractive index n_A and medium *B* with index n_B, in contact along a regular surface S_{AB}, and $n_A \leq n_B$. When a light ray (f_A) passes through medium *A* and reaches the S_{AB} interface, part of the incident ray is reflected (f_{Ar}) and part of the ray is refracted (f_B) into medium *B*, as dictated by Snell's Law. The θ_A, θ_{Ar} and θ_B are the angles that the incident, reflected and refracted rays make with the N_{AB} interface, normal to S_{AB} interface, as shown in Figure 2.1. Likewise, similar behavior happens between medium B and C, with $n_C \leq n_B$.

2.3.1 Total Internal Reflection

Concerning the S_{BC} interface, and considering the medium *B* more refringent than the *C* medium (i.e. $n_B \geq n_C$), then by Snell's law there will be a limiting angle of the incident beam θ_{Bc} for which $\theta_C = \pi/2$ rad . So,

$$n_B \, sen(\theta_{Bc}) = n_C \, sen(\theta_C) \tag{2.1}$$

$$sen(\theta_{Bc}) = \frac{n_C}{n_B} \tag{2.2}$$

Equation 2.2 expresses the boundary condition for total internal reflection given by $\theta_{RT} = arcsen(n_C / n_B)$, called the critical angle, as shown in Figure 2.2. For angles $\theta_{Bc} > \theta_{RT}$, the incident light ray f_B in Figure 2.1 is completely back reflected by the S_{BC} boundary towards medium *B*. Total internal reflection is the mechanism that forces the light present inside an optical fiber to remain confined within the fiber itself.

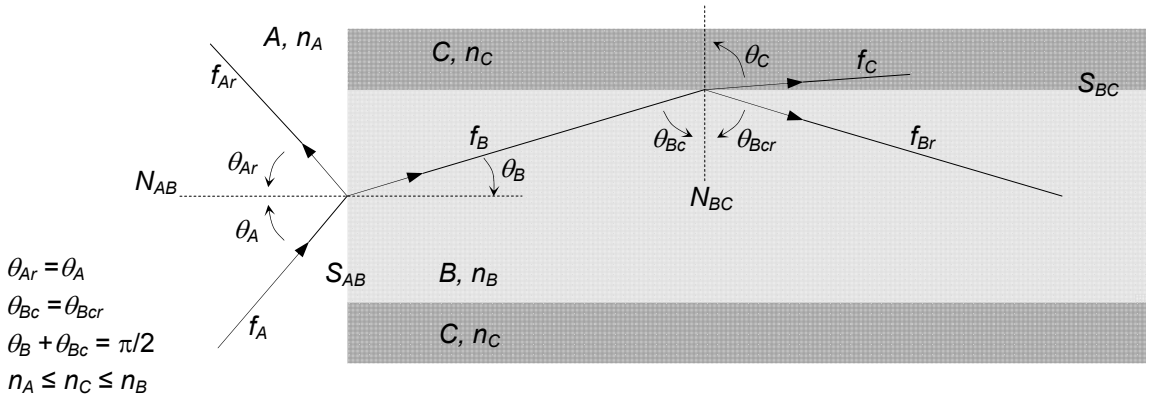

Figure 2.1: Refraction analysis of medium *A* to *B* and internal reflection within medium *B*

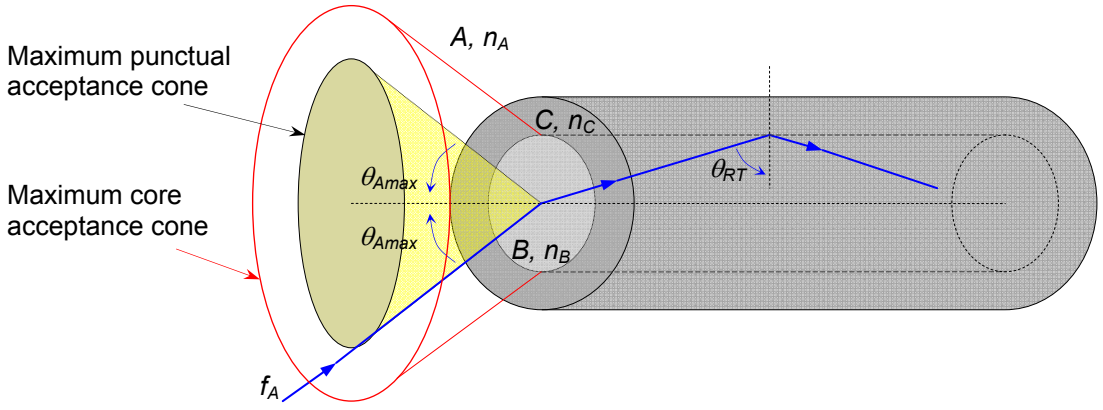

Figure 2.2: Maximum acceptance cone in the limit condition of total internal reflection

2.3.2 Numeric Aperture and Acceptance Angle

If the total internal reflection condition is respected at the S_{BC} interface, for light rays f_B traveling through medium *B*, then the rays f_A, traveling through medium A and reaching the S_{AB} surface, Figure 2.1, cannot exceed a certain maximum angle θ_{Amax}, otherwise, the total internal reflection of the f_B radius will not occur at the S_{BC} interface. The θ_{Amax} angle is obtained by applying Snell's Law to the S_{AB} interface, and considering the critical angle θ_{RT} in Figure 2.2 for the total reflection condition, then we have:

$$n_A\, sen(\theta_A) = n_B\, sen(\theta_B)$$

$$n_A\, sen(\theta_{A\max}) = n_B\, sen\left(\frac{\pi}{2} - \theta_{RT}\right) = n_B \cos(\theta_{RT})$$

$$n_A\, sen(\theta_{A\max}) = n_B \sqrt{1 - sen^2(\theta_{RT})} = n_B \sqrt{1 - \left(\frac{n_C}{n_B}\right)^2}$$

$$NA = sen(\theta_{A\max}) = \frac{\sqrt{n_B^2 - n_C^2}}{n_A} < 1 \qquad (2.3)$$

The angle θ_{Amax} satisfying the Equation (2.3) is called the acceptance angle and represents the angle of rotation of a cone of revolution, with a central axis parallel to the normal N_{AB}, as shown in Figure 2.2. The entire light beam f_A with angle of incidence contained in this cone $(\theta_A < \theta_{A\max})$ undergoes total internal reflection to medium *B* at the S_{BC} interface, propagating along the fiber.

The magnitude *NA* in Equation 2.3 is called the Numerical Aperture and measures the relative useful capacity that a given point on the S_{AB} surface has in capturing energy from the medium *A* and keeping it contained in the medium *B*. Table 2.2 shows the numerical aperture values for some fibers in POF and Glass optical fiber (GOF), according to [2].

Type	Profile	Radius (μm)	*NA*	Notes
PMMA-POF	SI	490	0.5	
PMMA-POF	GI	450	0.37	Fiber from *Optimedia*
MC PMMA-POF	SI	65*	0.5	MC37 Multi-Core Fiber. *Radius of a single core
PF-POF	GI	60	0.22	*Lucina*® Fiber from Asahi Glass
MM-GOF	GI	25	0.17	
SM-GOF	SI	5	0.1	

Table 2.2 – Profile, radius and numerical aperture characteristics of the core for some silicon and polymer fibers.
MM – Multimode, SM - Singlemode

2.3.3 Propagation Modes in Optical Fiber

Optical fibers are fundamentally classified by the way light rays propagate in the fiber core, that is, by the possible paths along the fiber optic core. If the path of all propagated rays always coincides with the core axis, as shown in Figure 2.3 b), then only one propagation mode is possible and the fiber is classified as single-mode fiber (SMF).

Depending on the radius *a* of the core and the difference between the refractive indexes of the core and the cladding, a light ray at a given wavelength may also take varying directions in inclined angles relative to the central axis of the core, as shown in the Figure 2.3 a). If, in addition to the axial path, the fiber core accepts the propagation of rays by inclined angles, then the fiber is classified as multimode fiber (MMF).

According to the wave equation for circular dielectric guides and respecting the boundary conditions at the core-cladding interface for the electric and magnetic field, it is possible to arrive at a designated parameter of Normalized Frequency (*V*), from which we can define if for a given wavelength the propagation will be single or multimode, according to [3], [4] by

$$V = \frac{2\pi a}{\lambda} NA$$

where *a* is the radius [m] of the fiber core, *NA* is the numerical aperture of the fiber and λ is the wavelength [m] of transmitted light. The cylindrical optical fibers are classified as SMF if $V < 2.405$ and in this case only the electromagnetic mode HE_{11} is propagated. For a higher *V* value, normally lower wavelengths, the fiber is classified as MMF and in this case, in addition to the lowest order HE_{11} mode, higher order modes [3] [4] are also propagated.

From the analysis of the radius of the glass fiber cores and the wavelengths in which they operate, we have SMF and MMF on the market. In the case of POFs, since the core diameter is normally ≥ 50 µm and the wavelength is predominantly in the visible region, we can classify them as MM. [5] [6]

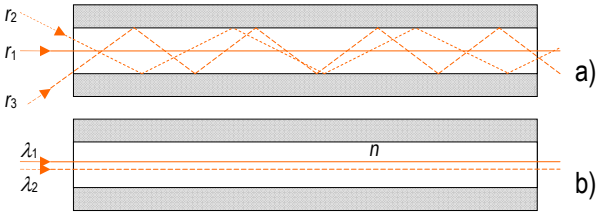

Figure 2.3: a) Multimode ray propagation, b) Singlemode ray propagation.

2.3.4 Attenuation

In an optical fiber, the power decreases exponentially along the length *z* according to the expression:

$$P(z) = P(0)\,10^{-\frac{\alpha z}{10}} \qquad \alpha = -\frac{1}{z}10\,Log\frac{P(z)}{P(0)}\ [dB/km]\ ,$$

where $P(z)$ is the power at distance *z*, $P(0)$ is the power at the input of the fiber and α is called the attenuation coefficient [7].

2.3.5 Optical Fiber Propagation Profile

The step index (SI) and graded index (GI) fiber profile is defined by how the core refractive index value evolves along the fiber cross-section as shown in the Figure 2.4.

The number of modes (*N*) propagated can be given approximately according to the normalized frequency, as expressed in [2], by

$$N \approx \frac{V^2}{2} \quad \text{, for step-index fibers}$$

$$N \approx \frac{V^2}{4} \quad \text{, for graded-index fibers}$$

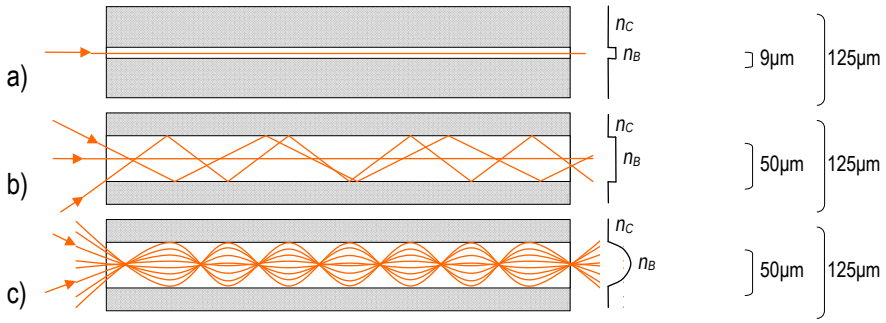

Figure 2.4 a) Single-mode fiber (SMF) with step index (SI), b) Multimode fiber (MMF) with SI, c) MMF with graded-index (GI).

The construction of optical fibers requires precise mechanical techniques in order to achieve the necessary longitudinal and radial thickness and homogeneity as well as complex chemical processes in controlling the refractive index. In addition, optical transmission by confined dielectric media involves, among other problems, delays by multi-path of the light rays (modal dispersion) and problems because the spectral velocity of the optical field propagated along the fiber is not constant (chromatic dispersion). The search to overcome these problems led to the construction of optical fibers with varied materials and profiles. Transversal to this variety of fibers, however complex the profiles, is that each longitudinal layer

present in that profile individually has a constant (SI) or variable (GI) refractive index.

2.4 The Historical Evolution of POFs

The first POFs came in the 1960s, with DuPont (USA) and Mitsubishi Rayon (Japan) pioneering the research and development of these materials based on the transparent thermoplastic polymer Polymethylmethacrylate (PMMA). In the 1970s, *DuPont* achieved a minimum of 1000 dB/km of attenuation, marketed a number of fibers under the name of *Crofon*®, however, it reduced interest in these products and slowly left the market. On the other hand, *Mitsubishi Rayon* launches a fiber with PMMA core under the name of *Eska*® [5]. In 1978 *Mitsubishi* acquires this entire area of research and patents to *DuPont*. In the following years, the development of Japanese manufacturing and research techniques lead the fibers in PMMA to 150 dB/km attenuations at 650 nm, very close to the theoretical limit. These fibers are still in step index profile with bandwidths of 50 Mb/s in 100 m [5].

The next evolutionary step was given by a group of researchers led by Prof. Koike, from the University of Keio (Japan), who in 1990 developed a process of construction of a PMMA plastic fiber with a graded-index profile (GI-POF) which, by reducing the modal dispersion, allowed an increase bandwidth of 3 GHz x km in the 650 nm range and similar losses were the step index fibers which were nonetheless high [8].

In 1995 POF technology achieves a major advance in attenuation when Koike and other researchers at Keio University develop graded-index fibers from perfluorinated polymers (PF-POF) with attenuations of less than 50 dB/km in the range of 650-1300 nm. However, developments involving the form of fiber construction and improvements in the processes of elimination of chemical impurities have been investigated [9] in order to reach the theoretical limit identified in Figure 2.7.

At the commercial level, it is worth noting in 2002 the amendment of the IDB 1394 standards, a version of the IEEE 1394b for the automotive area, which regulates the use of POF in telematics and multimedia applications in motor vehicles, with the automotive industry pioneering and booster of POF technology [8].

In 2005, following a first commercial data link made by *Fuji Photo* (Japan) using PMMA GI-POF fiber under license from Keio University, *Optimedia* (South Korea) commercially made the first GI-POF wired.

Asahi Glass (Japan) starts production of its own PF-POF fiber called *Cytop*® and from 2002 installs this fiber in several buildings in Japan. In 2005, Chromis Optical Fiber (USA) licenses the production of *Lucina*® fiber to Asahi Glass, developing a good cost-effective extrusion and cabling process [8].

The graph in Figure 2.5 shows the evolution of attenuation of PMMA and perfluorinated (PF) plastic fibers over time, highlighting the main actors of the process.

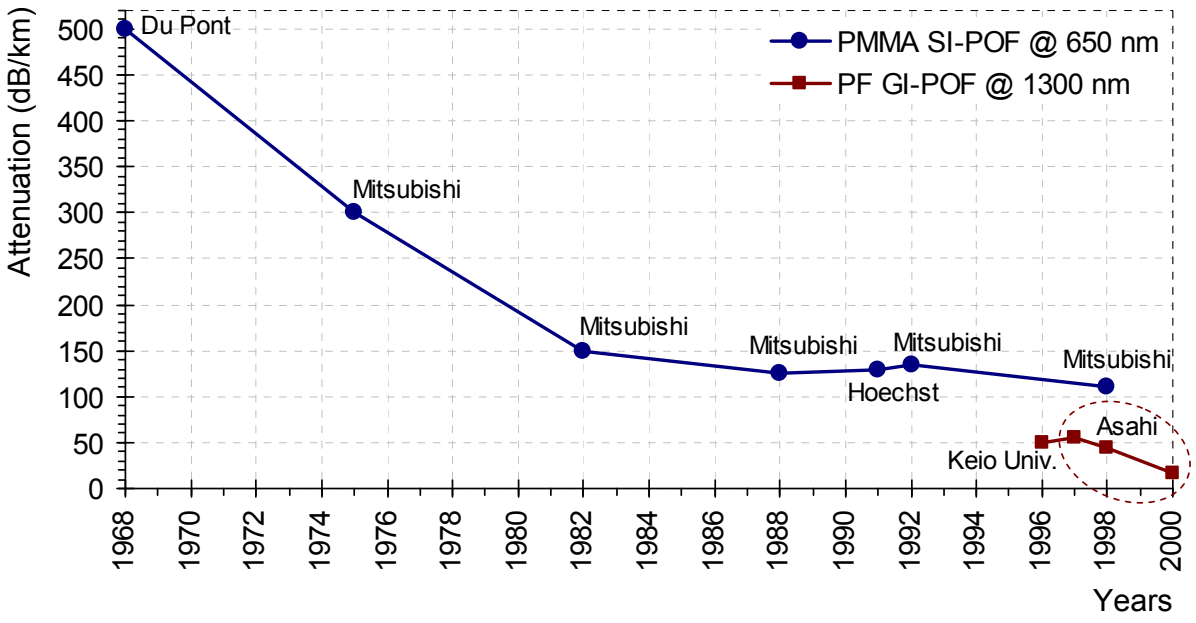

Figure 2.5: Historical evolution of POF attenuation and key players (adapted from [10]).

However, in recent years, amorphous polymers and fluoropolymers have been the subject of investigation and commercial interest by new manufacturers (DuPont, Solvay Solexis, 3M, Honeywell or Daikin) and new proposals for polymeric fibers have emerged on the market, of which are examples, microstructured polymer optical fibre (MPOF), multi-core POF (MCF), PMMA GI-POF, partially chlorinated GI-POF or GI-POF based on a new methacrylate composition (PTCEMA).

2.5 Types of POF

Glass optical fibers, more precisely single-mode fibers, are optical transmission media par excellence in WAN, PON, and optical LANs. These fibers initially using the 850 nm transmission window, have benefited from evolution in manufacturing. Currently, Low Peak Water (LWP) SMF has a virtually continuous transmission window, ranging from 800 to 1675 nm. Optical signal frequencies suffer uneven degradation due to attenuation and dispersion. In the 1550 nm window in SMF, Figure 2.7, an attenuation of 0.25 dB/km and a bandwidth-distance product of ~100 THz×km is possible. As shown in figure 2.7, the 1300 nm transmission window is one of the leaders in graded index MMF (GI-MMF), with attenuation of 1 dB/km and a bandwidth-distance product of 0.5 GHz×km. [11]

In general, despite the good characteristics of the transmission spectrum, handling and bonding the glass fibers requires complex equipment and qualified personnel. Furthermore, a low stress level and a bend radius of 25 mm make them unsuitable in optical access network and residential applications like FITH.

POFs have become increasingly important in automotive communications (MOST Program since 2001), in the construction of data networks, in specific residential communications or in the development of optical sensors. POFs have been developed with geometric, constructive and doping characteristics that give them unique characteristics. One of these well-known fibers has a polymethylmethacrylate (PMMA) core, a step-index profile and a 1 mm diameter

(1 mm SI-PMMA), with transmission windows defined in the visible spectrum- Figure 2.6. Another well-known polymer is PF-POF, which has a perfluorinated doped core and a graded index profile. These polymers were recognized as a cost-effective and competitive solution to copper lines in short-range broadband transmission, especially in the home-based broadband infrastructure for the provision of Gigabit Ethernet. These fibers have good connectorization, robustness, good tensile stress tolerance, and much better bending radius than those allowed by glass fibers or coaxial cables.

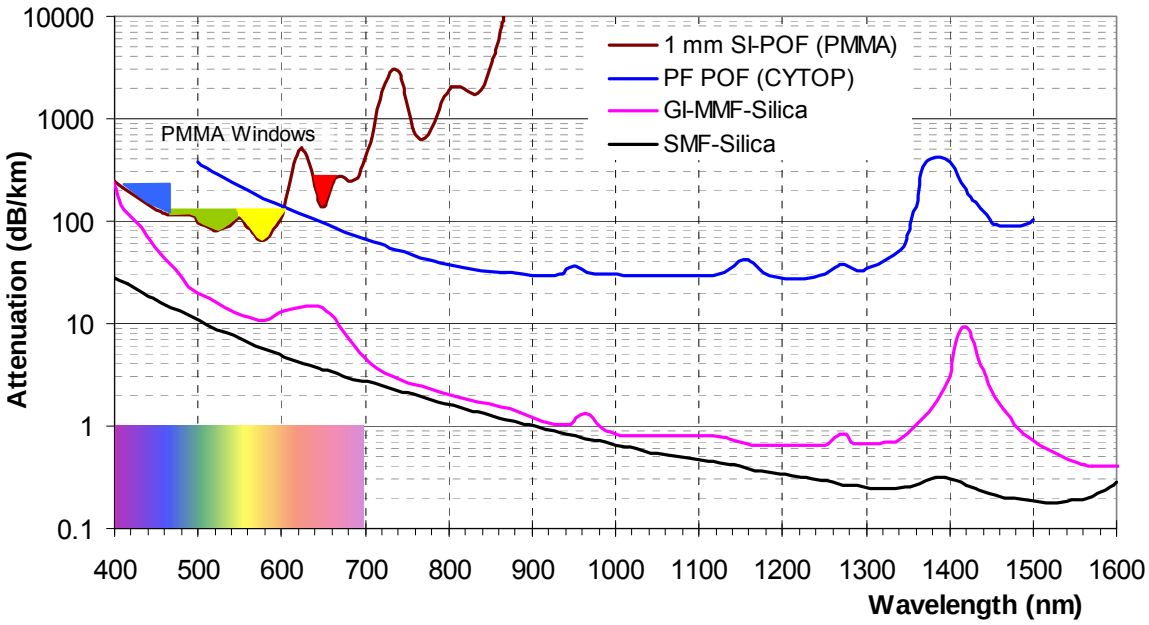

Figure 2.6: Wavelength attenuation for polymeric optical fibers (POF): 1 mm SI-PMMA and PF-POF [1], and silica optical fibers: GI-MMF and SMF (adapted from [1], [12])

Unique in high production, low cost and subject to standardization, the SI-PMMA POF has a loss of 110 dB/km at 520 nm (green) and a distance×bandwidth product of ~50 MHz×100 m. This POF was the first to be used in housing, however, its multimodal dispersion mode is very strong due to its high numerical aperture (~0.5). The transmission in SI-PMMA of 1 Gbps in 50 m proved to be viable, using strong equalization techniques.

An example for the impulse response model of this type of fibers is given by: [13]

$$h = \frac{A}{\sqrt{2\pi}\,\sigma} e^{-\frac{(t-\tau\, Lpof)^2}{2\,\sigma^2}}$$

Where: $A = 10^{-\frac{(\alpha\ Lpof)}{10}}$ fiber attenuation;

α - fiber losses in dB/m; *Lpof* - POF length in meters;

τ - group delay in s/m; σ - fiber dispersion.

Another useful approach to modeling the transfer function is given by POF: [14]

$$H(f) = Ae^{-\left(\frac{f}{1.7\ B_{3dB}}\right)^2}$$

Where: A - fiber attenuation; B_{3dB} - Bandwidth

In order to combat this high multimodal dispersion of the SI-PMMA fiber, increasing interest in GI-POF and Multicore-POF (MC-POF) has taken place [15].

With GI-POF it is possible to reach bandwidths above 2.0 GHz at 50 m. A transmission of 5.3 Gbps over 50 m, using GI-POF of 1 mm in diameter, was performed by [16].

MC-POF is usually composed of 19 or 37 parallel step-index small cores with similar propagation properties. The most important property of MC-POF is its high bending tolerance, ~ 2 mm, much smaller than 20-25 mm in SI-POF or GI-POF. A demonstration of 4.7 Gbit/s transmission on a 19-MC-POF core, 50 m long and 1 mm in diameter was performed by [17].

The PF-POF has better light transmission over a wide wavelength range of 650-1300 nm, with a minimum attenuation of 10 dB/km at 1050 nm and bandwidth×length product greater than 8 GHz-km [18] [19]. In Figure 2.6, the attenuation parameter is compared between the three materials that optical fibers are made of: glass, PMMA and perfluorinated polymer. The PF-POF attenuation is shown in detail in Figure 2.7.

The attenuation of PF-POF is 10 times lower than that associated with PMMA-based POF for both the visible and infrared spectrum. The relatively flat spectrum is a direct result of the low dispersion associated with perfluorinated polymers. This fiber is useful for applications at various wavelengths of 650, 850, 1310 and 1490 nm. For a 200 m link and 800 nm wavelength, the PF-POF presented a satisfactory performance at a transmission rate of 40 Gbps [19].

Therefore, optical POF is promising for short distances applications such as in the optical access network or FITH. Price is the most favorable feature of SI-PMMA POF. The MC-POF has greater bandwidth and a key element in the installation: the very low bending radius. However PF-POF is the best option if attenuation and bandwidth are key factors.

2.6 Bidirectional SMF and PF-POF Transmission on DP-QPSK Systems

2.6.1 Introduction

The growth in data traffic driven by the so-called Information Society and competition logic pushes telecom operators to offer new and faster services to customers. The increasing presence of the Internet in daily services and equipment to monitor/control them, the growth of mobile devices and the storage and processing in the Cloud, considerably increase the current data traffic in the networks. These facts lead to the increase and complexity of data center equipment, which must be flexible and capable of responding to increased data speed and processing. Therefore, data center modules should allow for a higher density of line boards, smaller transceivers, and embedded optical systems. This requires a large amount of short-range (patch-cord) cables with higher transmission bandwidth. RF copper cables are bulky, heavy and with limited bandwidth to accommodate rates of 10 Gbps or higher [7].

Silica optical fiber cables have low bending capabilities and require

connections with precise alignment of impurities-free cores. These facts hamper the short optical connections between devices in the Data Centers/Headends, where silica MMFs are often used, since the large core diameters of 50 and 62.5 μm facilitate the alignment in the connections, however they are more fragile and breakable [20].

An alternative to MMFs are multimode POFs, which exhibit optical attenuations higher than the corresponding MMFs. However, when applied to very short-range links [10], they are an interesting solution since they support compressions, strong curves and are more easily handled and connectorized due to the large coatings (0.5-1.0 mm). In addition, due to the large core diameters of POF (> 50 μm), the connections are less sensitive to impurities and the alignment is not as demanding, as seen in the MMF.

Multimode fibers are characterized by having several propagation modes with distinct speeds and corresponding group delays (GD). The optical fibers are subjected in their construction to geometric and density imperfections, impurities, irregularities in the refractive index, and also to external mechanical actions such as curvatures, kinks or compressions. These anomalies cause the optical field of a pulse traveling in a propagation mode to couple (transfer energy) to other modes with different GDs, in a so-called mode coupling process whose intensity is determined by the mode coupling coefficients [21]. The pulse obtained at the end of the fiber is the overlap of optical fields with distinct GDs whose scattering defines the modal dispersion.

When the optical field couples between modes, not only the magnitude of the field is redistributed but also the phase of the coupled field can be changed. In order to justify some results not explained by the power coupling models, the concept of field-coupling model [22] [23] was developed, which considers that modal GD values are not only dependent on power couplings, but also on the phase effects between modes. Thus, the GD values vary with the distance traveled and with the intensity of the couplings between modes, defining two coupling regimes. In the low-coupling regime, the GDs show little dependence on the reduced couplings between modes and the values of the GDs grow linearly with the transmission length. In this regime, the fiber response exhibits highly

polarized behavior. In the high-coupling regime, the GDs are strongly dependent on the high couplings between modes, growing with the square root of the fiber length and the fiber response exhibits a depolarized behavior. For a fixed length of the multimode fiber subject to a low coupling regime, the values of the GD observed at the fiber end will define a given modal spread. When the modal coupling intensity increases in the high-coupling regime, it is verified that the GD values are concentrated, reducing the modal scatter verified previously. This reduction in modal spreading and therefore in the modal dispersion leads to a consequent improvement in the fiber bandwidth-distance product characteristic [22]. The optical fiber length from which the optical transmission is subjected to a strong-coupling regime and an equilibrium mode distribution is defined as coupling length (Lc). In the graded-index MMF, the value of Lc is a few kilometers [21] while in the graded-index POF, the value of Lc is about 2 m [20].

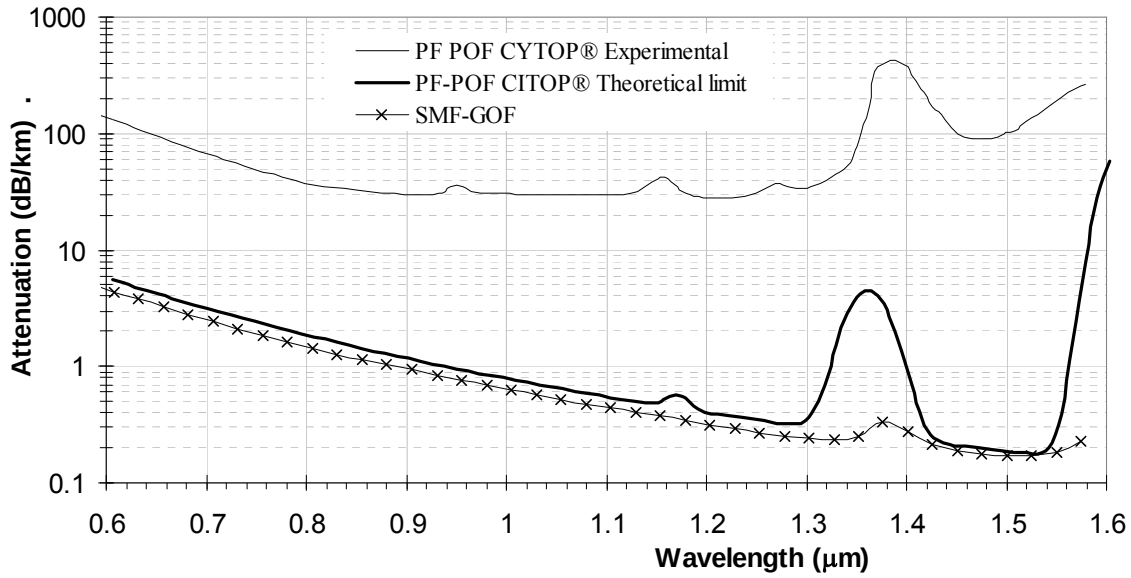

Figure 2.7: Spectral Attenuation curves to the PF-POF and SMF-GOF (adapted from [1], [24], [25])

In addition, research involving PF-POF has concluded that, in high-coupling modal regime, their bandwidths are insensitive to the optical beam launch conditions over a significant core area [26]. These characteristics allow less restricted connection conditions between different types of POF or these and

optical glass fibers, thus being motivating factors in the use of POF in applications of short distance (< 50 m) and high performance in detriment of the graded-index MMF.

The PF-POF shown < 40 dB/km attenuation in the 650-1310 nm range, with interesting near-infrared characteristics (10 dB/km at 1210 nm) [24]. Its experimental and theoretical limit attenuation curves to a *CYTOP*® POF as well as for silica SMF (SMF-GOF) are shown in Figure 2.7. Although currently PF-POF exhibits ~200 dB/km at 1550 nm, the theoretical limit curve shows that there is a wide margin of evolution for the PF-POF.

Researches were carried out [24] involving a graded-index POF (50 μm core) with unidirectional C-band transmission, quadrature phase-shift keying (QPSK) modulation, coherent detection with polarization diversity and FC-PC direct connections between different types of fibers. In this chapter, we analyze the use of patch-cords in PF-POF applied on short distances (~50 m) between SMF terminals in telecommunications equipment located in clusters/data centers, as well as the insertion of these patch-cords in the fast reestablishment on accidentally cut high-speed SMF links. For that, a C-band system with a data rate of 400 Gbps in each direction was implemented, consisting of four bidirectional wavelength channels with orthogonal polarizations and coherent receivers with polarization diversity. We also analyzed the use of free-space optical interfaces between SMF and PF-POF couplings.

2.6.2 Experimental Setup

To analyze the questions proposed above, I implemented a bidirectional system at 1550 nm formed by an optical link in SMF and PF-POF. A 400 Gbps data rate was sent in each transmission direction, using QPSK encoding, dual polarization (DP-QPSK) and Nyquist pulse shaping. The optical signal was detected by a coherent receiver allowing high sensitivity and then subjected to digital signal processing (DSP) in offline mode to recover the signal and estimate the bit error rate (BER) [28].

As shown in Figure 2.8, the implemented system has a Port-1 and a Port-2 located at the ends of the bidirectional optical transmission channel, both composed of a transmitter with DP-QPSK modulation (DP-QPSK-Tx) and a coherent receiver with polarization diversity (PD-CoRx).

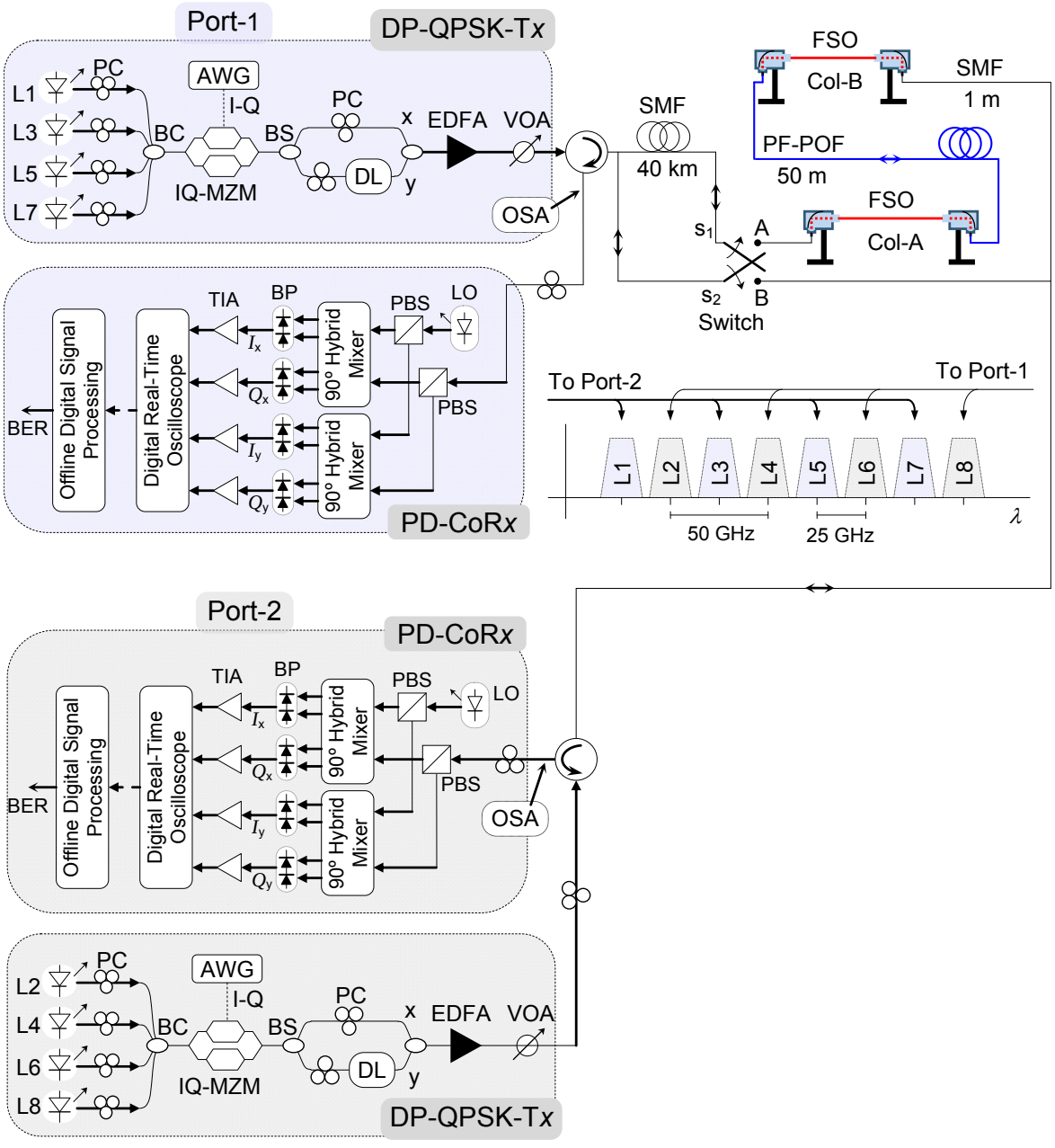

Figure 2.8: Experimental setup. Only one switch (s_1, s_2) at a time will be turned on in each implemented configuration.

The DP-QPSK-Tx in Port-1 consists of two Distributed Feedback lasers (DFB: L1, L3) of < 20 MHz linewidth and two External Cavity Lasers (ECL: L5, L7) of < 100 kHz linewidth. The four lasers are tuned on equally spaced wavelengths of 50 GHz between 1546.96 and 1548.14 nm and later grouped into a 4:1 Beam Combiner (BC) whose output signal feeds a Mach-Zehnder modulator.

An Arbitrary Waveform Generator (AWG: Agilent M8195A) with 65 Gs/s and a 25 GHz analog bandwidth produces a 25 Gbaud electrical signal in QPSK with 2^{11}-1 pseudo random binary sequence (PRBS) and improved Nyquist pulse shaping (roll-off factor 0.05) [29], which drives through the in-phase (I) and quadrature (Q) components the Mach-Zehnder modulator (IQ-MZM). The output modulated optical signal is then divided equally by two branches (BS) and polarized orthogonally by polarization controllers (PC) to emulate a DP system. The data signals are de-correlated (x, y) through a delay line (DL) and coupled in power, thereby forming a DP-QPSK transmission signal at 100 Gbps replicated in four wavelength channels, i.e. 400 Gbps total capacity. The launch power for this DP-QPSK signal was set by the Erbium-Doped Fiber Amplifier (EDFA) and a variable optical attenuator (VOA) before entering the 3-port circulator necessary for the establishment of bi-directionality in the transmission channel. The optical channel consisted of 40 km of SMF and 50 m of graded-index PF-POF (*CYTOP*® 50 μm core).

The difference between the core diameters of the SMF (9 μm) and the PF-POF (50 μm) as well as their numerical apertures (NA) pose optical beam coupling issues when directly connected. In fact, only part of the optical beam emitted by the PF-POF is captured by the smaller core and NA of the SMF, implying ~20 dB attenuation in this interface, measure in the course of the work. On the other hand, ~0.3 dB attenuations are recorded at the interface when the SMF optical beam is injected over the wide PF-POF core.

Due to the high attenuation resulting from the two PF-POF/SMF interfaces along the link, the connections were replaced by two pairs of optical fiber collimators (Thorlabs®), Col-A and Col-B, spaced 20 cm apart in free space as shown in Figure 2.8. In each direction of transmission, a minimum attenuation of

~4.5 dB was obtained for Col-A as for Col-B, conditioned by the available refinements in the collimators.

Therefore, the optical signal sent from Port-1 is routed through the 3-port circulator to the PD-CoRx in Port-2, which has an ECL with < 100 kHz of linewidth operating as local oscillator (LO) tuned to the center channel to be demodulated.

The received signal and the LO signal pass through polarization beam splitters (PBS), obtaining the orthogonally polarized components x, y. Then, the co-polarized components feed two 90º optical hybrid, one for each polarization. The coherently demodulated optical outputs are converted by two pairs of balanced photodiodes (BP) into electrical baseband signals (in-phase (I) and quadrature (Q) components of each polarization), then amplified by transimpedance amplifiers (TIA).

In PD-CoRx, the phases of the LO and the tuned optical carrier are not locked together making the detection of the information received challenging. On the other hand, optical propagation in the fibers produces impairments to the received signal such as polarization mode dispersion and chromatic dispersion. The widely used solution for later retrieval of the data in coherent receivers consists in the digital signal processing (DSP) [30] [31]. Thus, the I and Q signals at the TIA output are sampled by a real-time digital Oscilloscope (Tektronix® DPO72004B) at 50 Gs/s and digitally post-processed in offline mode using appropriate algorithms in Matlab®. This DSP seeks to compensate for the degradation caused along the channel by the chromatic dispersion and polarization-mode dispersion, as well as to recover the frequency and phase of the DP-QPSK signal. For polarization tracking, we use the constant modulus algorithm (CMA) and for frequency and phase the differential phase-based method and the Viterbi & Viterbi algorithm [32], respectively. The BER is calculated by bit error counting, obtained through the mean between the two polarizations.

The DP-QPSK-Tx module in Port-2 consists of four ECL lasers (L2, L4, L6 and L8) with linewidh < 100 kHz, tuned to the wavelengths of 1547.15 - 1548.34 nm and equally spaced from 50 GHz, which transmit to the DP-CoRx in Port-1

through the 3-port circulators. The eight bidirectional optical carriers (four in each direction) spaced consecutively at 25 GHz, then form the spectral structure between the optical circulators, as shown in Figure 2.8. Thus, the unidirectional spectrum at the input of each PD-CoRx has guard bands of 25 GHz, minimizing interference between the adjacent wavelengths received. In addition, the remaining description of the information processing from Port-2 to Port-1 is equivalent to that described in the reverse direction.

2.6.3 Experimental Results

Spectral responses were observed for the transmission media considered in Figures 2.9a, 2.9b and 2.9c. The graphs were obtained through a High Resolution Optical Spectrum Analyzer (OSA: APEX® AP2043B) with resolution of 40 fm (5 MHz). The bidirectional data transmission of 400 Gbps in DP-QPSK was initially established through a direct connection between 3-port circulators in a Back-to-Back (B2B) configuration, with switch s_2 in B in Figure 2.8.

The optical power spectrum then captured at the input of the PD-CoRx at Port-1 is shown in Figure 2.9a, where a separation of 50 GHz and guard spacing of 25 GHz between channels is observed, as well as the simultaneous reception of the two polarizations, Pol-X and Pol-Y, which do not present relevant relative spectral variations.

Subsequently, a 40 km SMF link was introduced between the two optical circulators, shown in Figure 2.8 with switch s_1 in B. The optical power spectra captured separately by the OSA at the inputs of the two PD-CoRx modules are superimposed and shown combined in Figure 2.9b. This figure illustrates bidirectional transmission through the SMF as well as the spectral distribution of the eight optical channels spaced ~25 GHz and attenuated by 8.4 dB when compared to B2B transmission.

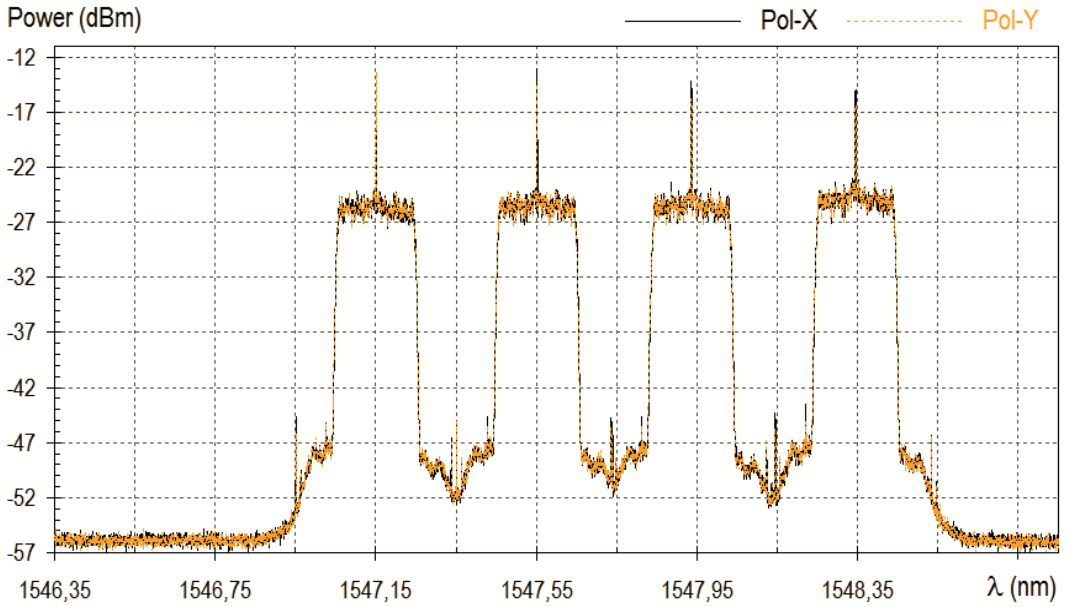

Figure 2.9a: Received spectrum at the input of the PD-CoRx on Port-1 in a B2B configuration and for the polarizations, Pol-X and Pol-Y.

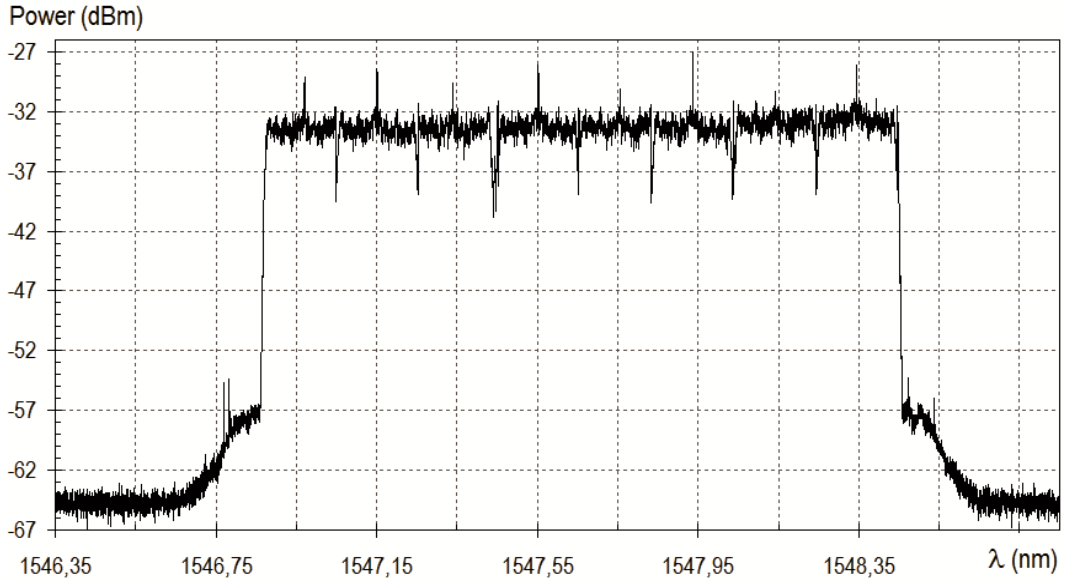

Figure 2.9b: Bidirectional spectrum composed of the overlap of received spectra at the inputs of both PD-CoRx, after transmission through 40 km of SMF and for Pol-X polarization.

Then 50 m of PF-POF was introduced between the Col-A and Col-B collimators which were connected to the optical circulators through 1 m patch cords in SMF, as shown in Figure 2.8 with s_2 in A. An attenuation of 20 dB was measured for the Col-A, Col-B and PF-POF section used. The use of Col-A and Col-B is to adapt the different NA of SMF and PF-POF in order to standardize the behavior of bidirectional transmission. Figure 2.9c shows the power spectrum for the two polarizations at the input of the PD-CoRx in Port-1, with an attenuation of 20 dB when compared to the B2B assembly in Figure 2.9a.

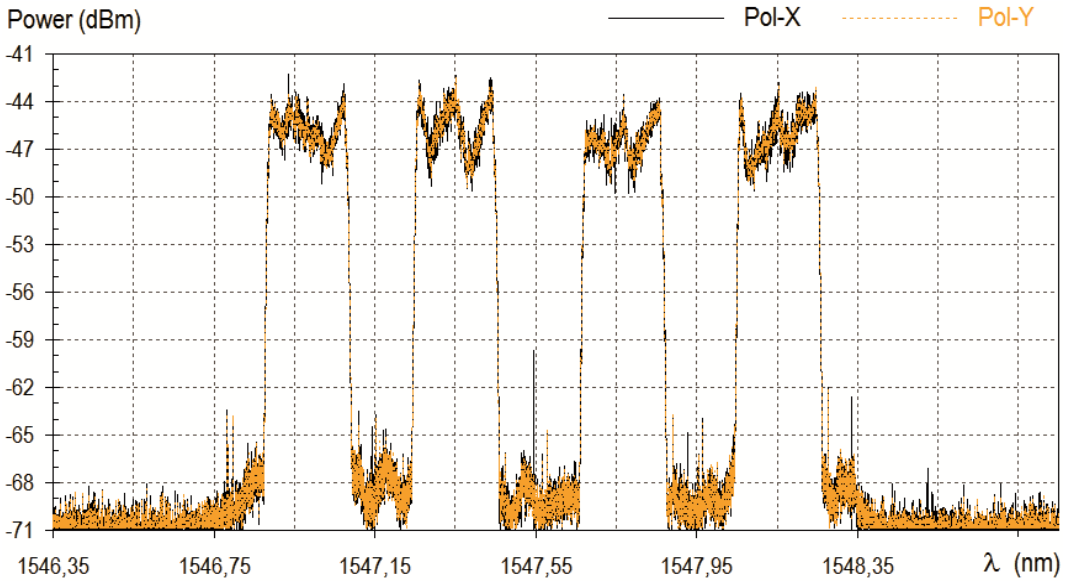

Figure 2.9c: Received spectrum at the input of PD-CoRx of Port-1, after transmission by 50 m of PF-POF and in the Pol-X and Pol-Y polarizations.

It is noted in Figure 2.9c for the transmitted wavelengths that the constituent polymer of the PF-POF used in this experiment introduces irregular distortions in the spectral response as compared to the SMF medium in Figure 2.9b. In addition, there is a minimal relative variation between Pol-X and Pol-Y polarizations in the transmission through the plastic fiber, showing spectra with relatively close envelopes.

In this configuration, for PF-POF with the transmission in the opposite direction, it was verified for the channels received at the PD-CoRx input of Port-2 that the spectral distortion, caused by some reflection, and the attenuation values were in all identical to those found in the forward transmission direction.

System performance was observed through the BER on the channel L5 (1547.75 nm) in the PD-CoRx of Port-1 of Figure 2.8. The BER measurements shown in Figure 2.10 are obtained for the system connections in B2B, 40 km in SMF, 50 m in PF-POF and SMF + PF-POF (for switch s_1 in A). Considering the BER threshold of 3.8×10^{-3} in the absence of applied forward error correction (FEC) codes (7 % hard-decision FEC), the optical power penalty measured in relation to the B2B system was 0.3 dB and 1.5 dB for the optical connections in SMF and PF-POF, respectively.

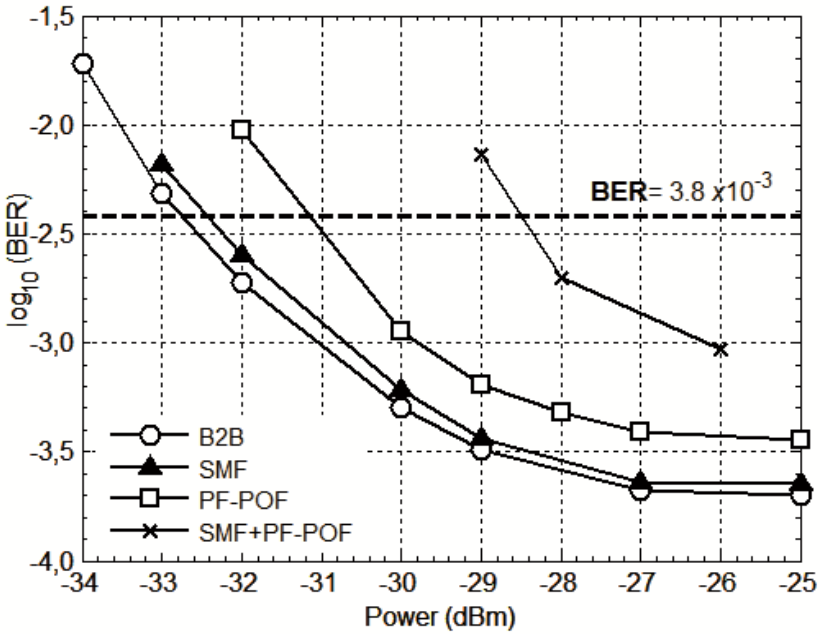

Figure 2.10: BER measurements obtained for the analyzed transmission media.

2.6.4 Conclusions

To the best of our knowledge, we present in this paper the first bidirectional dual-polarization QPSK system with a total capacity of 400 Gbps in each direction. The system transmission viability in optically transparent and diverse media such as silica, polymer and space-free have been demonstrated and implemented. It was found that the option of using fiber collimator pairs to couple the optical beam between the SMF and PF-POF with different fiber cores and NA allowed uniform bidirectional attenuation in the connections and a lower total link attenuation value.

The 50 m length of the PF-POF is higher than the coupling length (Lc) assigned to this type of optical fiber, placing this fiber in a high-coupling modal regime and making its impulse response independent of polarization [22]. In this respect, it was observed that the orthogonal polarizations of the SMF transmission retained their integrity after multimode propagating by the PF-POF.

In addition to the greater attenuation of plastic fibers and the need for an appropriate interface between SMF and PF-POF, the feasibility of using short-length cables in PF-POF was verified when inserted in high-capacity SMF transmission media.

References

[1] Christophe Lethien, Christophe.Loyez, J.P. Vilcot, N. Rolland, Paul Rolland, “Exploit the Bandwidth Capacities of the Perfluorinated Graded Index Polymer Optical Fiber for Multi-Services Distribution”, *Polymers*, vol. 3, no. 3, pp. 1006-1028, September 2011, DOI:10.3390/polym3031006

[2] Olaf Ziemann, Jürgen Krauser, Peter E. Zamzow, Werner Daum, “POF Handbook - Optical Short Range Transmission Systems”, Springer, 2nd Ed., 2008, ISBN: 978-3-540-76629-2

[3] Goran Einarsson, “Principles of Lightwave Communications”, Wiley, 1st Ed., 1996, ISBN: 9780471952978

[4] Gerd Keiser, “Optical Fiber Communications”, McGraw-Hill, 3rd Ed. 1999, ISBN: 9780072321012

[5] Mark G. Kuzyk, “Polymer Fiber Optics - Materials, Physics, and Applications”, CRC Press, 1st Ed., 2007, ISBN: 9781574447064

[6] “The Market for Plastic Optical Fiber in Data Communications: A Market and Technology Assessment”, IGI Consulting, 1996

[7] Joseba Zubia, Jon Arrue, “Plastic Optical Fibers: An Introduction to Their Technological Processes and Applications”, *Optical Fiber Technology*, Vol. 7, Issue 2, April 2001, pp. 101-140, DOI: 10.1006/ofte.2000.0355

[8] Paul Polishuk, “Plastic Optical Fiber Branch Out”, *IEEE Communications Magazine*, vol. 44, no. 9, pp. 140-148, September 2006, DOI: 10.1109/MCOM.2006.1705991

[9] Werner Daum, Jürgen Krauser, Peter E. Zamzow, Olaf Ziemann, "POF - Polymer Optical Fibers for Data Communication", Springer, Berlin - Heidelberg, 2002, ISBN: 978-3-662-04863-4, DOI: 10.1007/978-3-662-04861-0.

[10] Koike, Y.; Ishigure, T., “High-Bandwidth Plastic Optical Fiber for Fiber to the Display”, *Journal of Lightwave Technology*, vol. 24, no. 12, pp. 4541-4553, Dec. 2006, DOI: 10.1109/JLT.2006.885775

[11] Lennie Lightwave's New Guide to Fiber Optics, *VDV Works*, [Online]. http://www.jimhayes.com/lennielw/fiber.html

[12] Olaf Ziemann et al, "Home Networks - they have to work standard compliant, very fast and reliable", Institute of the University of Applied Sciences Nuernberg – POF Application Center, May, 2010.

[13] L. C. Nadales, “Tomlinson Harashima Precoding for Multi-Gigabit short-haul Transmission over Plastical Optical Fibers”, Universität Stuttgart, September 7, 2010.

[14] Jürgen Krapp, “Dependencies of bandwidth of polymer optical fiber for MOST systems”, *MOST Forum 2010: International MOST Conference & Exhibition*, Frankfurt, March 23, 2010.

[15] D. Visani, A.M.J. Koonen et al, “Towards Converged Broadband Wired and Wireless In-home Optical Networks”, *15th International Conference on Optical Network Design and Modeling - ONDM*, Bologna, pp. 1-6, Feb. 8-10, 2011, ISBN: 978-1-4244-9596-2

[16] D.Visani, A. M. Koonen, H. Yang et al “Record 5.3 Gbit/s Transmission over 50m 1mm Core Diameter Graded-Index Plastic Optical Fiber”, *2010 Conference on Optical Fiber Communication (OFC/NFOEC), collocated National Fiber Optic Engineers Conference*, San Diego - CA, 21-25 March 2010, pp. 1-3, DOI: 10.1364/NFOEC.2010.PDPA3

[17] H. Yang, A. M. Koonen et al., “4.7 Gbit/s Transmission over 50m Long 1mm Diameter Multi−core Plastic Optical Fiber”, *2010 Conference on Optical Fiber Communication (OFC/NFOEC), collocated National Fiber Optic Engineers Conference*, San Diego - CA, 21−25 March 2010, paper OWA4, DOI: 10.1364/OFC.2010.OWA4

[18] Olaf Ziemann, Jurgen Krauser et al. “POF handbook: optical short range transmission systems”, *Springer Verlag*, page 193, 2008, ISBN 978-3-540-76629-2

[19] R. J. Gandhi, A. Polley and S. E. Ralph, "40 Gbps Short Reach Links Using Plastic Optical Fiber," *LEOS 2006 - 19th Annual Meeting of the IEEE Lasers and Electro-Optics Society*, Montreal, Quebec, 2006, pp. 637-638, DOI: 10.1109/LEOS.2006.278857

[20] A. F. Garito, J. Wang, R. Gao, “Effects of Random Perturbations in Plastic Optical Fibers”. *Science*, vol. 281, no. 5379, pp. 962-967, 1998, DOI: 10.1126/science.281.5379.962

[21] Joseph M Kahn, Keang-Po Ho, Mahdieh Bagher Shemirani. Mode Coupling Effects in Multi-Mode Fibers. *Opt Fiber Commun Conference, OSA Technical Digest.* Optical Society of America, 2012: OW3D.3. DOI: 10.1364/OFC.2012.OW3D.3

[22] Mahdieh B. Shemirani, Wei Mao, Rahul Alex Panicker, Joseph M. Kahn, “Principal Modes in Graded-Index Multimode Fiber in Presence of Spatial and Polarization-Mode Coupling”, *Journal of Lightwave Technology*, Vol. 27, no. 10, pp. 1248-1261, 2009, DOI: 10.1109/JLT.2008.2005066

[23] Keang-Po Ho, Joseph M. Kahn, “Statistics of Group Delays in Multimode Fiber with Strong Mode Coupling”, *Journal Lightwave Technology*, vol. 29, no. 21, pp. 3119-3128, Nov.1, 2011, DOI: 10.1109/JLT.2011.2165316

[24] I. Tafur Monroy, H.P.A. vd Boom, A.M.J. Koonen, G.D. Khoe, Y. Watanabe, Y. Koike, T. Ishigure. “Data transmission over polymer optical fibers”, *Optical Fiber Technol*ogy, Vol. 9, Issue 3, July 2003, pp 159-171. DOI: 10.1016/S1068-5200(03)00006-3

[25] H.P.A. van den Boom, W. Li, P.K. van Bennekom, I.T. Monroy, G.–D. Khoe, “High-capacity transmission over polymer optical fiber”, *IEEE Journal of Selected Topics in Quantum Electronics*, vol. 7, no. 3, pp. 461-470, May-June 2001, DOI: 10.1109/2944.962269

[26] G. Giaretta, W. White, M. Wegmuller, T. Onishi, “High-speed (11 Gbit/s) data transmission using perfluorinated graded-index polymer optical fibers for short interconnects (<100 m)”, *IEEE - Photonics Technology Letters*, vol. 12, no. 3, pp. 347-349, March 2000, DOI: 10.1109/68.826936

[27] Yin Shao, Rui Cao, Yue-Kai Huang, P.N. Ji, Shaoliang Zhang, “112-Gb/s transmission over 100m of graded-index plastic optical fiber for optical data center applications”, *Optical Fiber Communication and the National Fiber Optic Engineers*

Conference (OFC/NFOEC), Los Angeles, CA, 2012, pp. 1-3,
DOI: 10.1364/OFC.2012.OW3J.5

[28] Joe Berthold, *et al*, "100G Ultra Long Haul DWDM Framework Document", *Optical Internetworking Forum (OIF)*, June 2009, [Online].
https://www.oiforum.com/documents/white-papers/technical-white-papers/

[29] N.C. Beaulieu, C.C. Tan, M.O. Damen, "A "better than" Nyquist pulse", *IEEE Communication Letters*, vol. 5, no. 9, pp. 367-368, Sept. 2001,
DOI: 10.1109/4234.951379

[30] Umashanker Sahu, B.C. Jinaga, A. Venkataramana, "Digital Signal Processing Techniques for LTI Fiber Impairment Compensation", *International Journal of Research in Engineering and Technology*, vol. 2, no. 10, pp. 168-172, October 2013, DOI: 10.15623/ijret.2013.0210024

[31] Ezra Ip, J M Kahn, "Digital Equalization of Chromatic Dispersion and Polarization Mode Dispersion", *Journal of Lightwave Technology*, vol. 25, no. 8, pp. 2033-2043, Aug. 2007, DOI: 10.1109/JLT.2007.900889

[32] Ricardo M. Ferreira, Ali Shahpari, Jacklyn D. Reis, António L. Teixeira, "Coherent UDWDM-PON With Dual-Polarization Transceivers in Real-Time", *IEEE Photonics Technology Letters*, vol. 29, no. 11, pp. 909-912, June 1, 2017,
DOI: 10.1109/LPT.2017.2693419

Chapter 3

Free-Space Optical Communication Systems

Free-space optical (FSO) communications have been attracting significant attention as a broadband access technology, which is capable of presenting high-speed as well as enhanced capacity, allowing a variety of information transmission techniques. In addition, optical wireless communication (OWC) is an attractive technology in very sensitive environments where is not allowed radio frequency (RF) technology. In addition, OWC can be assumed as a technology that enhances "green" communications as the required components use low power consumption compared to equivalent RF components [B2]. Therefore, it has been taken into consideration as an alternative method to the existing RF solutions.

In this chapter, based on manuscripts [J3, B1, B2], a broad and general overview of the FSO systems is considered. Additionally, besides to the radio transmission technology on FSO (RoFSO), transmission schemes with enhancement performance such as hybrid RF/FSO and relay-assisted transmission technologies, which can be implemented in the access networks, are also presented.

3.1 Introduction

It is noticeable that Internet communications undergo extraordinary development in all areas of human activity, through their use in the most varied types of applications, which consume bandwidth on an exceptionally increasing scale. One of the factors of this growth can be attributed to the increasing appearance of new characteristics based on Internet access, in the varied devices that surround us in the day-to-day. This network access feature is commonly referred to as "Internet of Things" (IoT), and the number of potential devices is expected to be enormous. In theory, the IoT concept would be ubiquitous in different types of devices/objects, such as actuators, mobile phones, household appliances, vehicles, sensors or RF identification (RFID) tags [J4]. These objects would be able to cooperate with each other, regardless of distance, in order to perform common tasks [1]. It is expected that by the year 2020, billions of these devices will be connected to the Internet [2]. Fifth generation (5G) wireless communication systems, which will integrate millimeter wave antennas and "Massive" multiple-input and multiple-output (MIMO) technology, present promising features in terms of the ability to support internet traffic on the devices. However, the existing regulated RF spectrum restricts the transmission speeds of wireless RF-based mobile technologies. This is due to several state-of-the-art wireless technologies and standards such as Wi-Fi (IEEE 802.11), WiMAX (802.16) as well as third-generation (3G) and fourth generation (4G) cellular systems [3, 4]. In addition, because of innumerable innovative technologies being used in optical communication systems, considerable advances have been obtained in the optical network reach, capacity and number of users supported. For example, optical-fiber-based architectures such as FTTH and FTTB (fiber-to-the-building) provide profitable solutions to the communication hurdles, making services increasingly close to customers through PON technologies such as Ethernet Passive Optical Network (EPON), GPON, and XG-PON. At present, one of the main challenges is the ability to support many service requirements in order to accomplish elastic as well as ubiquitous connections [5]. Therefore, wireless and optical networks convergence is very important for network

penetration with a cost-effective in the next-generation networks (NGNs). This will help in taking advantage of the mobility feature presented by the wireless network and the inherent bandwidth offered by the optical systems. Therefore, this will help in realizing the expected energy-efficiency and capacity objectives of the NGNs [3]. In addition, OWC systems are one of the promising access technologies with capability for offering high-speed in addition to improved capacity. Accordingly, OWC can address the bandwidth requirements of numerous services and applications of the NGNs in cost-effective manners [3, 7].

OWC can serve as an alternative and/or complementary technology to existing wireless RF solutions. For example, the OWC to be transmitted in the 350 to 1550 nm wavelength range can offer a high-data-rate of about 100 Gbit/s. This benefit makes it a good solution for tackling the usual “last mile” and “last-leg” problems of the access network. Additionally, resources re-use is an essential requirement when operators seek to improve network capacity and coverage. OWC technologies are capable to meet requirements using diversity schemes [6, 7, 8]. OWC can use the following configurations:

1. Directed line-of-sight (LOS)
2. Multi-spot LOS
3. Non-directed LOS
4. Diffuse
5. Quasi diffuse

In these arrangements, the performance of LOS links presents the lowest bit error rates (BER), higher data rates and less complicated protocols. These qualities make LOS links the most widely used configuration in outdoor applications. However, the main LOS links shortcomings are the lack of mobility and vulnerability to blockage. On the other hand, non-directed or diffuse LOS configurations offer enhanced mobility benefits and are less vulnerable to shading. However, the path attenuation, noise, and multi-path induced dispersion prevent the data rate from being comparatively high at high-speed connections. Intensity modulation and direct detection (IM/DD) is the widely method employed

in OWC systems. In addition, coherent scheme can be used to improve the channel usage. The application of coherent scheme comparatively enhances the system performance at the cost of increased system complexity. On the other hand, the coherent scheme can be used to improve channel usage, comparatively improving system performance at the expense of greater complexity. This is due to the need for accurate wavefront matching between the input signal and the local oscillator (LO) that is required to ensure effective coherent reception. In turn, the DD technique is simple as only low-cost transceiver devices are required without the need for the complex high-frequency circuit designs as compared with coherent systems [7, 8].

This chapter presents a comprehensive overview of the OWC systems as well RoFSO transmission schemes. Furthermore, we analyze the effects of different parameters such as wavelength and refractive index on RoFSO transmissions under different operating conditions.

In section 3.2, the OWC system block diagram is discussed. Section 3.3 focuses on the safety and regulations of optical beam transmissions as well as related international standardization organizations. In section 3.4, the OWC system categorizations are broadly discussed. Moreover, in section 3.5, RoFSO is considered and section 3.6 presents technologies for enhancing the system performance. Research contributions are discussed in section 3.7 and conclusions are given in section 3.8.

3.2 OWC System Blocks Diagram

Normally, a terrestrial OWC system comprises the transmitter, channel, and receiver, as illustrated by the block diagram of Figure 3.1. The transmitter source generates waveform information by modulating an optical carrier and the resulting optical field is then radiated through the atmospheric channel to the destination. The collected optical field at the receiver is afterward converted into an electrical current that is then processed in order to retrieve the information originally transmitted [9]. Nevertheless, due to expected degradations in the

transmission channel, there is a tendency for the incoming information will not be a replica of the information actually transmitted. Defective transmission may greatly limit the performance of wireless communication systems [B1].

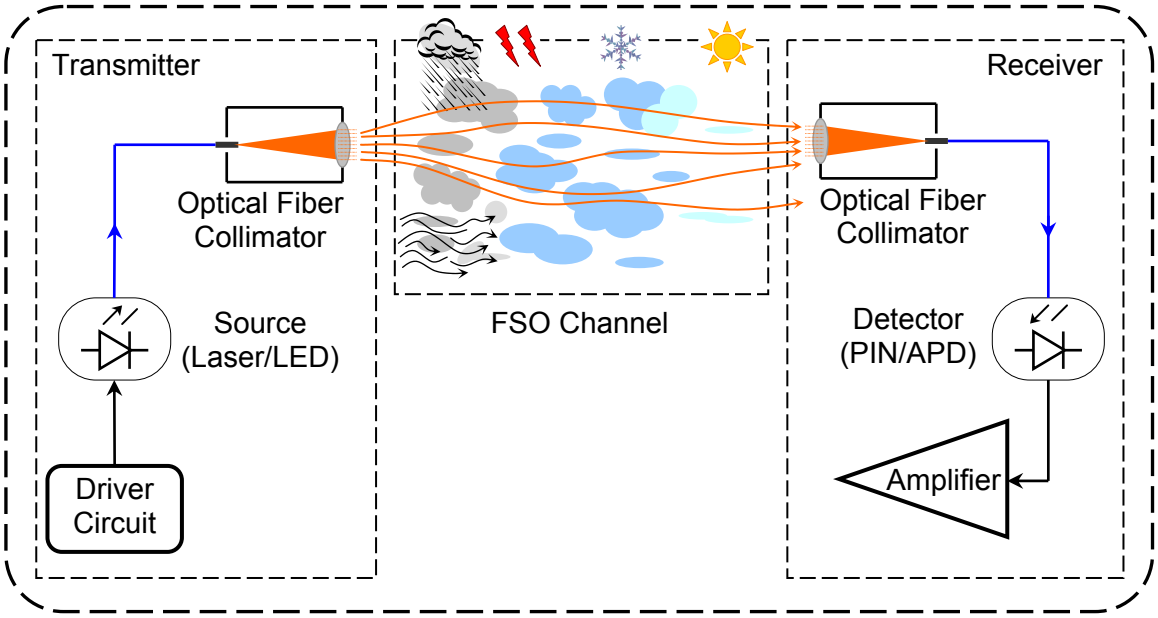

Figure 3.1: Block diagram of a terrestrial OWC system.

It is remarkable that the loss in transmission is mostly a consequence of the resulting absorption and scattering effects, which are presented by the aerosols and molecular constituents along the transmission path. Consequently, wavelength dependence by absorption and scattering are the main causes of atmospheric attenuation. Since absorption is not just a function of wavelength, but also of specific wavelengths, it is possible to identify wavelength windows that undergo relatively insignificant absorption.

At large, wavelength ranging from 780 to 850 nm and 1520 to 1600 nm, which are usually employed in existing OWC equipment, are located in atmospheric transmission windows where molecular absorption is insignificant. In fact, this contributes to the alleviation of atmospheric absorption losses. Moreover, windows located around four exact wavelengths such as 850 nm, 1060 nm, 1250 nm and 1550 nm usually suffer an attenuation of less than 0.2 dB/km. It should be noted that 850 nm and 1550 nm transmission windows correspond to

the typical transmission windows of fiber optic systems. Based on this, most commercial OWC systems work on one of these windows to support the existing off-the-shelf components. Moreover, wavelengths such as 10 μm and ultraviolet (UV) have been studied for the OWC systems. The 10 μm wavelength has a better fog transmission characteristic, however, the UV wavelength is more robust against transmission constraints such as beam blocking and pointing errors. Besides, the UV wavelength is less vulnerable to sunlight as well as other background interferences [9].

In addition, wavelengths from 1520 nm to 1600 nm are compatible with EDFA technology. This is very important to achieve high-data rate and high-power systems. Likewise, wavelengths from 1520 to 1600 nm allow the transmission of about 50 to 65 times more average output power than that transmitted from 780 to 850 nm, given the sighted safety rating. This can be ascribed mainly to the low transmission of the human eye at those wavelengths [10].

3.3 Safety and Regulations

It is noteworthy that an important factor in the design of a laser transmitter is the safety issue. If infrared (IR) light sources are operated incorrectly, they may become potential threats to human safety. Moreover, exposure to some optical wavelengths can injure the human eye and skin. It should be noted that possible damage to the eyes is relatively more dangerous because of their ability to focus and concentrate optical energy. However, some wavelengths can be absorbed by the front part of the eye before they can be focused on the retina, making handling safer. It should be noted that a laser considered “eye-safe” is also considered “skin-safe” [7, 10].

In addition, it has been established that the absorption coefficient of the eye front part is significantly higher at longer wavelengths (> 1400 nm). Therefore, the typical power allowed for lasers transmitting at 1550 nm is comparatively higher. Consequently, these larger wavelengths are commonly used to obtain a longer transmission range [7, 10].

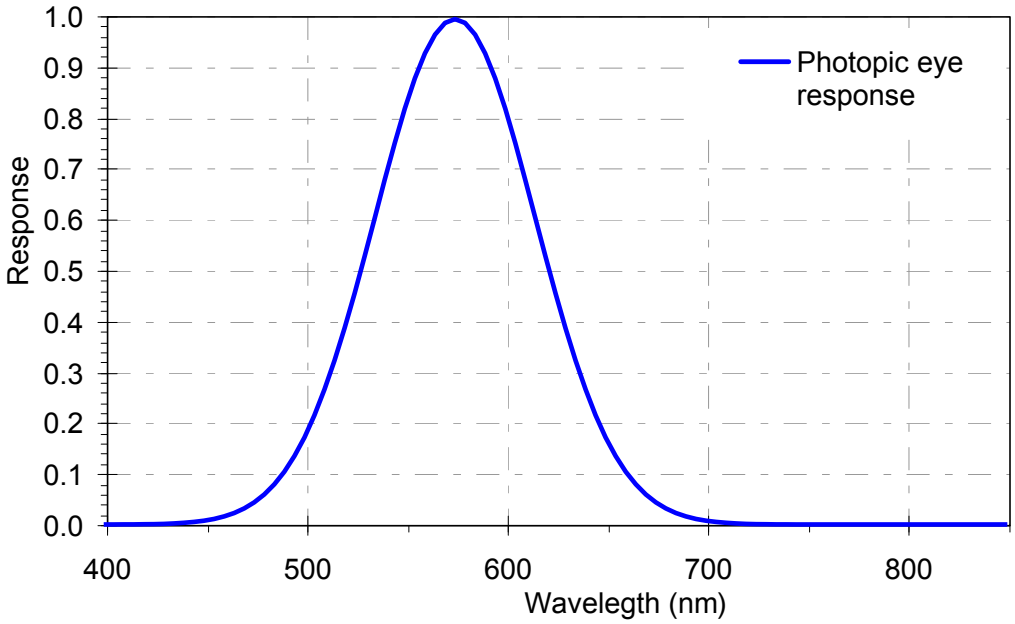

Figure 3.2: Response of the human eye at different wavelengths (adapted from [7, 10]).

The eye response at different wavelengths is shown in Figure 3.2. It is known that the cost of optical sources and detectors is comparatively low in the spectral range of 700 to 1000 nm, however, the eyes safety regulations in this range are generally stringent. Also, the maximum permissible exposure (MPE) at the 900 nm wavelength is ~143 mW/sr. Ocular safety standards are found to be relatively less severe at higher wavelengths (≥ 1500 nm), nevertheless, devices operating at these wavelengths are relatively expensive. In addition, optical beam safety recommendations have been established by various international standards organizations, such as [7, 10]

1. American National Standards Institute (ANSI)
2. Laser Institute of America (LIA)
3. International Electrotechnical Commission (IEC)
4. Center for Devices and Radiological Health (CDRH)
5. European Committee for Electrotechnical Standardization (CENELEC)

The aforementioned groups provided the mechanisms for classifying the lasers according to their type and power. Normally, categorization is established in four classes, ranging from Class 1, with the lowest restrictions, to Class 4, with the highest restrictions on use, in terms of safety. Moreover, each of the classes is identified by the accessible emission limits (AEL) metric. The AEL is regulated by the intensity and wavelength of the optical source as well as by the emitter geometry [7, 10]. Therefore, the AEL differs from one OWC class to another. In the following section, the main OWC classifications are presented.

3.4 OWC System Classification

OWC systems have been increasingly gaining research interest as a feasible method to effectively meet the NGNs requirements. The two general categories of these systems are indoor and outdoor OWCs. The unlimited OWC bandwidth can be ascribed to the use of several bands for communication purposes such as visible (VL), infrared (IR) and ultraviolet (UV) bands. Figure 3.3 illustrates the electromagnetic spectrum for different applications, as well as the relative positions of the wavelength and frequency ranges that have been employed in OWC applications. VL or IR emission is applied to an in-building wireless solution.

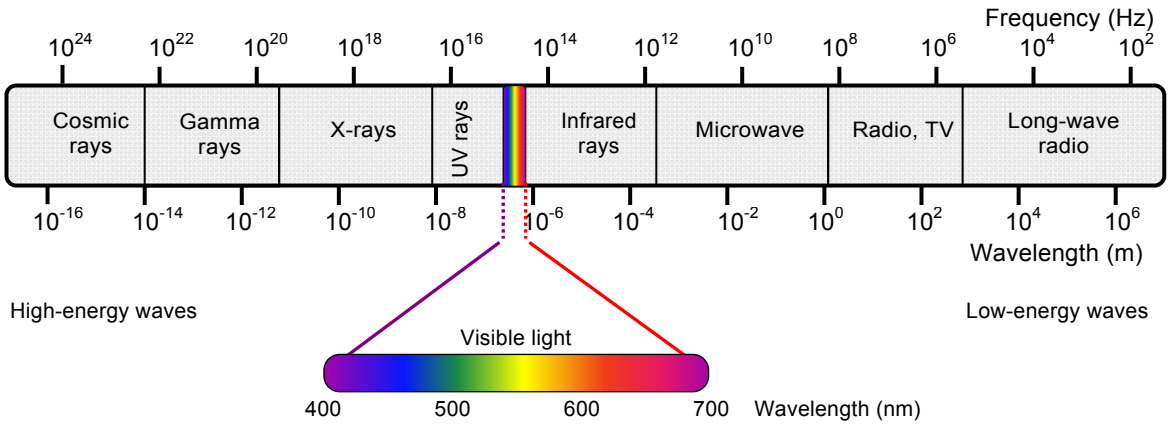

Figure 3.3: Electromagnetic spectrum

This application is very useful especially in situations where the possibility of providing network connectivity through wire connections is a challenge. In addition, the indoor OWC systems can generally be grouped into four arrangements, such as Directed LOS, Diffused, Non-directed LOS, and Tracked. Moreover, optical carriers are used in the outdoor OWC for conveying information through an unguided channel, which may be in free-space (Out-of-Earth) or in the atmosphere.

Consequently, this external OWC scheme is also known as the FSO communications system, which generally operates at near-IR frequencies. They are categorized into space and terrestrial optical links, whose applications include building-to-building, ground-to-satellite, satellite-to-ground, satellite-to-airborne, and satellite-to-satellite platforms [11]. Figure 3.4 illustrates the classification of OWC systems in a tree diagram.

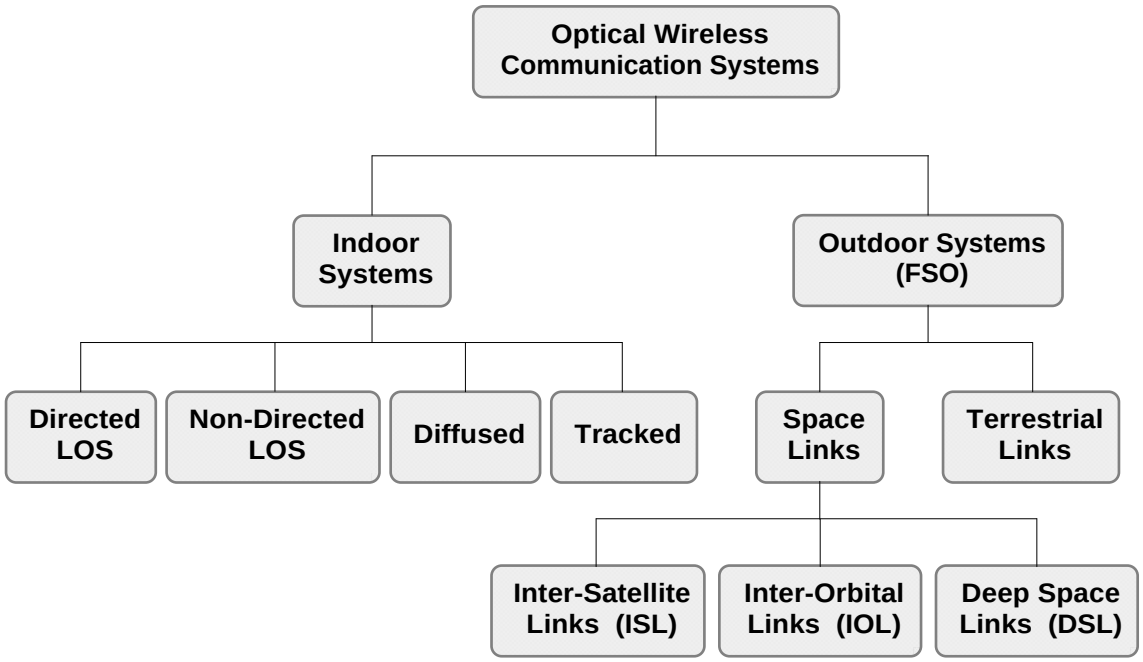

Figure 3.4: Optical wireless communication system classification (adapted from [11]).

3.4.1 Visible Light Communication (VLC) Systems

Visible light communication (VLC) systems have been gaining considerable attention due to the existing improvement in the light-emitting diode (LED) chip design. The chips are capable of offering fast switching times of the order of nanoseconds. Besides, the wide deployment of LEDs in energy-efficient applications paves the way for VLC systems [12, 13]. Therefore, VLC systems are an appealing solution to meet different challenges such as bandwidth limitation, energy efficiency, electromagnetic radiation, as well as safety in wireless communications [14, 15]. It is noteworthy that VLC systems work in the wavelength range of ~ 390 to 750 nm. Furthermore, due to the simultaneous support for lighting and communication in VLC, it presents the following benefits compared with RF communications:

Low Power Consumption

The VLC offers both lighting and communication and is able to provide Gbit/s data rates with simple LEDs and photodiodes (PDs) that consume low power relative to expensive RF options that require high power consumption for processing and sampling when transmitting data in Gbit/s [13].

Huge Bandwidth

VLC shows virtually boundless and unlicensed bandwidth ranging from 380 to 780 nm. Hence, VLC has 350 THz capacity, which can serve multi-gigabit-per-second data rates using LED arrays with the aids of the MIMO configuration [13]. This advantage makes VLC a good option to the indoor IR transmission, which uses the range between 780 to 950 nm [8].

No Health Concerns

The VLC system presents no human health concerns, as it does not produce radiation that leads to public health problems. Moreover, it helps to reduce carbon dioxide emissions due to the low increase in power required for

communication [16].

Low Cost

The associated optical components such as PD and LEDs are compact, cheap, lightweight, and have extended lifespan [12]. Additionally, with much lower power-per-bit cost and large unlicensed optical spectrum, the VLC is economical compared with the RF communications.

Inherent Security

VLC gives relatively better security owing to the fact that it is extremely difficult for a network intruder to pick up the optical signal in order to launch any form of attack on the system [13].

Ubiquitous Computing

Owing to a series of incandescent devices, such as TVs, commercial displays, traffic lights, indoor/outdoor lamps, car headlights/taillights, which are used in various places, the VLC can be exploited for an extensive range of network connectivity [17].

3.4.2 Terrestrial Free-Space Optical (FSO) Communications

It is noteworthy that there have been additional research efforts regarding terrestrial transmission in FSO owing to a number of positive field trials and commercial implementations [18-22]. A representative setup for exploiting FSO systems as an effective solution for universal provisioning of wireless service is illustrated in Figure 3.5. Considerations received by the FSO schemes are mainly the result of their characteristic benefits like lower power consumption, cost-effectiveness, higher capacity, ease of deployment, low mass equipment, immunity to electromagnetic interference (EMI), reduced time-to-market, license-

free operation, high degree of security against eavesdropping, in addition to an improved protection against interferences, relative to the conventional RF communication systems [23, 24].

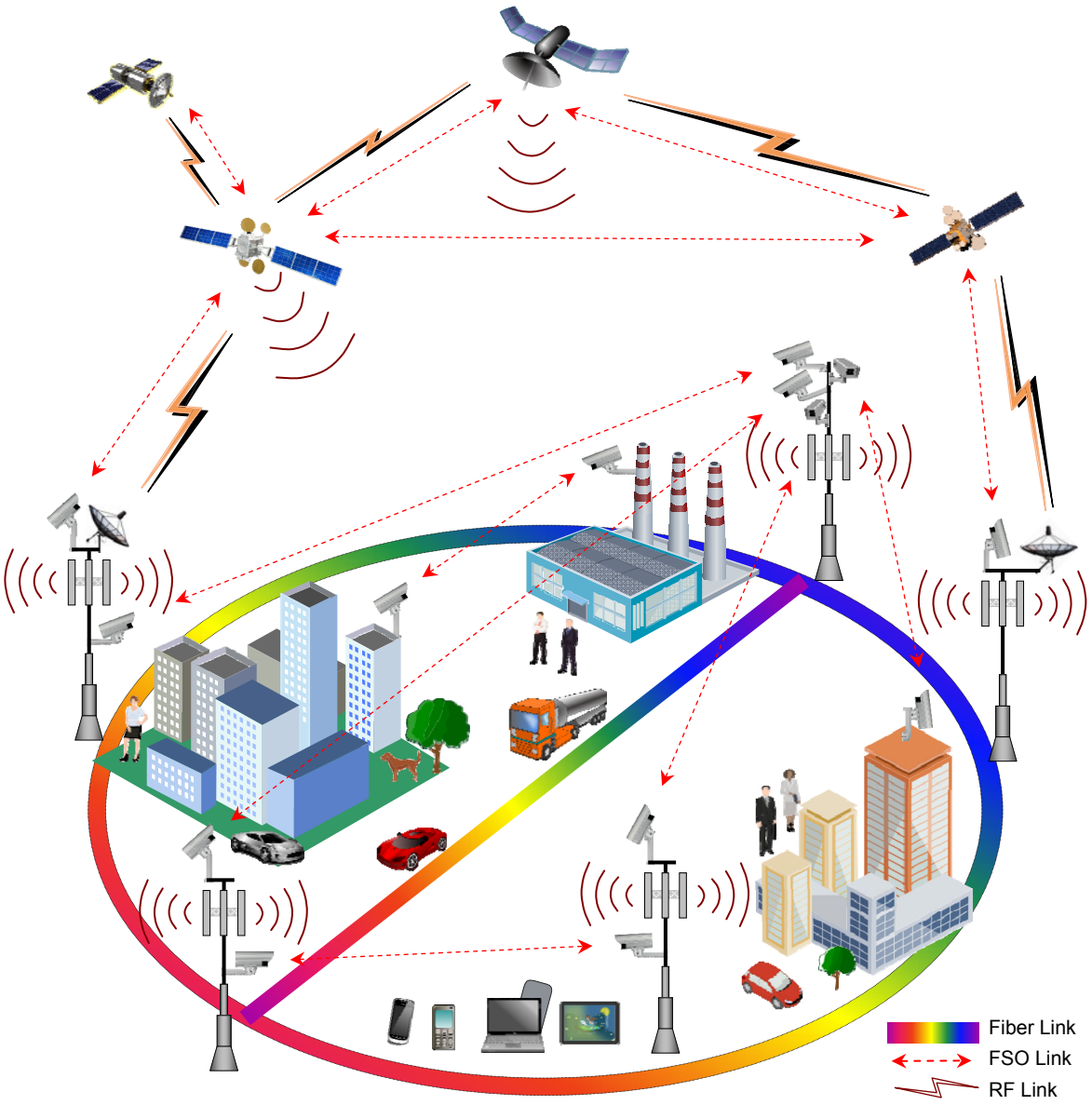

Figure 3.5: Scenarios for deploying OWC systems in access networks.

However, apart from the benefits of the FSO system and its diverse applications, a number of challenges in practical situations hamper its

employment. For example, FSO links are prone to scattering, resulting from adverse weather conditions such as rain, snow, and fog [9, 24]. Moreover, building-sway is another effect that impairs the FSO link performance, which originates from factors like wind loads, thermal expansion, and weak earthquakes [24]. Additionally, the key cause of the FSO link impairment is the fading induced by atmospheric turbulence [24, 25]. Therefore, system performance is hindered owing to atmospheric effects, that bring about beam spreading, loss of spatial coherence, and temporal irradiance fluctuation well-known as scintillation or else fading [J3, 9]. Scintillation is established as the spatial and temporal variation in the light intensity along the transmission path. This is due to the random variations in the refractive index due to the lack of homogeneity of temperature and air pressure [9, 23]. Based on this, the random nature of the link requires significant planning when an FSO system is being modeled. So, this will aid in addressing the severe requirements of several bandwidth-intensive mobile applications [3]. Section 5.2 discusses the FSO link impairment modeling. The tree diagram in Figure 3.6 shows several methods of atmospheric turbulence alleviation.

3.5 Radio on Free-Space Optics (RoFSO)

The radio over fiber (RoF) is a scheme in which light is modulated by the RF signal and transmitted over the optical fiber links. RoF has been used as a high-capacity and cost-effective solution so as to simplify the system design. However, its employment considerably depends on the accessibility of fiber cable infrastructure. Therefore, in a scenario without fiber cable installations, FSO links can be suitably used for RF signal transmissions. It should be noted that FSO system is similar to RoF scheme however, it demands no fiber medium like RoF. Consequently, the notion of transmitting RF signals through FSO systems is known as radio on FSO (RoFSO). RoFSO systems integrate the ease of deployment of the wireless links and the high-transmission capacity presented by optical technologies. The RoFSO schemes are normally employed for last-mile

access solutions in terrestrial communication systems. This application aids in broadening connectivity to the poorly served areas. Besides, it can be employed as a backup connection for both fiber and RF links as examined in chapter 3.6. Nonetheless, the RoFSO link performance can be constrained by factors like fog, rain, atmospheric turbulence, and non-ideal features of optical transmitters and receivers [3, 4, 26, 27].

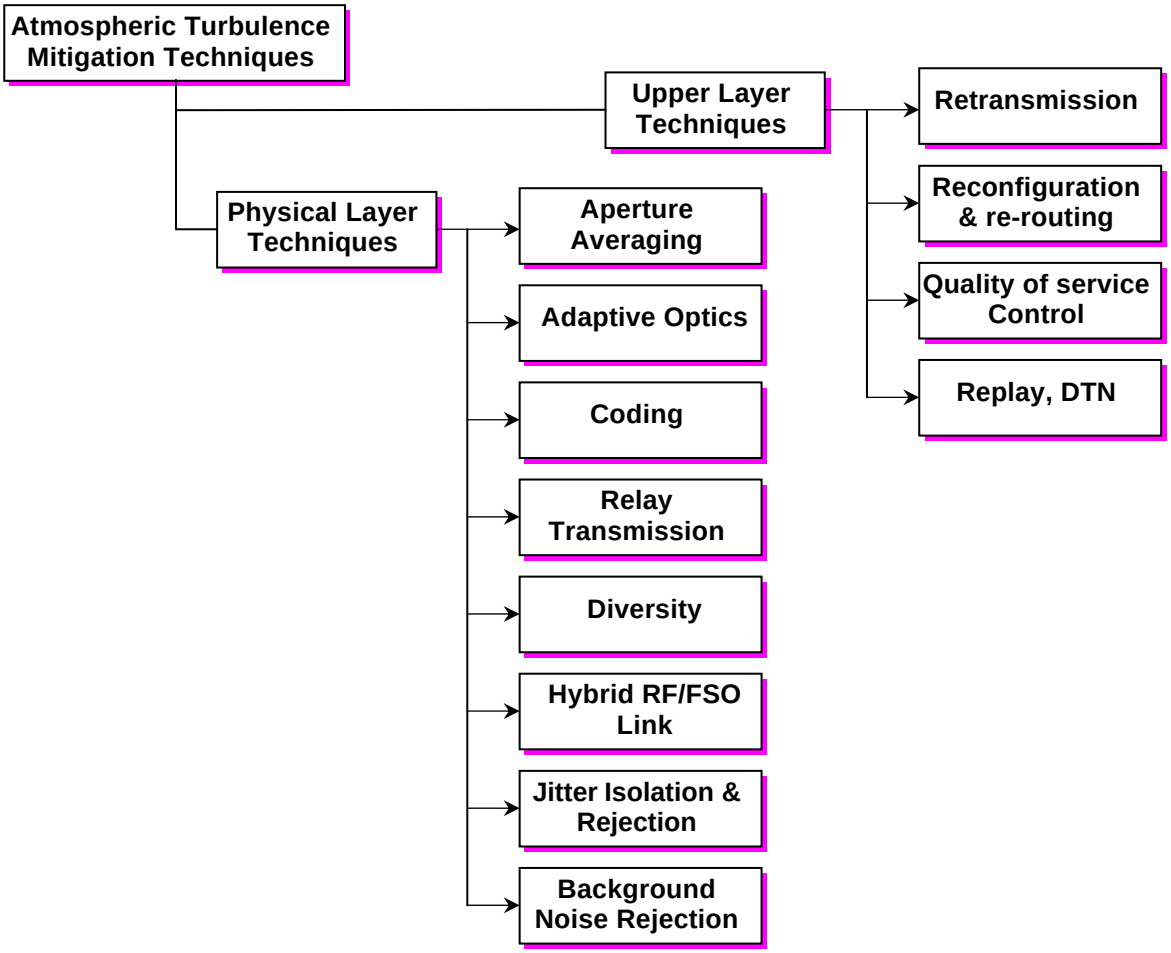

Figure 3.6: Atmospheric turbulence mitigation techniques (adapted from [11]).

Orthogonal frequency-division multiplexing (OFDM) has been implemented in several high-speed digital communication standards because of its outstanding benefits like robustness against fading, narrow-band interference, as well as high channel efficiency. Normally, the OFDM signal is bipolar and complex. On the

other hand, OFDM transmission using intensity modulated direct detection (IM/DD) wireless optical communication scheme demands a real and positive RF signal for driving the laser diode (LD). Therefore, Hermitian symmetry can be applied on the input vector to the transmitter inverse fast Fourier transform (IFFT) block in order to produce the real OFDM signal. In addition, OFDM signal can be converted into unipolar by applying a direct current (DC) bias to the OFDM signal (DC-OFDM). This procedure helps in guaranteeing that the consequent signal is positive. To prevent distortion and clipping in optical domain, the DC bias has to be suitably large. Normally, IM/DD multiple-subcarrier modulation (MSM) schemes have fundamental drawbacks like average optical power inefficiency that is a result of the large added DC bias as well as distortions that are owing to the LD and optical channel nonlinearity [27].

3.6 Technologies for Performance Enhancement

C-RAN (Cloud-Radio Access Network) architecture has been proposed as a promising paradigm for the next generation access network. C-RAN architecture is capable of managing the NGNs and the related evolving complexity efficiently. This can be associated with various related advantages of C-RAN such as cost-effectiveness and performance optimization [28, 29]. The foremost method for signal transmission in the C-RAN fronthaul is by digital baseband oversampled IQ streams. The IQ streams transmission can be easily achieved with the help of CPRI or OBSAI interface [30]. Nevertheless, optical links that employ these interfaces demand enormous bandwidth, which is owing to the high-resolution bits demanded by the digitalization process [31]. Therefore, the associated bandwidth inadequacy can restrain or make C-RANs unrealistic for the next generation mobile system [32, 33]. As a result, to achieve a bandwidth-efficient mobile fronthaul, the employment of innovative measures is highly essential. An example of a viable measure is the implementation of analog optical

transmission scheme that is based on RoF technology [26, 30, 33].

It is worth mentioning that RoF technology deployment depends largely on the availability of optical fiber cables installed in the network. Nevertheless, when deploying network installations is considered dense, dark fiber deployment is not only time- consuming but also cost-intensive. As result of these issues, as well as the limited amount of fiber cables installed in the network, the viability of the FSO communication system has been increasingly recognized. Like in RoF, RF signal transmission can be implemented in FSO. The major advantage of this is that the installation of fiber cables is not mandatory. The idea of RF signal transmission through the FSO medium (i.e. RoFSO) takes advantage of the ease of deployment of wireless systems as well as high transmission capacity present by optical technologies [34].

As aforementioned, FSO transmission is an attractive and viable optical technique that can be implemented for a number of emerging applications. Nevertheless, the trade-off between the constraints of the atmospheric channel and the required data rates are the main issues for reliable application of FSO schemes in the access networks [J3, C1]. Consequently, these challenges prevent FSO technology from being an efficient as well as dependable standalone fronthaul scheme. This section presents FSO performance enhancement schemes, such as hybrid RF FSO, and relay-assisted transmission technologies that can be implemented in the access networks.

3.6.1 Hybrid RF/FSO Technology

It is interesting to note that RF wireless systems, operating at frequencies greater than approximately 10 GHz, are harmfully influenced by rainfall; however, the fog has a negligible effect on them. Conversely, FSO systems are extremely prone to fog, while the rain has an insignificant effect on them. Thus, it is essential to enhance link reliability in order to alleviate undesirable influences from weather conditions. This issue can be effectively addressed through the simultaneous implementation of RF and FSO links for signal transmission. It is

noteworthy that fog and rain seldom happen simultaneously in nature. Subsequently, the two links provided by the hybrid scheme can operate in a complementary way. This idea motivates the RF/FSO hybrid link scheme, as shown in Figure 3.7. Conceptually, the RF/FSO is a hybrid system that joins the advantages of the typical high-capacity transmission of optical systems and the ease of deployment of wireless links. Furthermore, the notion of hybrid RF/FSO system is based on attending to the associated weaknesses and taking the benefits of both technologies simultaneously to ensure reliable transmission wireless services [B1, 4, 9, 35].

A RF/FSO hybrid scheme has two parallel links between the transmitter and the receiver. Furthermore, based on the application and implementation scenario, both parallel links are capable of transmitting data. However, depending on the weather conditions and the Electro-Magnetic Interference (EMI) levels, either of the links can be employed for data transmission [36]. For example, during adverse atmospheric conditions (e.g. fog) with FSO link outage, the hybrid system ensures that the RF link operates as a backup. Nevertheless, the resulting data rate of the RF link is considerably lower than the one offered by the real FSO link [B1, 4, 9, 35]

3.6.2 Relay-assisted FSO Transmission

It has been observed that a practical method for turbulence-induced fading alleviation is the spatial diversity scheme. In spatial diversity, multiple transmitter/receiver apertures are deployed with the aim of creating and exploring additional degrees of freedom offered by the spatial domain. The scheme is an attractive method for fading alleviation owing to its characteristic redundancy. Nonetheless, the application of multiple apertures poses a number of challenges like an increase in system cost and complexity. Besides, the distance between the apertures has to be sufficiently large to prevent the harmful effects of spatial correlation. The basic means of achieving spatial diversity is dual-hop relaying. The scheme has been implemented significantly in RF

communication systems. The dual-hop relaying employment aids greatly in extending the network coverage area and in enhancing the receive signal quality [37]. A mixed RF/FSO communication system is shown in Figure 3.8.

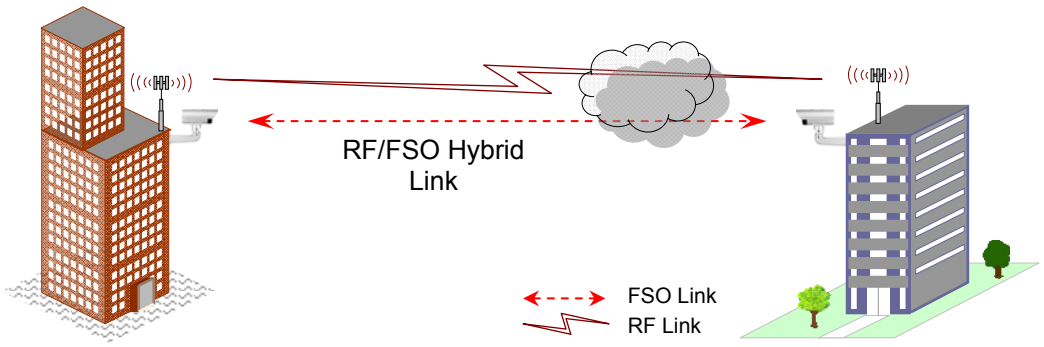

Figure 3.7: Schematic of a RF/FSO hybrid link.

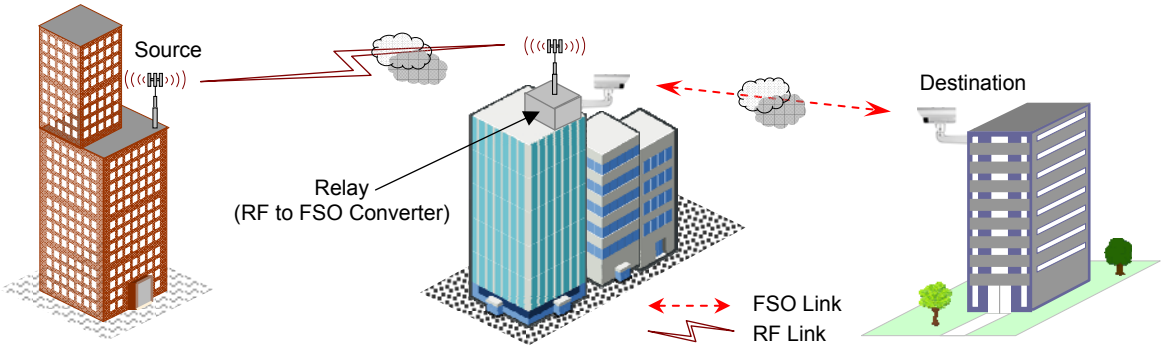

Figure 3.8: Schematic of a mixed RF/FSO communication system.

In addition, the idea of relay-assisted transmission is established on generating a virtual multiple-aperture scheme so as to achieve the benefits of MIMO systems. This is accomplished by taking advantage of the salient features in both FSO and RF transmissions with the intention of ensuring an effective system in a real-life condition.

Moreover, a relay-assisted transmission, also known as a mixed RF/FSO dual-hop communication scheme, comprises the RF links from the source to the

relay, as well as the FSO links between the relay and the destination. Basically, RF transmission is employed at one hop in the system while the FSO transmission is utilized at the other hop. It is worth mentioning that, the mixed RF/FSO dual-hop relay scheme is relatively different from the RF/FSO hybrid scheme. In the RF/FSO hybrid scheme, parallel RF and FSO links are usually employed for the same path [37]. However, in the former scheme, the major function of the FSO link is to allow the RF users to communicate with the backbone network. This aids and serves as a major method of bridging the connectivity gap between the backbone network and the last-mile access network [38, 39].

3.7 Research Contributions

In this section, the contributions of the manuscripts [J3, B1, B2] are referenced in the construction of this chapter. From these documents, several perspectives are presented for the implementation of wireless optical communication technologies in different sectors. In addition, they provide a comprehensive overview of the challenges surrounding the applications of optical-wireless systems. These documents will be a good start for researchers to better understand the concepts of OWC systems.

3.8 Conclusion

In this chapter, several opportunities for application of OWC technologies have been presented for various segments of the communication networks. Additionally, challenges were presented for optical-wireless network applications and considered different possible solutions.

References

[1] C. Yu, L. Yu, Y. Wu, Y. He, and Q. Lu, “Uplink Scheduling and Link Adaptation for Narrowband Internet of Things Systems”, *IEEE Access*, vol. 5, pp. 1724-1734, 2017, DOI: 10.1109/ACCESS.2017.2664418.

[2] W. Ejaz, A. Anpalagan, M. A. Imran, M. Jo, M. Naeem, S. B. Qaisar, and W. Wang, “Internet of Things (IoT) in 5G Wireless Communications”, *IEEE Access*, vol. 4, pp. 10310–10314, 2016, DOI: 10.1109/ACCESS.2016.2646120.

[3] I. Alimi, A. Shahpari, V. Ribeiro, N. Kumar, P. Monteiro, and A. Teixeira, “Optical Wireless Communication for Future Broadband Access Networks”, *2016 21st European Conference on Networks and Optical Communications (NOC)*, Lisbon, June 2016, pp. 124–128, DOI: 10.1109/NOC.2016.7506998.

[4] I. A. Alimi, A. L. Teixeira, and P. P. Monteiro, “Toward an Efficient C-RAN Optical Fronthaul for the Future Networks: A Tutorial on Technologies, Requirements, Challenges, and Solutions”, *IEEE Communications Surveys & Tutorials*, vol. 20, no. 1, pp. 708–769, Firstquarter 2018, DOI: 10.1109/COMST.2017.2773462.

[5] G. Parca, A. Tavares, A. Shahpari, A. Teixeira, V. Carrozzo, and G. T. Beleffi, “FSO for broadband multi service delivery in future networks”, in *2013 2nd International Workshop on Optical Wireless Communications (IWOW)*, Oct 2013, pp. 67–70, DOI: 10.1109/IWOW.2013.6777779

[6] Abu Jahid, Mohammed H. Alsharif and Trevor J. Hall, *A Contemporary Survey on Free Space Optical Communication: Potential, Technical Challenges, Recent Advances and Research Direction*. ArXiv – Information Theory, Nov. 2020, DOI: arxiv-2012.00155.

[7] Z. Ghassemlooy, W. Popoola, and S. Rajbhandari, *Optical Wireless Communications: System and Channel Modelling With MATLAB*. CRC Press, 2012, ISBN 9781138074804.

[8] Z. Ghassemlooy, S. Arnon, M. Uysal, Z. Xu, and J. Cheng, “Emerging Optical Wireless Communications-Advances and Challenges”, *IEEE Journal on Selected Areas in Communications*, vol. 33, no. 9, pp. 1738–1749, Sept 2015, DOI: 10.1109/JSAC.2015.2458511.

[9] M. A. Khalighi and M. Uysal, “Survey on Free Space Optical Communication: A Communication Theory Perspective”, *IEEE Communications Surveys & Tutorials*, vol. 16, no. 4, pp. 2231–2258, 2014, DOI:10.1109/COMST.2014.232950

[10] S. Bloom, E. Korevaar, J. Schuster, and H. Willebrand, “Understanding the performance of free-space optics [Invited]”, *Journal of Optical Network.*, vol. 2, no. 6, pp. 178-200, Jun 2003, DOI:10.1364/JON.2.000178

[11] H. Kaushal and G. Kaddoum, “Optical Communication in Space: Challenges and Mitigation Techniques”, *IEEE Communications Surveys & Tutorials*, vol. 19, no. 1, pp. 57–96, Firstquarter 2017, DOI: 10.1109/COMST.2016.2603518.

[12] A. Sevincer, A. Bhattarai, M. Bilgi, M. Yuksel, and N. Pala, “LIGHTNETs: Smart LIGHTing and Mobile Optical Wireless NETworks - A Survey”, *IEEE Communications Surveys & Tutorials*, vol. 15, no. 4, pp. 1620–1641, Fourth 2013, DOI: 10.1109/SURV.2013.032713.00150.

[13] S. Rajagopal, R. D. Roberts, and S. K. Lim, “IEEE 802.15.7 visible light communication: modulation schemes and dimming support”, *IEEE Communications Magazine*, vol. 50, no. 3, pp. 72–82, March 2012, DOI: 10.1109/MCOM.2012.6163585.

[14] K. Ying, Z. Yu, R. J. Baxley, H. Qian, G. K. Chang, and G. T. Zhou, “Nonlinear distortion mitigation in visible light communications”, *IEEE Wireless Communications*, vol. 22, no. 2, pp. 36–45, April 2015, DOI: 10.1109/MWC.2015.7096283.

[15] F. Yang and J. Gao, “Dimming Control Scheme With High Power and Spectrum Efficiency for Visible Light Communications”, *IEEE Photonics Journal*, vol. 9, no. 1, pp. 1–12, Feb 2017, Art no. 7901612, DOI: 10.1109/JPHOT.2017.2658025.

[16] M. Wang, J. Wu, W. Yu, H. Wang, J. Li, J. Shi, and C. Luo, “Efficient coding modulation and seamless rate adaptation for visible light communications”, *IEEE Wireless Communications*, vol. 22, no. 2, pp. 86–93, April 2015, DOI: 10.1109/MWC.2015.7096290.

[17] Visible light communication - VLC & PUREVLC™, *ANDY*, Accessed: February 2017, [Online]. http://andy96877.blogspot.pt/p/visible-light-communication-vlc-is-data.html.

[18] M. D’Amico, A. Leva, and B. Micheli, “Free-space optics communication systems: first results from a pilot field-trial in the surrounding area of Milan, Italy”, *IEEE Microwave and Wireless Components Letters*, vol. 13, no. 8, pp. 305–307, Aug 2003, DOI: 10.1109/LMWC.2003.815699.

[19] D.-Y. Song, Y.-S. Hurh, J.-W. Cho, J.-H. Lim, D.-W. Lee, J.-S. Lee, and Y. Chung, “4 x 10 Gb/s terrestrial optical free space transmission over 1.2 km using an EDFA preamplifier with 100 GHz channel spacing”, *Optics Express*, vol. 7, no. 8, pp. 280-284, Oct 2000, DOI: 10.1364/OE.7.000280, [Online]. http://www.opticsexpress.org/abstract.cfm?URI=oe-7-8-280

[20] R. T. Carlson and S. Paciorek, “Environmental qualification and field test results for the SONAbeam™ 155 and 622”, *fSONA Communications Corp*, Tech. Rep. [Online]. http://www.fsona.com/tech/white_papers/tech_qual-test.pdf

[21] P. Bandera, “Defining a Common Standard for Evaluating and Comparing Free-Space Optical Products”, *fSONA Communications Corp*, Tech. Rep., [Online].

http://www.fsona.com/tech/white_papers/WHTPAP-Generalized_Link_Margin.pdf

[22] "Ultra-Low Latency Point-to-Point Wireless Bridge", *LightPointe*, white paper, [Online].http://nebula.wsimg.com/793e82b2beac48cb90c347bd86776d12?AccessKeyId=C1431E109BF92B03DF85&disposition=0&alloworigin=1.

[23] Z. Wang, W. D. Zhong, S. Fu, and C. Lin, "Performance comparison of different modulation formats over free-space optical (FSO) turbulence links with space diversity reception technique", *IEEE Photonics Journal*, vol. 1, no. 6, pp. 277–285, Dec 2009, DOI: 10.1109/JPHOT.2009.2039015.

[24] S. M. Navidpour, M. Uysal, and M. Kavehrad, "BER Performance of Free-Space Optical Transmission with Spatial Diversity", *IEEE Transactions on Wireless Communications*, vol. 6, no. 8, pp. 2813–2819, August 2007, DOI: 10.1109/TWC.2007.06109

[25] I. A. Alimi, A. M. Abdalla, J. Rodriguez, P. P. Monteiro, and A. L. Teixeira, "Spatial Interpolated Lookup Tables (LUTs) Models for Ergodic Capacity of MIMO FSO Systems", *IEEE Photonics Technology Letters*, vol. 29, no. 7, pp. 583–586, April 2017, DOI: 10.1109/LPT.2017.2669337

[26] I. Alimi, P. Monteiro, and A. Teixeira, "Analysis of Atmospheric Effects on RF Signal Transmission Over the Optical Wireless Communication Links", in *XIII Symposium on Enabling Optical Networks and Sensors (SEONS)*, Covilhã – Portugal, pp. 35–38, July 2016.

[27] A. Bekkali, C. B. Naila, K. Kazaura, K. Wakamori, and M. Matsumoto, "Transmission Analysis of OFDM-Based Wireless Services Over Turbulent Radio-On-FSO Links Modeled by Gamma-Gamma Distribution", *IEEE Photonics Journal*, vol. 2, no. 3, pp. 510–520, June 2010, DOI: 10.1109/JPHOT.2010.2050306.

[28] P. P. Monteiro, D. Viana, J. da Silva, D. Riscado, M. Drummond, A. S. R. Oliveira, N. Silva, and P. Jesus, "Mobile fronthaul RoF transceivers for C-RAN applications", in *2015 17th International Conference on Transparent Optical Networks (ICTON)*, Budapest, July 2015, pp. 1–4, DOI: 10.1109/ICTON.2015.7193452.

[29] M. Peng, Y. Li, Z. Zhao, and C. Wang, "System architecture and key technologies for 5G heterogeneous cloud radio access networks", *IEEE Network*, vol. 29, no. 2, pp. 6–14, March-April 2015, DOI: 10.1109/MNET.2015.7064897.

[30] C. Liu, L. Zhang, M. Zhu, J. Wang, L. Cheng, and G. K. Chang, "A Novel Multi-Service Small-Cell Cloud Radio Access Network for Mobile Backhaul and Computing Based on Radio-Over-Fiber Technologies", *Journal of Lightwave Technology*, vol. 31, no. 17, pp. 2869–2875, Sept 2013, DOI: 10.1109/JLT.2013.2274193..

[31] R. S. Oliveira, C. R. L. Francês, J. C. W. A. Costa, D. F. R. Viana, M. Lima, and A. Teixeira, "Analysis of the cost-effective digital radio over fiber system in the NG-

PON2 context", in *2014 16th International Telecommunications Network Strategy and Planning Symposium (Networks)*, Funchal, Sept 2014, pp. 1–6, DOI: 10.1109/NETWKS.2014.6959262.

[32] G.-K. Chang, C. Liu, and L. Zhang, "Architecture and applications of a versatile small-cell, multi-service cloud radio access network using radio-over-fiber technologies", in *2013 IEEE International Conference on Communications Workshops (ICC)*, Budapest, June 2013, pp. 879–883, DOI: 10.1109/ICCW.2013.6649358.

[33] N. J. Gomes, P. Assimakopoulos, L. C. Vieira, and P. Sklikas, "Fiber link design considerations for cloud-Radio Access Networks", in *2014 IEEE International Conference on Communications Workshops (ICC)*, June 2014, pp. 382–387, DOI: 10.1109/ICCW.2014.6881227.

[34] K. Kazaura, P. Dat, A. Shah, T. Suzuki, K. Wakamori, M. Matsumoto, T. Higashino, K. Tsukamoto, and S. Komaki, "Studies on a Next Generation Access Technology Using Radio over Free-Space Optic Links", in *2008 The Second International Conference on Next Generation Mobile Applications, Services, and Technologies*, Cardiff, Sept 2008, pp. 317–324, DOI: 10.1109/NGMAST.2008.54.

[35] M. Uysal, C. Capsoni, Z. Ghassemlooy, A. Boucouvalas, and E. Udvary, *Optical Wireless Communications: An Emerging Technology*, ser. Signals and Communication Technology, Springer International Publishing, 2016, ISBN 978-3-319-30201-0.

[36] H. Dahrouj, A. Douik, F. Rayal, T. Y. Al-Naffouri, and M. S. Alouini, "Cost-effective hybrid RF/FSO backhaul solution for next generation wireless systems", *IEEE Wireless Communications*, vol. 22, no. 5, pp. 98–104, October 2015, DOI: 10.1109/MWC.2015.7306543.

[37] J. Zhang, L. Dai, Y. Zhang, and Z. Wang, "Unified Performance Analysis of Mixed Radio Frequency/Free-Space Optical Dual-Hop Transmission Systems", *Journal of Lightwave Technology*, vol. 33, no. 11, pp. 2286–2293, June 2015, DOI: 10.1109/JLT.2015.2409570.

[38] K. Yang, N. Yang, C. Xing, J. Wu, and Z. Zhang, "Space-Time Network Coding With Transmit Antenna Selection and Maximal-Ratio Combining", *IEEE Transactions on Wireless Communications*, vol. 14, no. 4, pp. 2106–2117, April 2015, DOI: 10.1109/TWC.2014.2381217.

[39] I. S. Ansari, F. Yilmaz, and M. S. Alouini, "Impact of Pointing Errors on the Performance of Mixed RF/FSO Dual-Hop Transmission Systems", *IEEE Wireless Communications Letters*, vol. 2, no. 3, pp. 351–354, June 2013, DOI: 10.1109/WCL.2013.042313.130138.

Chapter 4

Channel Model and Characterization

As stated earlier, links in FSO are able to offer high data rates for different applications. Nonetheless, their availability and reliability depend heavily on the associated weather conditions. As a result, it is really essential that FSO systems have accurate channel measurements based on different atmospheric conditions. This chapter presents both simulated and experimental results reported in [J3, B2]. In these manuscripts, the performance of a FSO link is experimentally examined and reported, when influenced by real-life atmospheric turbulence conditions. The atmospheric related scintillation index, σ_N^2 , is determined from the samples obtained from the channel, in an attempt to determine the extent of the atmospheric turbulence, as well as the consequent effects on the FSO link features. Additionally, the refractive-index structure parameter, C_n^2, can be subsequently estimated. Therefore, in this chapter, apart from the simulation results considered, the experimental results of the channel characterization for the SISO FSO link, obtained from the channel measurements, are presented. The FSO channel samples histograms, in addition to the atmospheric turbulence distribution fittings, are given concurrently with the measured σ_N^2 . Furthermore, the effects of scintillation on system

performance are studied for different turbulence conditions. In addition, a proof-of-concept real-time long-reach, gigabit-capable, hybrid coherent PON and FSO systems are presented. The presented hybrid systems are capable of supporting several applications in shared fiber-optic infrastructure.

4.1 Introduction

The increase in the number of mobile devices like laptops, cell phones, and tablets significantly influences the already growing annual rate of broadband connections. Furthermore, several applications and services that are bandwidth-intensive are contributing also to the remarkable increase [7–9]. Networks capable of presenting improved-capacity, as well as high-speed at comparatively low-cost, are required to support the different use cases [10]. As aforementioned in chapter 4, a remarkable and attractive solution that converges the mobility and flexibility characteristics of RF networks with the high data rates offered by the optical systems is the FSO communication system [J2, 3, 11, 12]. Nevertheless, FSO links are actually prone to local weather conditions and atmospheric turbulence [10, 13–17], affecting system performance. The effect can give rise to beam spreading, loss of spatial coherence, and temporal irradiance fluctuation, also known as scintillation [1, 6, 12, 16, 18–21]. Consequently, an accurate channel characterization is highly essential for the practical FSO links development and can help in the definition of the system performance for different transmission scenarios [3]. Moreover, with a perfectly characterized channel, ergodic channel capacity can be estimated [22–24].

Various theoretical and experimental attempts have been reported in the literature in an effort to characterize the FSO communication link [12]. Closed-form expressions to estimate the average capacity of the MIMO FSO systems, using $\Gamma\Gamma$ fading channel for an equal gain combining (EGC) and maximum ratio combining (MRC) diversity techniques, were presented in [23]. In the work, it has been demonstrated that the average capacity can be improved with the employment of spatial diversity methods. In addition, [24] analyzes the influence

of weather and turbulence conditions on the average channel capacity of the FSO link. Aperture averaging and MIMO techniques are employed in the study. It has been shown that an increase in the number of transmits and receives apertures results in an increase in capacity regardless of the weather conditions. Moreover, the BER performance was studied in [4] in the FSO links, which are based on spatial diversity over the channels with fading and log-normal atmospheric turbulence, with the assumption of independent and correlated channels between transceiver apertures. The results presented in the work indicated that the FSO links with transmit and receive diversity can be represented by corresponding SISO schemes with appropriate scaling in the channel variance.

Furthermore, in [25], double generalized gamma model expressed the turbulence-induced fading in the FSO channel, as well as, at work, beam-pointing errors were taken into account. Likewise, performance measurement metrics such as the outage probability, the BER, and system ergodic capacity were stated using unified closed-form expressions. In addition, [26] presented a MIMO FSO system, which was based on Vertical-Bell Laboratories Layered Space-Time (V-BLAST) detection algorithm. At work, it was established through simulation that an increase in the number of antennas results in larger channel capacity. Also, as a result of the offered diversity, the error rate significantly decreases. Besides, the optical signal fluctuation during propagation through the FSO link was defined by the Log-Normal (LN) and Gamma-Gamma ($\Gamma\Gamma$) distribution models. Additionally, closed-form expressions for the estimation of the average channel capacity of the FSO system were provided in [27]. Moreover, in [28], maximum likelihood estimation was employed for characterizing the log-normal-Rician turbulence model parameters. Also, the unknown parameters were calculated through the expectation-maximization algorithm. Besides, an experimentally quantified channel model based on a finite-state Markov chain, which was derived for autocorrelation and the distribution of fading, was proffered in [12].

This chapter presents the effects of several factors, such as wavelength and refractive index, which are investigated in FSO transmissions. Additionally, a

10 Gbps link with an external FSO channel of 54 meters (round trip) and 1548.51 nm wavelength is also considered, which is characterized based on the gain measurement of the channel. In addition, we propose closed-form expressions, which are established on the channel measurement, to evaluate the ergodic channel capacity of MIMO FSO communication systems over the atmospheric turbulence fading channels.

With the noticeable importance of the FSO systems and the state-of-the-art description of the area under discussion, Section 4.2 presents an optical system as well as channel models, considering atmospheric attenuation, pointing error, and atmospheric turbulence. The system performance is analyzed in Section 4.3. In Section 4.4, simulation results are presented along with comprehensive discussions. In Section 4.5, experimental setup as well as channel measurement and characterization results are examined. Research contributions are discussed in Section 4.6 and conclusions are presented in Section 4.7.

4.2 Optical System and Channel Model

A practical FSO link was assumed, based on IM/DD and using the on-off keying (OOK) modulation format, where the data modulates the instantaneous intensity of the carrier's optical beam at the transmitter. The optical power coming from the transmission aperture passes through the free-space channel and is then influenced by various factors such as atmospheric turbulence-induced fading, misalignment fading, and background noise along with the link before reaching the receiving aperture. The aforementioned factors bring about optical signal intensity to fluctuate. Therefore, the resulting electrical signal, r, received in the receive aperture can be expressed as [J3, 1, 29, 30]

$$r = \eta_e \, h \, x + n \tag{4.1}$$

where η_e denotes the effective photoelectric conversion ratio of the receiver, $x \in \{0,\ 1\}$ represents the information bit transmitted, n is the additive white

Gaussian noise (AWGN) with zero mean and variance $\sigma_n^2 = N_0/2$ (for 1 Hz), N_0 is the noise power spectral density value in W/Hz, and $h = h_l\, h_a\, h_p$ denotes the irradiance that influences the channel state. The channel irradiance h present in Equation (4.1), is the product of the deterministic path loss, h_l; the random attenuation (i.e. atmospheric turbulence-induced fading), h_a; and random attenuation (due to geometric spread and pointing errors), h_p. The h_a and h_p are random variables with probability density functions (pdf) $f_{h_a}(h_a)$ and $f_{h_p}(h_p)$, respectively.

4.2.1 Atmospheric Attenuation

The transmission of an optical beam through the atmosphere results in an atmospheric loss. The attenuation experienced by signal power can be defined by the exponential law of Beers-Lambert and can be expressed as [29–31]

$$h_l(\lambda, z) = \frac{P(\lambda, z)}{P(\lambda, 0)} = \exp(-\sigma(\lambda)\, z) \tag{4.2}$$

where $h_l(\lambda, z)$ represents the loss that is a function of propagation path of length z at wavelength λ, $P(\lambda, 0)$ and $P(\lambda, z)$ denote the signal power at the beginning and the emitted power at distance z, respectively and $\sigma(\lambda)$ denotes the attenuation coefficient.

The attenuation coefficient, for a given wavelength λ (in nanometer), can be empirically expressed in terms of visibility as [B2, 29]

$$\sigma(\lambda) = \frac{3.912}{V}\left(\frac{\lambda}{550}\right)^{-q} \tag{4.3}$$

where V represents visibility in kilometers, and q is a parameter that is a function of the particle size distribution in the atmosphere. It can be expressed by the Kruse model as [B2, 29]

$$q = \begin{cases} 1.6 & V > 50 \text{ km} \\ 1.3 & 6\text{km} < V < 50 \text{ km} \\ 0.585V^{1/3} & V < 6 \text{ km} \end{cases} \tag{4.4}$$

Furthermore, Kim presented an extended model with the intention of achieving a better accuracy in lower visibility scenarios. The Kim model is defined as [B2, 29]

$$q = \begin{cases} 1.6 & V > 50 \text{ km} \\ 1.3 & 6 \text{ km} < V < 50 \text{ km} \\ 0.16V + 0.34 & 1\text{km} < V < 6 \text{ km} \\ V - 0.5 & 0.5 \text{ km} < V < 1\text{km} \\ 0 & V < 0.5 \text{ km} \end{cases} \tag{4.5}$$

4.2.2 Pointing Error or Misalignment Fading

The FSO link is a LOS communication in which a narrow optical beamwidth is employed. This presents severe requirements for pointing accuracy for effective performance as well as the reliability of optical systems. The signal fading, as well as pointing errors typically take place at the receiver owing to the wind loads, in addition to thermal expansions that result in random oscillations of buildings. Suppose a Gaussian spatial intensity profile with beam waist w_z in the receiving plane, located at a distance z away from the transmitter. Moreover, assume a receiver circular aperture of radius r. The collected power fraction due to the geometric spread with radial displacement α, from the detector origin, can be estimated in Gaussian form as [B2, 30, 31]

$$h_p(\alpha) \approx A_0 \exp\left(-\frac{2\alpha^2}{w_{z_{eq}}^2}\right) \tag{4.6}$$

where $w_{z_{eq}}$ denotes equivalent beamwidth, $w_{z_{eq}}^2 = w_z^2\left[\frac{\sqrt{\pi}\ \text{erf}(v)}{2v\ \exp(-v^2)}\right]$,

$v = \frac{\sqrt{\pi}\, r}{\sqrt{2}\, w_z}$, A_0 = [erf(v)]^2, and erf(·) represents the error function given by [B2, 20]

$$erf(x) = \frac{2}{\sqrt{\pi}} \int_0^x e^{-u^2} \tag{4.7}$$

Assuming that the elevation as well as the horizontal sway is independent and identical Gaussian distributions, subsequently, the radial displacement α follows a Rayleigh distribution. In that case, the $f_{h_p}(h_p)$ can be expressed as [B2, 30, 31]

$$f_{h_p}(h_p) = \frac{\gamma^2}{A_0^{\gamma^2}} h_p^{\gamma^2 - 1} \qquad 0 \le h_p \le A_0 \tag{4.8}$$

where $\gamma = w_{z_{eq}} / 2\sigma_s$ denotes the ratio between the equivalent beam radius and the standard deviation (jitter) of the pointing error displacement at the receiver and σ_s^2 represents the jitter variance at the receiver.

4.2.3 Atmospheric Turbulence

In the literature, several statistical models have been employed to define the intensity fluctuation over the FSO channel for different turbulence regimes. A good example of those models is the Log-Normal (LN) distribution. The LN has been widely used owing to its substantial match with different experimental measures. Furthermore, other extensively employed models are Gamma-Gamma ($\Gamma\Gamma$) distribution, K distribution, I-K distribution, Málaga ($\mathcal{M}$)-distribution, and Negative Exponential distribution. This work focuses mainly on the LN and $\Gamma\Gamma$ distribution.

Log-normal (LN) Distribution

Generally, the LN model is just appropriate for weak turbulence conditions. It is also applicable to links with a range of less than 100 m [32]. Consequently, the pdf model of weak intensity turbulence fluctuation using the LN distribution can be defined as [J3, B2, 1]

$$f_{h_a}\left(h_a\right)=\frac{1}{2h_a\sqrt{2\pi\sigma_x^2}}\exp\left(-\frac{\left(\ln\left(h_a\right)+2\sigma_x\right)^2}{8\sigma_x^2}\right) \tag{4.9}$$

where $\sigma_x^2=\sigma_I^2/4$ denotes the log-amplitude variance which can be defined for plane and spherical waves, respectively as [J3, B2, 1]

$$\sigma_x^2\Big|_{plane}=0.307C_n^2k^{7/6}L^{11/6} \tag{4.10a}$$

$$\sigma_x^2\Big|_{spherical}=0.125C_n^2k^{7/6}L^{11/6} \tag{4.10b}$$

$$\sigma_I^2\Big|_{plane}=1.23C_n^2k^{7/6}L^{11/6} \tag{4.10c}$$

$$\sigma_I^2\Big|_{spherical}=0.50C_n^2k^{7/6}L^{11/6} \tag{4.10d}$$

where $k = 2\pi/\lambda$ denotes the optical wave number, σ_I^2 represents the log-irradiance variance, L is the distance, and C_n^2 represents the refractive-index structure parameter that is altitude-dependent. The C_n^2 is one of the major parameters for characterizing the quantity of refractive index fluctuation through the atmospheric turbulence. Moreover, it depends on features such as temperature, wavelength, and atmospheric altitude. Several C_n^2 profile models have been offered in the literature considering different features. Nevertheless, that extensively employed and that takes the altitude into consideration is the Hufnagel-Valley model defined as [J3, B2, 1, 2, 20]

$$C_n^2=0.00594\left(\frac{v_w}{27}\right)^2\left(10^{-5}h\right)^{10}\exp\left(\frac{-h}{1000}\right)+2.7\times10^{-16}\exp\left(\frac{-h}{1500}\right)+\hat{A}\exp\left(\frac{-h}{100}\right) \tag{4.11}$$

where h is the altitude in meters (m) and $\hat{A}$ represents the nominal value of $C_n^2(0)$ at the ground level in $m^{-2/3}$. The C_n^2 values for the FSO links near the ground level are estimated to be approximately 1.7×10^{-14} $m^{-2/3}$ and 8.4×10^{-15} $m^{-2/3}$ during the day and at night, respectively. Usually, C_n^2 is estimated between 10^{-13} $m^{-2/3}$ for strong turbulence to 10^{-17} $m^{-2/3}$ for weak turbulence. However, its usual average value is 10^{-15} $m^{-2/3}$ [2, 20]. The v_W represents the root mean square of wind speed in meters per second (m/s) [20].

The LN pdf for different values of log-irradiance variance is illustrated in Figure 4.1. Considering $\sigma_I^2 \in (0.01,\ 0.1,\ 0.4,\ 0.9)$, the $\sigma_x^2\big|_{plane}$ values corresponding to Equation (4.10a) are introduced in Equation (4.9), to estimate the pdf of the intensity fluctuation for the LN distribution. From the plot, it could be seen that as the value of σ_I^2 increases, the distribution becomes more and more tilted. This shows the magnitude of the system irradiance fluctuation.

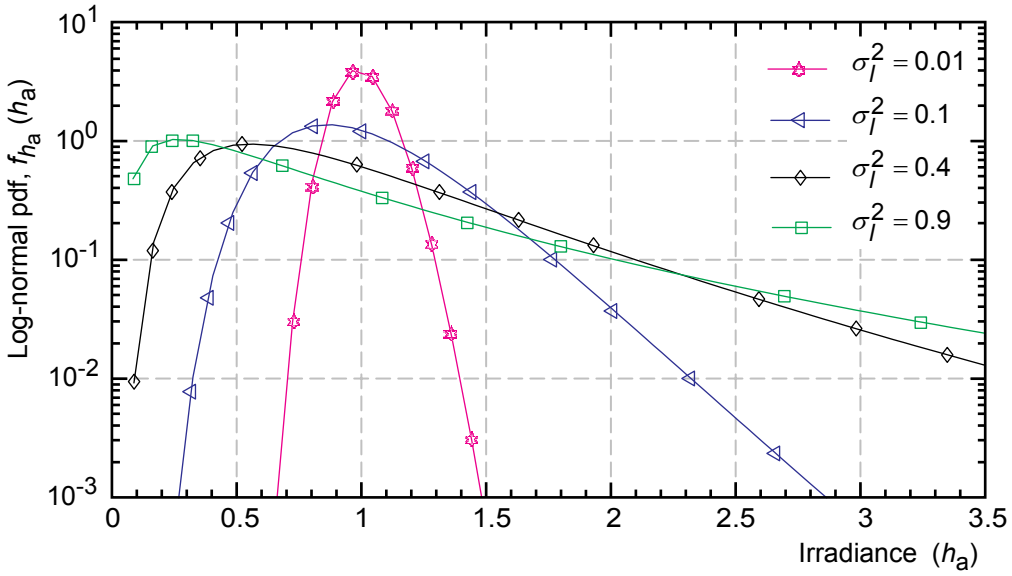

Figure 4.1: Log-normal pdf for different values of log-irradiance variance

Gamma-Gamma ($\Gamma\Gamma$) Distribution

It is noteworthy that, the LN distribution characterization is not valid in the

strong turbulence regimes. Consequently, the widely implemented model for defining the scintillation effects in such regimes is the $\Gamma\Gamma$ distribution. Besides, the $\Gamma\Gamma$ model can be employed for the characterization of the fading gain from weak to strong turbulence conditions. The h_a pdf with the implementation of $\Gamma\Gamma$ distribution can be defined as [J3, 1, 2, 20]

$$f_{h_a}(h_a) = \frac{2\,(\alpha\,\beta)^{(\alpha+\beta)/2}}{\Gamma(\alpha)\,\Gamma(\beta)}\,(h_a)^{\frac{\alpha+\beta}{2}-1}\,K_{\alpha-\beta}\left(2\sqrt{\alpha\,\beta\,h_a}\right) \tag{4.12}$$

where $K_V(\cdot)$ represents the modified Bessel function of the second kind of order v, $\Gamma(\cdot)$ denotes the gamma function, α and β are the effective numbers of large-scale and small-scale eddies of the scattering process, respectively. The parameters α and β are expressed, respectively, for the plane wave as [J3, B2, 1, 2, 20]

$$\alpha = \left[\exp\left(\frac{0.49\,\sigma_R^2}{\left(1+1.11\sigma_R^{12/5}\right)^{7/6}}\right)-1\right]^{-1} \tag{4.13a}$$

$$\beta = \left[\exp\left(\frac{0.51\sigma_R^2}{\left(1+0.69\,\sigma_R^{12/5}\right)^{5/6}}\right)-1\right]^{-1} \tag{4.13b}$$

and likewise, for the spherical wave, they are given by [J3, B2]

$$\alpha = \left[\exp\left(\frac{0.49\,\sigma_R^2}{\left(1+1.18\,d^2+0.56\,\sigma_R^{12/5}\right)^{7/6}}\right)-1\right]^{-1} \tag{4.14a}$$

$$\beta = \left[\exp\left(\frac{0.51\sigma_R^2\left(1+0.69\sigma_R^{12/5}\right)^{-5/6}}{\left(1+0.9\,d^2+0.62\,d^2\,\sigma_R^{12/5}\right)^{5/6}}\right)-1\right]^{-1} \tag{4.14b}$$

where $d \triangleq (k\,D^2/4L)^{1/2}$, D is the diameter of the receiver aperture, the parameter σ_R^2 represents the Rytov variance which is a metric that determines the strength of the turbulence fluctuations. The σ_R^2 can be expressed for the plane and

spherical waves, respectively, as [J3, B2, 2, 20]

$$\sigma_R^2\Big|_{plane} = 1.23 C_n^2 k^{7/6} L^{11/6} \tag{4.15a}$$

$$\sigma_R^2\Big|_{spherical} = 0.492 C_n^2 k^{7/6} L^{11/6} \tag{4.15b}$$

It is remarkable that the normalized variance of the irradiance which is also well- known as the scintillation index (σ_N^2) can be defined as a function of σ_x^2 and eddies of the scattering process (α and β), respectively, as [J3, B2, 20], where $\langle \cdot \rangle$ represents the average over the scintillation.

$$\sigma_N^2 \triangleq \frac{\langle h_a^2 \rangle - \langle h_a \rangle^2}{\langle h_a \rangle^2} = \frac{\langle h_a^2 \rangle}{\langle h_a \rangle^2} - 1 \tag{4.16a}$$

$$= \exp\left(4\sigma_x^2\right) - 1 \tag{4.16b}$$

$$= 1/\alpha + 1/\beta + 1/(\alpha\beta) \tag{4.16c}$$

The $\Gamma\Gamma$ pdf is illustrated in Figure 4.2 for the turbulent regimes that correspond to weak, moderate, and strong atmospheric scenarios.

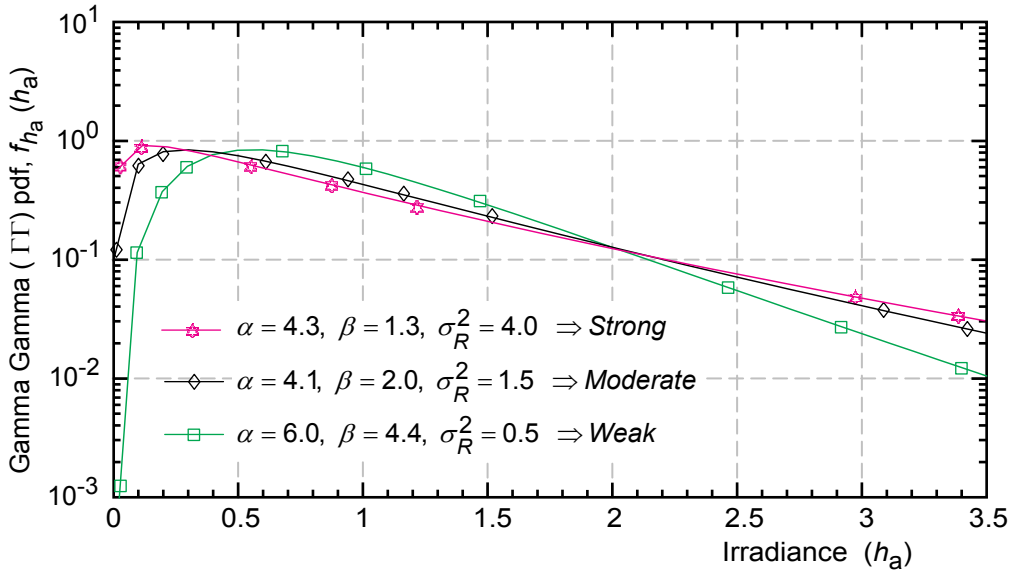

Figure 4.2: Gamma-gamma pdf for turbulence regimes from weak to strong.

It can be inferred from the results that, an increase in the turbulence from the weak to the strong regimes brings about resulting increase in the distribution spreading.

4.2.4 Combined Attenuation Statistics

The irradiance pdf, $h = h_l\ h_a\ h_p$ that represents the above-mentioned propagation channel factors can be written as [B2, 30, 31]

$$f_h(h; w_z) = \int f_{h|h_a}(h \mid h_a)\, f_{h_a}(h_a)\, d\, h_a \tag{4.17}$$

where $f_{h|h_a}(h|h_a)$ denotes the conditional probability with a turbulence state h_a and its distribution can be expressed as [30, 31]

$$f_{h|h_a}(h \mid h_a) = \frac{1}{h_a\, h_l} f_{h_p}\left(\frac{h}{h_a h_l}\right) = \frac{\gamma^2}{A_0^{\gamma^2} h_a\, h_l}\left(\frac{h}{h_a\, h_l}\right)^{\gamma^2 - 1}, \quad 0 \le h \le A_0\, h_a\, h_l \tag{4.18}$$

Consequently, $f_h(h; w_z)$ can be expressed as [30]

$$f_h(h; w_z) = \frac{\gamma^2}{\left(A_0\ h_l\right)^{\gamma^2}} h^{\gamma^2 - 1} \int_{h/A_0\, h_l}^{\infty} h_a^{-\gamma^2} f_{h_a}(h_a) d\, h_a \tag{4.19}$$

4.3 OWC Systems Performance Analysis

This section presents the BER performance and ergodic channel capacity of the considered models.

4.3.1 BER

It is noteworthy that the channel state distribution $f_h(h;\ w_z)$ can be estimated by using a suitable atmospheric model for the turbulence regimes in equation 4.19 as follows:

1. **For a weak turbulence**

   In this atmospheric regime, $f_{h_a}(h_a)$ is based on LN distribution, therefore, $f_h(h;\ w_z)$ can be written as [B2, 30]

$$f_h(h;w_z) = \frac{\gamma^2}{2(A_0\, h_l)^{\gamma^2}} h^{\gamma^2-1} \times erfc\left(\frac{\ln\left(\frac{h}{A_0\, h_l}\right) + \mu}{\sqrt{8}\,\sigma_x} \right) e^{\left(2\sigma_x^2\,\gamma^2\left(1+\gamma^2\right)\right)} \tag{4.20}$$

2. **For a strong turbulence**

   As stated earlier, this atmospheric regime is characterized by the $\Gamma\Gamma$ distribution, hence, $f_h(h;\ w_z)$ can be defined as [B2, 30, 31]

$$f_h(h;\ w_z) = \frac{2\gamma^2\left(\alpha\,\beta\right)^{(\alpha+\beta)/2}}{\left(A_0\, h_l\right)^{\gamma^2}\,\Gamma(\alpha)\,\Gamma(\beta)} h^{\gamma^2-1} \times \int_{h/(A_0\, h_l)}^{\infty} h_a^{(\alpha+\beta)/2-1-\gamma^2} K_{\alpha-\beta}\left(2\sqrt{\alpha\,\beta\, h_a}\right) d\, h_a \tag{4.21}$$

   where $K_v(\cdot)$ can be written in terms of the Meijer's G-function $G_{p,\,q}^{m,n}[\cdot]$ as [J3]

$$K_v(x) = \frac{1}{2} G_{0,\,2}^{2,\,0}\left[\frac{x^2}{4} \middle|_{v/2,\,-v/2}^{-} \right] \tag{4.22}$$

   Therefore, from equation 4.22, $K_{\alpha-\beta}\left(2\sqrt{\alpha\,\beta\, h_a}\right)$ can be written as [J3]

$$K_{\alpha-\beta}\left(2\sqrt{\alpha\beta h_a}\right)=\frac{1}{2}G_{0,2}^{2,0}\left[\alpha\beta h_a\middle|\begin{matrix}-\\(\alpha-\beta)/2,(\beta-\alpha)/2\end{matrix}\right] \tag{4.23}$$

Hence, $f_h(h)$ can be expressed as [31]

$$f_h(h)=\frac{\alpha\beta\gamma^2}{A_0 h_l\,\Gamma(\alpha)\,\Gamma(\beta)}\left(\frac{\alpha\beta h}{A_0 h_l}\right)^{(\alpha+\beta/2)-1}\times G_{1,3}^{3,0}\left[\frac{\alpha\beta}{A_0 h_l}h\middle|\begin{matrix}1-\frac{\alpha+\beta}{2}+\gamma^2\\-\frac{\alpha+\beta}{2}+\gamma^2,\frac{\alpha-\beta}{2},\frac{\beta-\alpha}{2}\end{matrix}\right] \tag{4.24}$$

Moreover, the average BER, $P(e)$, in term of $f_h(h)$ can be defined as [31]

$$P(e)=\int_0^\infty P(e|h)\,f_h(h)\,dh \tag{4.25}$$

4.3.2 Ergodic Channel Capacity

Besides the BER, achievable average (ergodic) channel capacity is another relevant figure of merit that has been widely used for characterizing the communication link performance. Thus, channel capacity is one of the key performance metrics that has to be taken into consideration in the design of FSO systems. Furthermore, the capacity of a MIMO FSO system with M lasers and N PDs in bits/s/Hz can be defined as [B2, 5, 22, 33]

$$C=Log_2\left[\det\left(I_M+\frac{\gamma_{inst}}{M}R\right)\right] \tag{4.26}$$

where I_M denotes a $M \times M$ identity matrix, $R=\begin{cases}\boldsymbol{H}\,\boldsymbol{H}^\dagger & \text{if } N<M\\ \boldsymbol{H}^\dagger\,\boldsymbol{H} & \text{if } N\le M\end{cases}$, $\boldsymbol{H}$ is a $N \times M$ channel state matrix, $(\cdot)^\dagger$ is the Hermitian transpose, $\gamma_{inst}=\eta_e^2 h^2/N_0$ represents the instantaneous electrical SNR whose average $\xi_a=\eta_e^2 E\langle h\rangle^2/N_0$

The MIMO FSO link ergodic capacity, C_{erg}, can be expressed using the expected value of instantaneous mutual information C, between the transmitter and receiver apertures. Therefore, the FSO system parameter C_{erg} is a random variable as well as a function of SNR. The C_{erg} can be determined by employing numerical integration approach as [J3, 5, 22, 34], where $E(\cdot)$ represents the expectation operator and $f_{\gamma_{inst}}(\gamma_{inst})$ denotes the pdf of γ_{inst}.

$$C_{erg} \triangleq E\langle C\rangle = \int_0^{\infty} Log_2\left(1+\gamma_{inst}\right) f_{\gamma_{inst}}\left(\gamma_{inst}\right) d\,\gamma_{inst} \tag{4.27}$$

4.4 Simulation Results and Discussions

In this section, the simulation results of the study of the atmospheric effects on BER performance of a binary phase-shift keying (BPSK), considering different turbulence conditions, are presented. In addition, we also present the simulation result of the average channel capacity of the FSO link with heterodyne detection. We consider the effects of various parameters on system performance for different operating conditions. In the simulation, we assume that the FSO system has a link of 1 km and a bit rate of 10 Gbps.

The average BER, regarding the average SNR for the BPSK and for different values of turbulence strength, is presented in Figure 4.3. In the study, when equation 4.25 is considered, a value is assumed for the effect of atmospheric turbulence. With the aim of estimating the system BER performance in the 1550 nm window, the atmospheric turbulence parameters with the following corresponding values are employed: $\alpha \in$ (4.34, 4.05, 5.98, 204.64), $\beta \in$ (1.31, 1.98, 4.40, 196.03), and $\sigma_I^2 \in$ (4.00, 1.50, 0.50, 0.01). These values represent conditions from weak to strong turbulence. The result shows that the SNR required to obtain a given BER increase with increasing atmospheric turbulence

strength. Take, for instance, a BER of 10^{-6} in a channel with σ_I^2 = 0.01, then the required SNR is about 18 dB. Conversely, for a fading strength of σ_I^2 = 0.50, the required SNR increases to 28 dB. In addition, with this BER and for σ_I^2 = 0.01 and σ_I^2 = 0.50, an additional 2 dB and 12 dB respectively are needed when compared with an ideal channel where no turbulence condition is assumed. Consequently, it can be inferred that the BER increases as turbulence strength becomes fiercer.

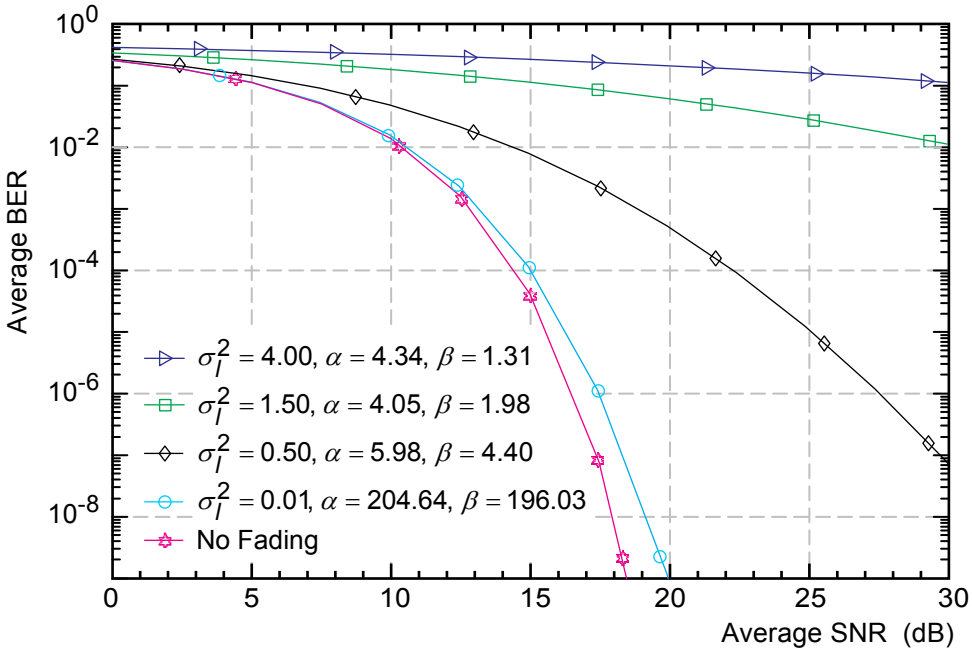

Figure 4.3: Average BER versus SNR for BPSK under different turbulence conditions at 1550 nm.

Furthermore, Figure 4.4 illustrates the average channel capacity of the FSO link as a function of average electrical SNR considering different values of turbulence strength. The atmospheric turbulence parameters $\sigma_N^2 \in$ (0.0120, 0.1486, 0.2078) give rise to $C_N^2 \in$ (6.03×10^{-16} $m^{-2/3}$, 7.62×10^{-15} $m^{-2/3}$, 1.09×10^{-14} $m^{-2/3}$) which correspond to the weak, moderate, and strong turbulence conditions, respectively. Additionally, on the same plot, the capacity for the non-turbulent channel condition (without fading) is present for

comparative analysis. It can be observed that the ergodic capacity of the FSO link can be influenced by the intensity of atmospheric turbulence. Accordingly, it is noted that the capacity of the ergodic channel for the situation of weak turbulence is relatively greater than in the case of moderate and strong turbulence regimes. Besides, the utmost capacity is given to the channel condition with no fading.

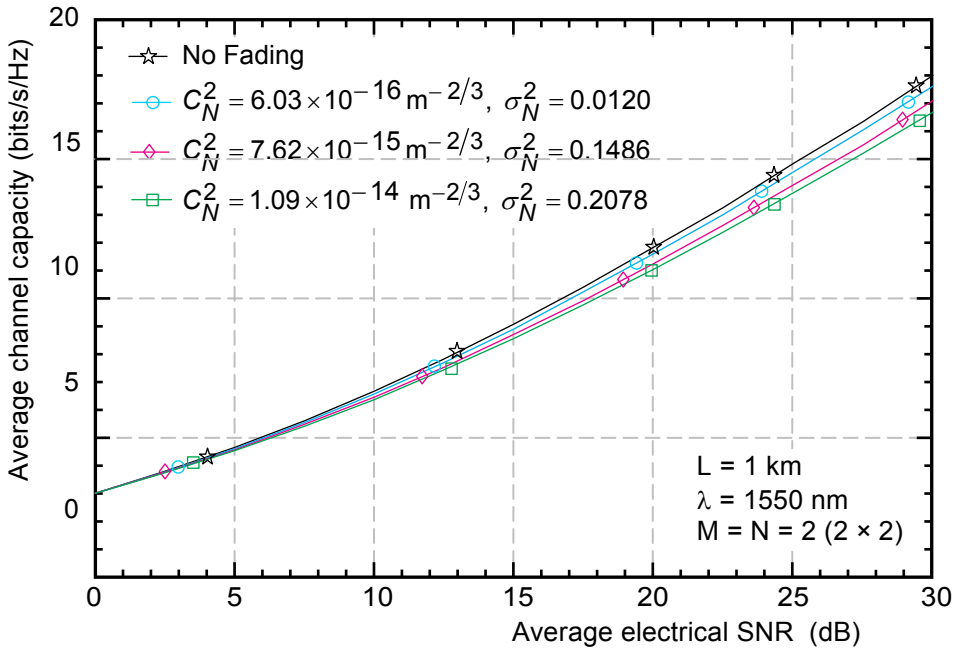

Figure 4.4: Average channel capacity of FSO link versus average electrical SNR.

Therefore, the result indicates that the atmospheric turbulence-induced fading brings about severe impairment in the FSO link performance. If care is not taken, this can result in persistent link failures in the long run. As a result, wireless optical systems are not as reliable as typical fiber optic systems. Thus, state-of-the-art technologies must be implemented to address the challenges and significantly enhance system performance.

4.5 Channel Measurement and Characterization

There has been an increase in efforts in the modeling of communication channels based on experimental measurements. One of such efforts presented in [35] considers a link operating at 1550 nm, estimating the fading distribution for several aperture sizes. Using an unmodulated continuous-wave source, the fitting parameters for the LN and the $\Gamma\Gamma$ fading distributions were compared based on the analytical model and experimental data. The analysis was done according to the receiver diameter. In addition, the FSO channel measurements completed the evaluation of the parameters for the fading distributions by means of an unmodulated continuous-wave source at 1550 nm in [36]. Based on the method, the authors jointly assessed parameters of the LN and $\Gamma\Gamma$ fading distributions taken the noise into consideration. Moreover, attenuation measurements on the FSO link channel operating at 1550 nm were reported in [37], however, no channel model was presented. Similarly, measurement results of a FSO link at 785 nm were reported in [38].

In the subsequent subsections, the experimental setup and the results for the FSO channel gain measurement, in which an outdoor link of 10 Gbps and 54 m operating at the wavelength of 1548.51 nm, are presented.

4.5.1 Experimental Setup

Figure 4.5 illustrates the experimental setup for the measurement of the outdoor FSO channel. The setup comprises a point-to-point FSO link in which the IM/DD technique is employed.

A 10 Gb/s NRZ signal is generated with the aids of a pattern generator that utilizes a PRBS of length $2^{23} - 1$ bits. Moreover, the generated electrical signal is then introduced into a JDSU® Integrated Laser Mach-Zehnder (ILMZ) being driven to the wavelength of 1548.51 nm.

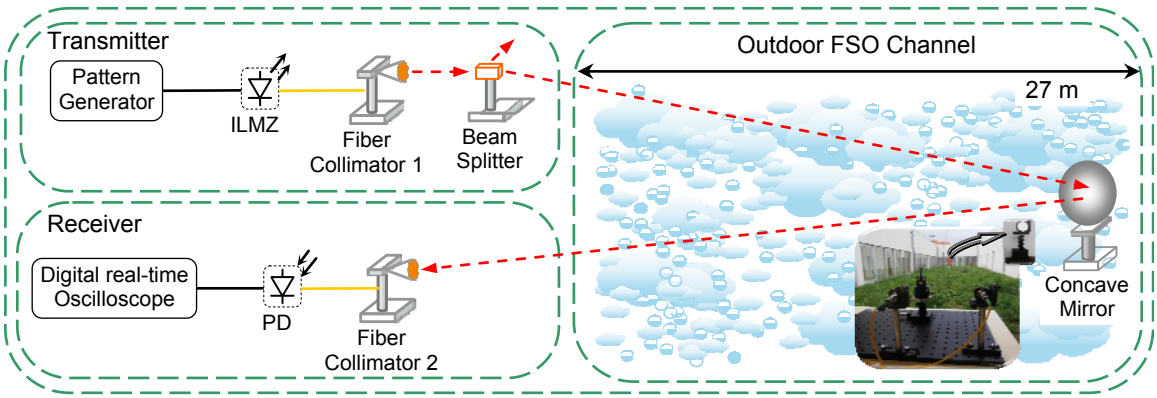

Figure 4.5: Outdoor experimental FSO setup.

A SMF is employed to transmit the optical signal from the laser to the fiber collimator, which then emits into the free space an optical beam 3 mm in diameter. In this experiment, an optical power of 0 dBm was set at the input of the fiber collimator. The collimated optical beam propagates over the FSO channel with a round-trip length of 54 m. The total transmission distance is realized when the optical beam of the fiber collimator 1 passes through the FSO channel and reaches the mirror ahead, at which point the reflected beam is returned back to the fiber collimator 2 at the receiver with approximately its initial diameter (2 mm). The mirror with 4 cm in diameter, has a concave profile and is located at a distance of 27 m from fiber collimators 1 and 2. The concave profile mirror minimizes beam scattering and significantly maximizes power transfer. The optical beam received by the fiber collimator 2 is focused on a SMF and subsequently converted to an electrical signal of 10 Gb/s, with the aid of PIN photodiode and then real-time sampled by an oscilloscope (Tektronix®: DPO72004B) at the sampling rate of 50 GS/s.

4.5.2 Experimental Results

In this study, we present the results of FSO channel samples collected from 9th - 20th November, 2015 for characterization. The acquired data on 12th

November 2015 at 01:45 pm as well as 09:30 pm are considered. The followings are the recorded weather conditions:

1. Scenario 1: 01:45 pm

   Temperature, 22 ^{o}C; wind, 6 mph; humidity, 69%; pressure, 1031 mb; visibility, 10 km; precipitation, 0 mm; and rain rate, 0%.

2. Scenario 2: 09:30 pm

   Temperature, 17 ^{o}C; wind, 4 mph; humidity, 80%; pressure, 1030 mb; visibility, 9 km; precipitation, 0 mm; and rain rate, 0%.

In order to carry out the FSO channel measurement, an unmodulated laser signal was injected into the FSO channel. The mean value recorded for the FSO channel path loss for the configuration and atmospheric conditions was 9 dB. With the aid of statistical calculations, the signal detected and received by the oscilloscope in real time was later evaluated offline by MATLAB.

The refractive-index structure parameter C_N^2 characterization is accomplished by fitting the nearest LN and the $\Gamma\Gamma$ pdf curves to the pdf of the received data. The obtained fittings are depicted in Figure 4.6.

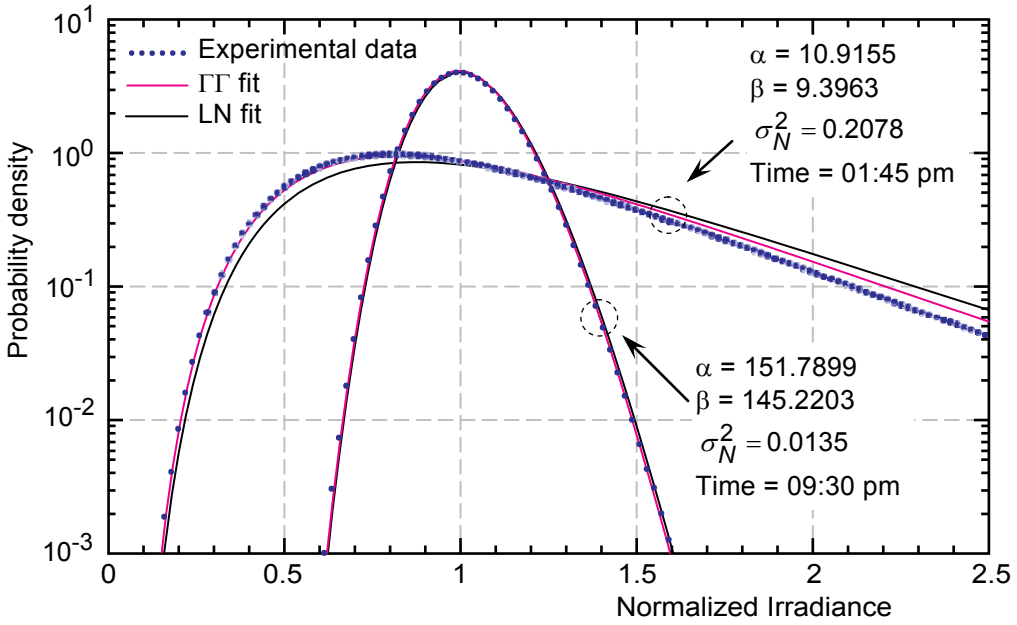

Figure 4.6: Experimental and fit histogram of normalized irradiance with log-normal (LN) and gamma-gamma ($\Gamma\Gamma$) fits under different scintillation index values.

We measure the scintillation index σ_N^2 for the two considered scenarios. The acquired values are 0.0135 and 0.2078 for 09:30 pm and 01:45 pm, respectively. For the former scenario in which σ_N^2 = 0.0135, the LN as well as the $\Gamma\Gamma$ fit very well with the measured channel samples σ_N^2. On the other hand, when σ_N^2 = 0.2078, the LN fitting is slightly loose and unable to offer an accurate result for the fading model. However, the $\Gamma\Gamma$ fitting still keeps a comparatively better outcome for the fading model. The result indicates that the LN model is inappropriate for the characterization of strong atmospheric fading.

In addition, the evaluated values of the refractive-index structure parameters C_N^2, are 6.7807×10^{-16} $m^{-2/3}$ (σ_N^2 = 0.0135) and 1.0864×10^{-14} $m^{-2/3}$ (σ_N^2 = 0.2078). Consequently, the first (σ_N^2 = 0.2078) and the second (σ_N^2 = 0.0135) scenarios match with the strong as well as weak turbulence regimes, respectively.

4.6 Research Contributions

The contributions of this chapter regarding the optical system, as well as to the channel models and channel characterization, are presented. With reference to the manuscripts [J3, B2], the SISO link is characterized by the data obtained from the experimental channel measurements. Moreover, the scintillation effects on system performance are evaluated for various turbulent conditions. In addition, the SISO FSO studies were extended to diversity schemes and proposed closed-form expressions for assessing the channel capacity of the MIMO FSO communication systems, considering atmospheric turbulence fading channels.

4.7 Conclusion

This chapter presents the experimental results of the channel characterization of the SISO FSO communication link. The presented results are based on channel measurements. Moreover, were presented the histograms of the FSO link samples in conjunction with the associated LN and $\Gamma\Gamma$ distributions fitting. Furthermore, it was established that the reliability of the FSO scheme is influenced considerably by the weather conditions.

References

[1] I. Alimi, A. Shahpari, V. Ribeiro, N. Kumar, P. Monteiro, and A. Teixeira, "Optical wireless communication for future broadband access networks", in *2016 21st European Conference on Networks and Optical Communications (NOC)*, Lisbon, June 2016, pp. 124–128, DOI: 10.1109/NOC.2016.750699.

[2] Z. Ghassemlooy, W. Popoola, and S. Rajbhandari, *Optical Wireless Communications: System and Channel Modelling with MATLAB*, 1st Edition, Taylor & Francis, August 2012, DOI: 10.1201/b12687, ISBN: 978-1-4398-5188-3.

[3] M. A. Khalighi and M. Uysal, "Survey on Free Space Optical Communication: A Communication Theory Perspective", *IEEE Communications Surveys & Tutorials*, vol. 16, no. 4, pp. 2231–2258, 2014, DOI:10.1109/COMST.2014.2329501

[4] S. M. Navidpour, M. Uysal, and M. Kavehrad, "BER Performance of Free-Space Optical Transmission with Spatial Diversity", *IEEE Transactions on Wireless Communications*, vol. 6, no. 8, pp. 2813–2819, August 2007, DOI: 10.1109/TWC.2007.06109

[5] I. A. Alimi, A. M. Abdalla, J. Rodriguez, P. P. Monteiro, and A. L. Teixeira, "Spatial Interpolated Lookup Tables (LUTs) Models for Ergodic Capacity of MIMO FSO Systems", *IEEE Photonics Technology Letters*, vol. 29, no. 7, pp. 583–586, April 2017, DOI: 10.1109/LPT.2017.2669337

[6] I. Alimi, P. Monteiro, and A. Teixeira, "Analysis of Atmospheric Effects on RF Signal Transmission over the Optical Wireless Communication Links", in *XIII Symposium on Enabling Optical Networks and Sensors (SEONS)*, Covilhã, July 2016, pp. 35–38.

[7] T. S. Rappaport, S. Sun, R. Mayzus, H. Zhao, Y. Azar, K. Wang, G. N. Wong, J. K.

Schulz, M. Samimi, and F. Gutierrez, “Millimeter Wave Mobile Communications for 5G Cellular: It Will Work!” *IEEE Access*, vol. 1, pp. 335–349, 2013, DOI: 10.1109/ACCESS.2013.2260813.

[8] J. G. Andrews, S. Buzzi, W. Choi, S. V. Hanly, A. Lozano, A. C. K. Soong, and J. C. Zhang, “What Will 5G Be?” *IEEE Journal on Selected Areas in Communications*, vol. 32, no. 6, pp. 1065–1082, June 2014, DOI: 10.1109/JSAC.2014.2328098.

[9] H. Mehrpouyan, M. R. Khanzadi, M. Matthaiou, A. M. Sayeed, R. Schober, and Y. Hua, “Improving Bandwidth Efficiency in E-Band Communication Systems”, *IEEE Communications Magazine*, vol. 52, no. 3, pp. 121–128, March 2014, DOI: 10.1109/MCOM.2014.6766096.

[10] K. Wakamori, K. Kazaura, and I. Oka, “Experiment on Regional Broadband Network Using Free-Space-Optical Communication Systems”, *Journal of Lightwave Technology*, vol. 25, no. 11, pp. 3265–3273, Nov 2007, DOI: 10.1109/JLT.2007.906825.

[11] A. Shahpari, A. Abdalla, R. Ferreira, G. Parca, J. D. Reis, M. Lima, V. Carrozzo, G. T. Beleffi, and A. Teixeira, “Ultra-High-Capacity Passive Optical Network Systems with Free-Space Optical Communications”, *Fiber and Integrated Optics*, vol. 33, no. 3, pp. 149–162, July 2014, DOI: 10.1080/01468030.2014.886751.

[12] A. Mostafa and S. Hranilovic, “Channel measurement and Markov modeling of an urban free-space optical link”, *IEEE/OSA Journal of Optical Communications and Networking*, vol. 4, no. 10, pp. 836–846, Oct 2012, DOI: 10.1364/JOCN.4.000836.

[13] L. Yang, M. O. Hasna, and X. Gao, “Performance of Mixed RF/FSO With Variable Gain over Generalized Atmospheric Turbulence Channels”, *IEEE Journal on Selected Areas in Communications*, vol. 33, no. 9, pp. 1913–1924, Sept 2015, DOI: 10.1109/JSAC.2015.2432471.

[14] G. Parca, A. Shahpari, V. Carrozzo, G. M. Tosi Beleffi, and A. L. J. Teixeira, “Optical wireless transmission at 1.6-Tbit/s (16 × 100 Gbit/s) for next-generation convergent urban infrastructures”, *Optical Engineering*, vol. 52, no. 11, pp. 116102 (1-5), November 2013, DOI: 10.1117/1.OE.52.11.116102.

[15] C. B. Naila, A. Bekkali, K. Wakamori, and M. Matsumoto, “Performance Analysis of CDMA-Based Wireless Services Transmission Over a Turbulent RF-on-FSO Channel”, *IEEE/OSA Journal of Optical Communications and Networking*, vol. 3, no. 5, pp. 475– 486, May 2011, DOI: 10.1364/JOCN.3.000475.

[16] H. E. Nistazakis, G. S. Tombras, A. D. Tsigopoulos, E. A. Karagianni, and M. E. Fafalios, “Capacity estimation of optical wireless communication systems over moderate to strong turbulence channels”, *Journal of Communications and Networks*, vol. 11, no. 4, pp. 384–389, August 2009,
DOI: 10.1109/JCN.2009.6391352.

[17] M. A. Esmail, H. Fathallah, and M. S. Alouini, “Outdoor FSO Communications Under Fog: Attenuation Modeling and Performance Evaluation”, *IEEE Photonics Journal*, vol. 8, no. 4, pp. 1–22, Aug 2016, DOI: 10.1109/JPHOT.2016.2592705.

[18] W. O. Popoola and Z. Ghassemlooy, “BPSK Subcarrier Intensity Modulated Free-Space Optical Communications in Atmospheric Turbulence”, *Journal of Lightwave Technology*, vol. 27, no. 8, pp. 967–973, April 2009, DOI: 10.1109/JLT.2008.2004950.

[19] B. Epple, “Simplified Channel Model for Simulation of Free-Space Optical Communications”, *IEEE/OSA Journal of Optical Communications and Networking*, vol. 2, no. 5, pp. 293–304, May 2010, DOI: 10.1364/JOCN.2.000293.

[20] Larry C. Andrews, Ronald L. Phillips, *Laser Beam Propagation through Random Media*, Second edition, Publisher: SPIE Optical Engineering Press, 2005, ISBN: 0819459488, DOI: 10.1117/3.626196

[21] A. Mansour, R. Mesleh, and M. Abaza, “New challenges in wireless and free space optical communications”, *Optics and Lasers in Engineering*, vol. 89, pp. 95-108, 2016, DOI: 10.1016/j.optlaseng.2016.03.027. [Online]. http://www.sciencedirect.com/science/article/pii/S0143816616300252

[22] J. Zhang, L. Dai, Y. Han, Y. Zhang, and Z. Wang, “On the Ergodic Capacity of MIMO Free-Space Optical Systems Over Turbulence Channels”, *IEEE Journal on Selected Areas in Communications*, vol. 33, no. 9, pp. 1925–1934, Sept 2015, DOI: 10.1109/JSAC.2015.2452631.

[23] D. A. Luong and A. T. Pham, “Average capacity of MIMO free-space optical gamma- gamma fading channel”, in *2014 IEEE International Conference on Communications (ICC)*, Sidney, June 2014, pp. 3354–3358, DOI: 10.1109/ICC.2014.6883839.

[24] P. Kaur, V. K. Jain, and S. Kar, “Capacity of free space optical links with spatial diversity and aperture averaging”, *2014 27th Biennial Symposium on Communications (QBSC)*, Kingston, June 2014, pp. 14–18, DOI: 10.1109/QBSC.2014.6841175.

[25] H. AlQuwaiee, I. S. Ansari, and M. S. Alouini, “On the Performance of Free-Space Optical Communication Systems Over Double Generalized Gamma Channel”, *IEEE Journal on Selected Areas in Communications*, vol. 33, no. 9, pp. 1829–1840, Sept 2015, DOI: 10.1109/JSAC.2015.2432529.

[26] M. Cao, H. Wang, K. Jia, and L. Hou, “Free Space Optical Communication Based on V-BLAST”, in *2010 Symposium on Photonics and Optoelectronics*, Chengdu, June 2010, pp. 1–4, DOI: 10.1109/SOPO.2010.5504146

[27] H. E. Nistazakis, E. A. Karagianni, A. D. Tsigopoulos, M. E. Fafalios, and G. S. Tombras, “Average Capacity of Optical Wireless Communication Systems Over Atmospheric Turbulence Channels”, *Journal of Lightwave Technology*, vol. 27,

no. 8, pp. 974–979, April 2009, DOI: 10.1109/JLT.2008.2005039.

[28] L. Yang, J. Cheng, and J. F. Holzman, “Maximum Likelihood Estimation of the Lognormal-Rician FSO Channel Model”, *IEEE Photonics Technology Letters*, vol. 27, no. 15, pp. 1656–1659, Aug 2015, DOI: 10.1109/LPT.2015.2433871.

[29] M. Al Naboulsi, H. Sizun, and F. de Fornel, “Fog attenuation prediction for optical and infrared waves”, *Optical Engineering*, vol. 43, no. 2, pp. 319–329, 2004, DOI: 10.1117/1.1637611

[30] A. A. Farid and S. Hranilovic, “Outage Capacity Optimization for Free-Space Optical Links With Pointing Errors”, *Journal of Lightwave Technology*, vol. 25, no. 7, pp. 1702– 1710, July 2007, DOI: 10.1109/JLT.2007.899174.

[31] H. G. Sandalidis, T. A. Tsiftsis, and G. K. Karagiannidis, “Optical Wireless Communications With Heterodyne Detection Over Turbulence Channels With Pointing Errors”, *Journal of Lightwave Technology*, vol. 27, no. 20, pp. 4440–4445, Oct 2009, DOI: 10.1109/JLT.2009.2024169.

[32] K. Kiasaleh, “Performance of APD-based, PPM free-space optical communication systems in atmospheric turbulence”, *IEEE Transactions on Communications*, vol. 53, no. 9, pp. 1455–1461, Sept 2005, DOI: 10.1109/TCOMM.2005.855009.

[33] C. L. Tran, T. A. Wysocki, A. Mertins, and J. Seberry, “Multiple-Input Multiple-Output Systems with Space-Time Codes”, in *Complex Orthogonal Space-Time Processing in Wireless Communications*, Springer-Verlag, Boston, US, 2006, ch. 2, pp. 9–58, DOI: 10.1007/978-0-387-29544-2_2.

[34] K. P. Peppas, A. N. Stassinakis, G. K. Topalis, H. E. Nistazakis, and G. S. Tombras, “Average capacity of optical wireless communication systems over I-K atmospheric turbulence channels”, *IEEE/OSA Journal of Optical Communications and Networking*, vol. 4, no. 12, pp. 1026–1032, Dec 2012,
DOI: 10.1364/JOCN.4.001026.

[35] F. S. Vetelino, C. Young, L. Andrews, and J. Recolons, “Aperture averaging effects on the probability density of irradiance fluctuations in moderate-to-strong turbulence”, *Applied Optics*, vol. 46, no. 11, pp. 2099–2108, Apr 2007, DOI: 10.1364/AO.46.002099.

[36] A. Khatoon, W. G. Cowley, and N. Letzepis, “Channel measurement and estimation for free space optical communications”, in *2011 Australian Communications Theory Workshop*, Melbourne, Jan 2011, pp. 112–117, DOI: 10.1109/AUSCTW.2011.5728747.

[37] F. S. Marzano, S. Mori, F. Frezza, P. Nocito, G. M. T. Beleffi, G. Incerti, E. Restuccia, and F. Consalvi, “Free-space optical high-speed link in the urban area of southern Rome: Preliminary experimental set up and channel modelling”, in *Proceedings of the 5th European Conference on Antennas and Propagation (EUCAP)*, Rome, April 2011, pp. 2737–2741.

[38] K. H. Kim, T. Higashino, K. Tsukamoto, and S. Komaki, “Optical fading analysis considering spectrum of optical scintillation in terrestrial free-space optical channel”, in *2011 International Conference on Space Optical Systems and Applications (ICSOS)*, Santa Monica, May 2011, pp. 58–66, DOI: 10.1109/ICSOS.2011.5783710.

Chapter 5

Real-Time Coherent PON OWC based on Dual-Polarization for the Mobile Backhaul/Fronthaul

This chapter presents the main achievements attained by conducting the experimental work in [J2, J4], and also, discuss the results obtained in laboratory work described in [J1, J3, C1-C3, B2]. In general, this chapter presents the work carried out experimentally from proof of concept, implemented on long-range coherent PON systems integrating OWC and capable to transmit in gigabit. Moreover, the performance of a system simultaneously transmitting data traffic in the GPON standard and the optical signal of a CATV system is experimentally validated using a bidirectional link in FSO and 20 km of SMF. In addition, the implementations of FSO interfaces used to couple the optical beam between the SMF and the PF-POF are studied. The considered configurations, implemented in a logic of optical transparency of transmission by paths of diverse nature, validate the ability of the optical paths can be shared simultaneously by several applications.

5.1 Introduction

The advent of the IoT has pushed the connections of billions of smart devices to the Internet. It has been surveyed that, almost 5 to 9 billion connected devices have been evaluated for a market size of about 700 billion in 2015. In addition, approximately 25 to 50 billion IoT devices are to be adopted each year. This denotes annual increments of 17 to 32 percent in the system [6]. Consequently, the growing Internet traffic demands for subsequent network upgrade. Therefore, network operators have been improving their systems with regard to 5G, taking advantage of the associated high-capacity of fiber-optic infrastructures and upgrading the spectral efficiency (SE) of their networks.[J4].

It should be noted that the existing FTTH scheme is based on TDM-PON in which one or two wavelengths are implemented. This commonly employed technique in the optical networks may be a limitation to support the envisioned bandwidth requirements by the system. In an effort to overcome this limitation, WDM-PONs have been widely studied as viable architectures for future access networks. WDM-PONs systems have good scalability features that can be scaled to dense WDM PON (DWDM-PON), as well as ultra-dense WDM PON (UDWDM-PON) schemes, which may be a solution when channel bandwidth is reduced [C1, C2, 7]. Additionally, a robust, flexible and spectrally efficient PON system can be achieved by employing coherent optical technologies that are established in software-defined transceivers based on digital signal processing (DSP) [J1, 8]. The SE as well as the number of users in the stipulated wavelength can be increased by the use of coherent PONs with complex modulation and dual-polarization (DP) transceivers [9,10]. Nevertheless, the application for commercial purposes by the mobile network operators is limited by the high cost of the transceiver. Therefore, research on cost-effective transceiver is very essential for system improvement [11]. In addition, the implementation of cost-effective DSP can aid in lessening the hardware implementation cost. Besides, DSP with polarization demultiplexing (PolDemux) technique can be of good assistance in automatic polarization control. Moreover, owing to its robustness, simplicity, and immunity to phase noise, constant modulus algorithm (CMA) can

also be implemented for blind equalization as well as PolDemux [J4, 5, 12].

Moreover, it should be noted that there are some geographic areas of the network where physical connections through fiber optic cables are unrealistic or in rural area where fiber infrastructure is not available, and where FSO connections may be the appropriate solution for connectivity [J2]. As previously stated, FSO connections has various advantages that encourages their use for broadband access connectivity in an effort to meet next-generation networks (NGN) bandwidth demands [J2, J3, C1, 1, 3]. Also, the notion of radio signal transmission over FSO (RoFSO) takes advantage of the high capacity provided by the optical technologies in addition to the ease of implementation of wireless systems. Consequently, the DWDM RoFSO system is capable of transmitting multiple wireless signals simultaneously [J4, 4].

The intensity-modulations (IM) schemes have been extensively used in FSO systems. It should be noted that schemes such as coherent UDWDM, advanced modulation formats, and DP can be employed to further improve the transmission coverage and capacity of the FSO system. Unlike the IM systems, the DP schemes are not conditioned by the non-linear response of the intensity modulators and are invulnerable to the laser phase noise. Furthermore, the DP schemes have the ability to prevent turbulence-induced fading. This is due to the fact that polarization states are better conserved than the phase and amplitude of the optical signal during propagation [12]. Moreover, coherent FSO systems exhibit greater sensitivity at the receiver and also allow substantial rejection of background noise as well as intentional interference. Besides, coherent FSO systems allow the transmission of information in the phase, amplitude or polarization of the optical field, aiding in the substantial enhancement of the system's SE. Nevertheless, as aforementioned, intensity-modulation/direct-detection (IM/DD) schemes are widely used because of their related low implementation cost and complexity. However, the current improvement involving integrated coherent receivers and high-speed DSP circuits stimulates interest in the implementation of coherent FSO systems [J4, 2].

The remaining chapter is organized as follows: In Section 5.2, experimental validation of coherent long-reach and gigabit-capable UDWDM-PON and FSO

systems is presented. Section 5.3, describes the experimental demonstration of a work that involved the GPON data traffic and the CATV optical signal transmission through a connection formed by two bidirectional FSO sections and 20 km of SMF. Research contributions are presented in Section 5.4 while conclusions are given in Section 5.5.

5.2 Real-Time Gigabit-capable Long-reach Coherent UWDM- PON and FSO Systems

This section describes and analyzes the results obtained experimentally by a coherent long-reach and gigabit-capable UDWDM-PON system as by the presence of a FSO section on the transmission link. The presented system is able to support several applications in the same fiber optic infrastructure in a mobile backhaul (MBH) network, as illustrated in Figure 5.1. Furthermore, for the first time, real-time and reconfigurable DSP reception of DP-QPSK signals through silicon SMF and FSO medium is presented. The receiver system employed is based on commercial field-programmable gate array (FPGA). The analyzed MBH network is structurally based on 20 UDWDM channels, distanced each other from 2.5 GHz and 625 Mbaud per channel. Signal transmission and reception over 100 km of SMF as well as over a hybrid 100 km of SMF and a 54 m outdoor FSO link is considered. The lowest sampling rate required for coherent digital PON was achieved by implementing four 1.25 Gs/s ADCs using an electrical front-end receiver that provides only 1 GHz of analog bandwidth. This is achieved using a coherent receiver with phase and polarization diversity, along with the DP-QPSK modulation format [12]. This technique is essential for lowering the electrical digital blocks required in the ONU, considering the radiofrequency (RF) rates. This transmission scenario meets the predicted data rate for next-generation coherent optical access networks [J4, C1, B2].

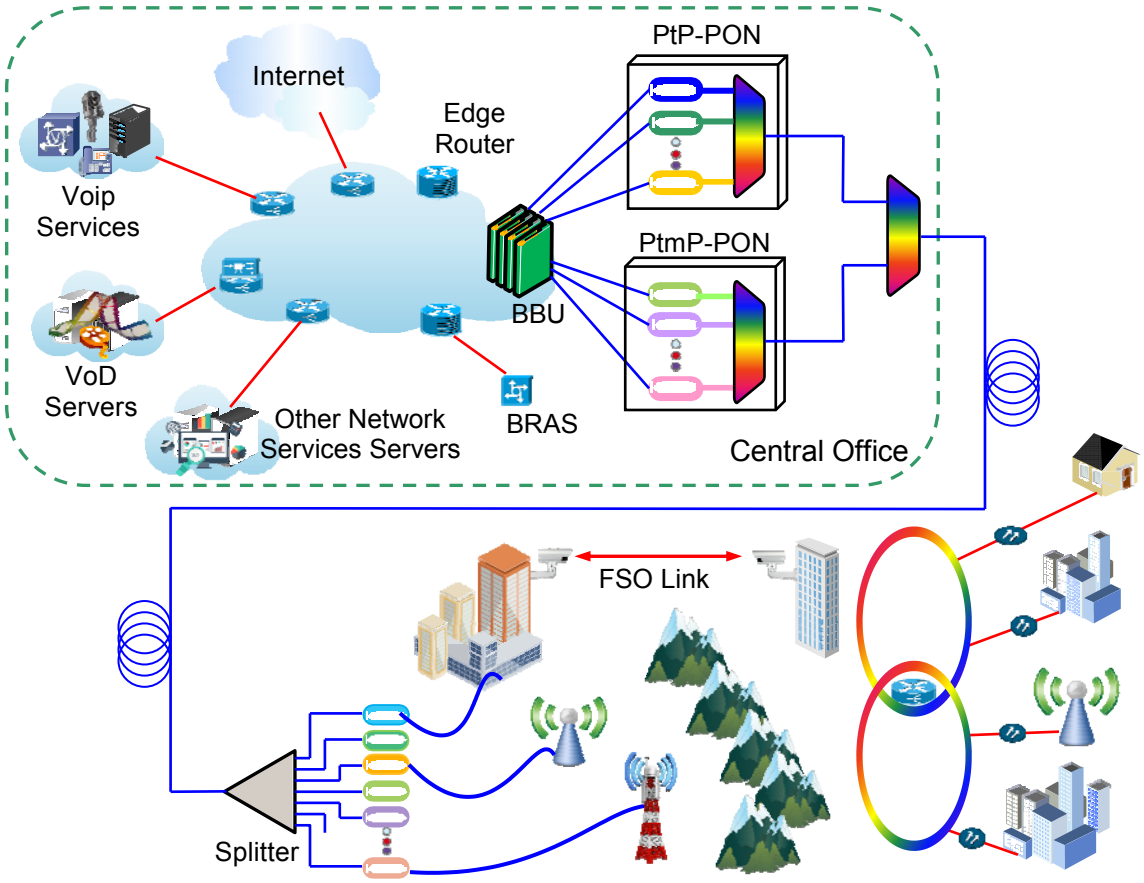

Figure 5.1: Gigabit-capable long-reach coherent UDWDM-PON and FSO systems for mobile backhaul (MBH) networks.
(BRAS: broadband remote access server; BBU: baseband unit)

5.2.1 Experimental Setup

The experimental configuration I use to validate the performance of the UDWDM-PON system containing a hybrid link formed by sections in SMF and FSO and with an optical signal in DP is shown in Figure 5.2 (a). In the implemented configuration, the information presented to the DSP in the receiver is estimated in real time. The UDWDM grid in the OLT is formed by injecting the light from four external cavity laser (ECL) with 100 kHz linewidth in the two IQ

modulators (IQMs). Regarding the configuration of the ECL lasers, wavelength λ_2 is centered at ~1549 nm. As for the wavelengths λ_1, λ_3 and λ_4, these are shifted from λ_2 by -5, -2.5 and +2.5 GHz, respectively. Next, the IQM_1 modulator is powered by lasers with wavelengths λ_1 and λ_2, and driven by a 65 Gs/s arbitrary waveform generator (AWG). By the same process, the λ_3 and λ_4 lasers power the IQM_2, which is driven by another AWG (AWG_2) generating 16 Gs/s.

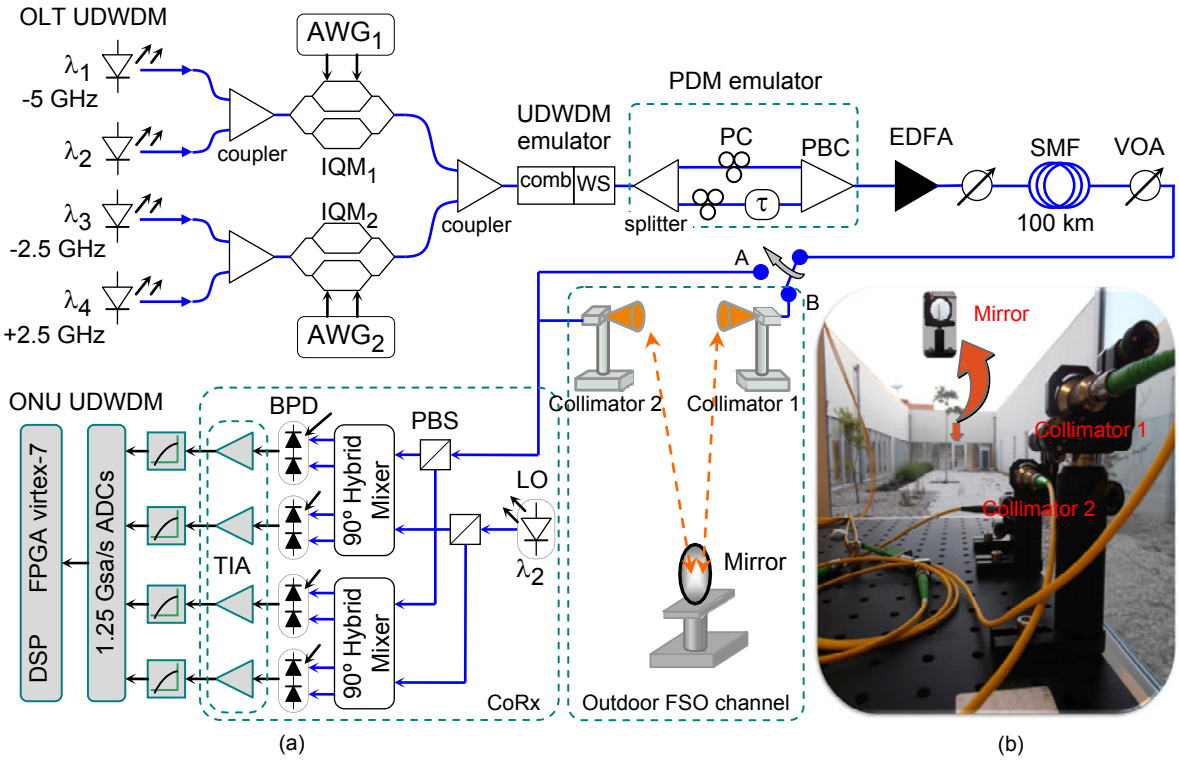

Figure 5.2: (a) Experimental setup for 20 × 625 Mbaud DP-QPSK signal; (b) Overall outdoor scenario; (PBS/C: polarization beam splitter/combiner; BPD: balanced photo-detector; CoRX: coherent receiver; WS: wavelength selective switch).

Therefore, the two AWGs generate signals at 625 Mbaud with a pseudo-random binary sequence (PRBS) with a pattern length of $2^{12}-1$. Furthermore, the subsequent signal is digitally filtered by means of a raised-cosine (RC) filter

with a roll-off factor of 0.1, in addition to 32-taps and 3-taps FIR filters, as well as a simple FIR filter of the pre-emphasis subsystem, respectively [J1, J4]. DP-QPSK is the modulation format implemented, which offers 2.5 Gb/s per end-user. Moreover, after modulation, the four created channels are subsequently combined and injected into an optical comb generator. This is the effort required to replicate the four channels to a total of 20 channels, with 2.5 GHz channel spacing. Figure 5.3 (a) illustrates the 4-channel spectrum. The resulting UDWDM grid for the 20 channels is shown in Figure 5.3 (b).

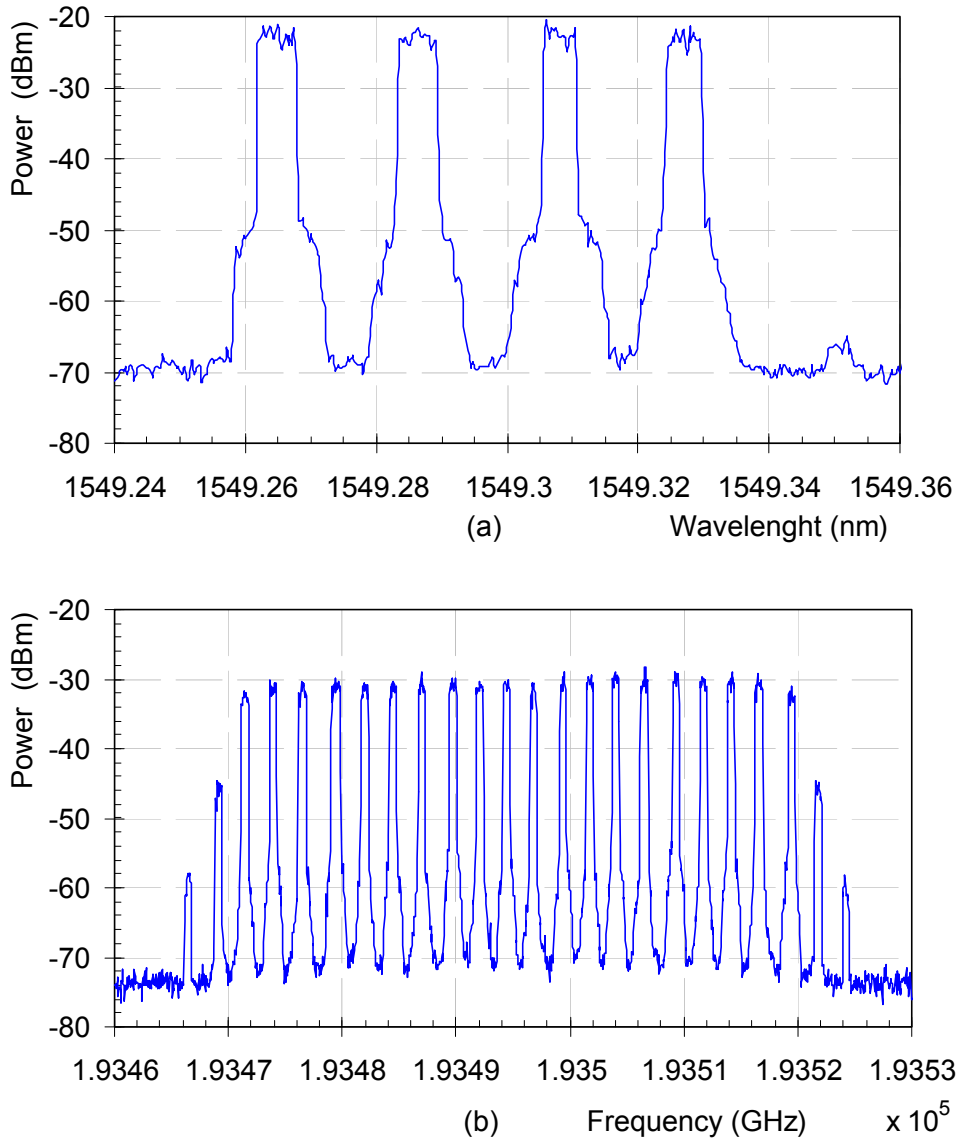

Figure 5.3: Spectrum of (a) 4-channels and (b) 20-channels.

The spectral width displayed by the UDWDM channels is about 750 MHz when measured at -20 dB of the wavelength peaks [J4].

The resulting signal is split into two branches by an optical splitter in order to emulate a polarization-division multiplexing (PDM) system. The two optical signals are then adjusted and orthogonally polarized through polarization controllers (PC). For reasons of information de-correlation between the two branches, a delay of 12 symbols is applied to the optical signal of one of the branches. Thereafter, the two orthogonally polarized signals are multiplexed in a single one through a polarization beam combiner (PBC). This gives rise to a resulting double polarization signal. Subsequently, the signal is transmitted only through a SMF with a length of 100 km (switch in the A position) or through the SMF and 54 m in outdoor FSO (switch in position B). The optical power delivered to the SMF input is regulated through a variable optical attenuator (VOA) and an EDFA operating in the C-band with 20 dB of optical gain and 4.5 dB of noise figure. The SMF input power was set to −10 dBm [J4, J5, B2].

At the receiver, the signal is coherently detected using a 4 × 90° optical hybrid on the receiver side. This is achieved through a free-running, 100 kHz linewidth ECL, acting as a local oscillator (LO), tuned to the frequency of the channel to be captured. In the development of this work, as shown in Figure 5.2, the center frequency of λ_2 channel was used as the value for LO frequency. Following the receiver, four balanced detectors (BD) are used for optical signal conversion to the electrical domain. Transimpedance amplifiers (TIAs) then amplify the resulting signal. Therefore, the process performed by the coherent detection module (CoRx) presents, at the output of the TIA, the in-phase and quadrature components of both polarizations of the channel previously selected by the LO. Low-pass filters of 1 GHz are then employed to filter the signals at the output of the TIAs, which are subsequently sampled through four 8-bit ADCs and 1.25 Gs/s.

Then the digitalized signal is sent to a Virtex-7 FPGA, where all 8-bit DSP post-detection is performed in real time. The DSP used is that based on [12] and the method to perform the required polarization tracking was the CMA. In

addition, the BER is measured in real-time using the bit error count, which is calculated by the average between the two polarizations. It should be noted that the DSP clock is set to 156.25 MHz. This result shows a degree of polarization (DOP) of 0.8, thus reaching 1.25 Gs/s for the sampling rate. The implementation is due to the fact that, the majority of my DSP operations are based on 8-bit of resolution [J1, J4, B2].

Also, I performed the implementation of an external FSO path as part of the transmission link of the considered UDWDM system. Figure 5.2 (b) shows the external configuration image of the FSO setup. The coherent FSO connection employed consists of two optical fiber collimators as well as a concave mirror with aluminum reflector. The meteorological conditions recorded for the FSO link were as follows: wind, 12 km/h; temperature, 10 °C; and relative humidity, 73%. The collimated laser beam emitted by the transmitter collimator passes through the atmospheric FSO channel, in a total length of 54 m. After traversing the initial 27 m, the emitted optical beam is reflected by a concave mirror, returning the beam to the neighborhood of the emitter collimator. Therefore, after traversing the 54 m of the FSO channel, the reflected beam with a final diameter of ~ 4 mm is collected by the receiver collimator [J3, 1]. It was estimated for the FSO outdoor communication link, an aggregate loss of about 8 to 9 dB. Therefore, after the signal is received in the collimator, it is channeled to the integrated phase and polarization-diversity coherent receiver [J4].

5.2.2 Experimental Results and Discussion

Figure 5.4 shows the receiver sensitivity to the measured BER for the center channel (λ_2). The measurement is made considering the DP-QPSK and the transmitted power per channel at the output of the transmitter is set at -10 dBm. Figure 5.4 shows the results for the back-to-back (B2B), 100 km SMF and 100 km SMF plus 54 m FSO scenarios. It should be noted that for each scenario, the transmissions of 1, 4, and 20 UDWDM channels are studied, respectively. In this study, the BER limit of 3.8×10^{-3}, which is compatible with the application of

the 7% hard-decision forward error correction (HD-FEC) codes, is taken into account. Considering 100 km of fiber and 20 channels, the observed sensitivity for the DP-QPSK is almost -44 dBm. For the stated BER limit and for 20 channels, the comparative penalty observed between the signals in B2B and with 100 km of SMF is ≤ 1 dB. Likewise, for the scenario of 20 channels through 100 km of SMF plus 54 m of a FSO link, the observed sensitivity is ~ -42 dBm. Relating this to the B2B scenario brings about a penalty of ~2 dB. Moreover, considering the scenario of 20 channels over 100 km of SMF plus 54 m of FSO, Figure 5.5 illustrates the BER variation in real-time during 1 h 40 min of link operation, considering the received power from the DP-QPSK of -38 dBm. The obtained result shows a comparatively stable performance during the measurement [J4].

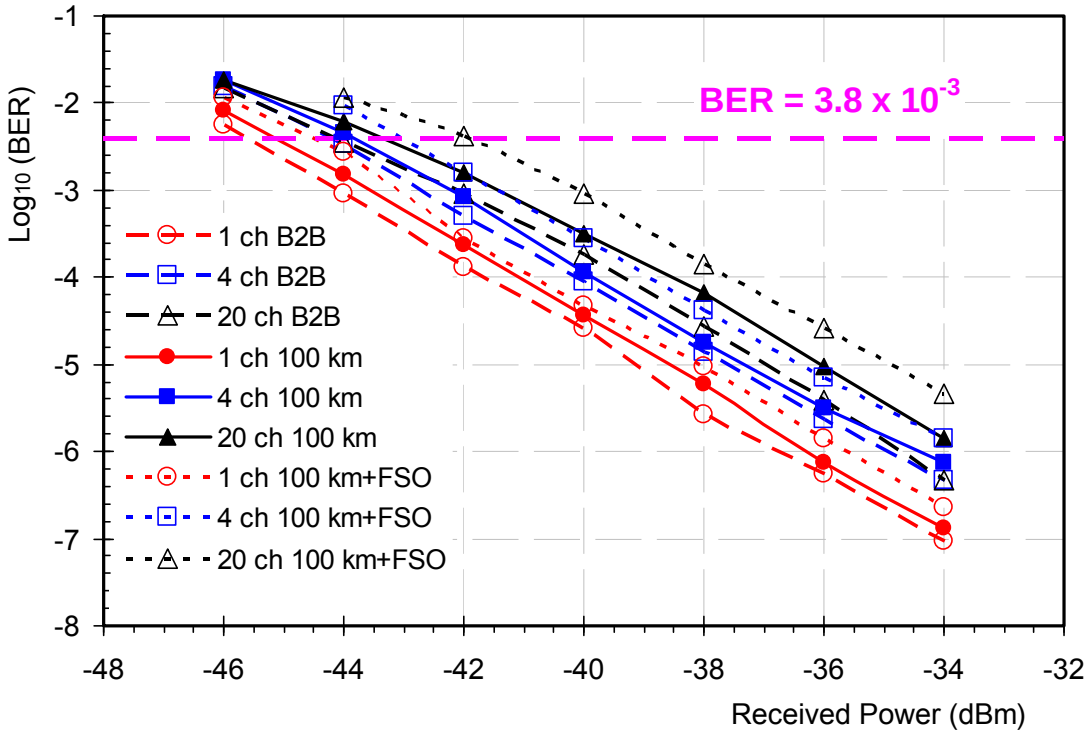

Figure 5.4: Receiver sensitivity in terms of BER, for DP-QPSK signals and obtained for the center channel (λ_2).

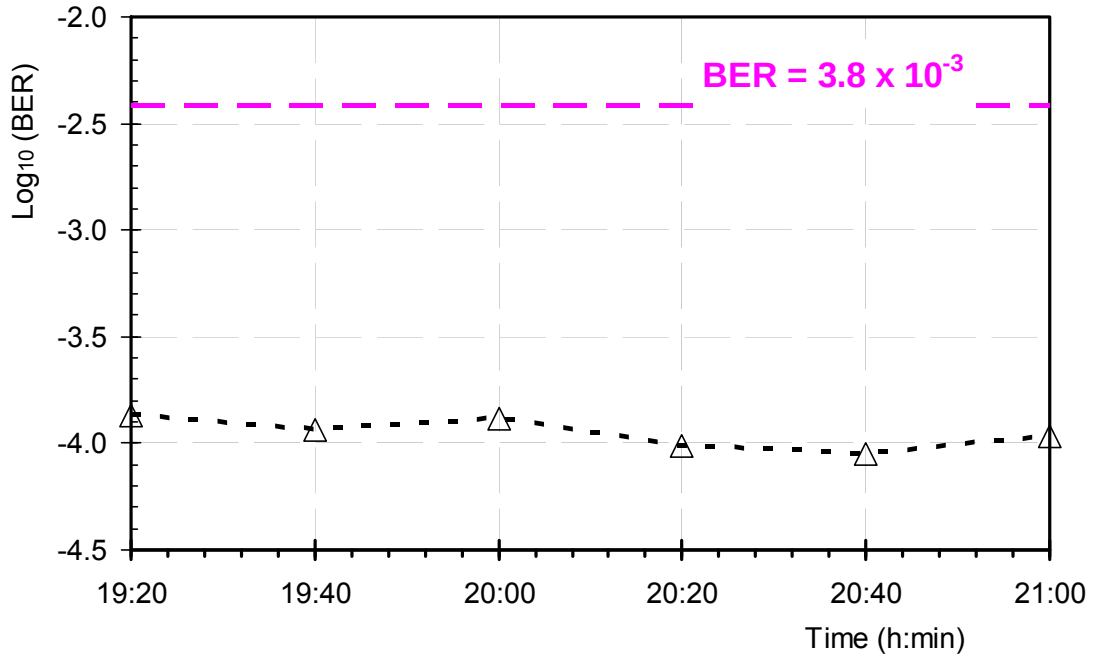

Figure 5.5: Variation of BER versus time, for 20 channels transmitted through a link of 100 km in SMF and 54 m in FSO, for the DP-QPSK data format and -38 dBm of received power.

5.3 Gigabit PON and CATV over Hybrid FSO and SMF with Bidirectional Transmission

In this section, the performance of a system involving the combined transmission of data traffic in GPON and the CATV optical signal is demonstrated experimentally through a bidirectional connection formed by two sections in FSO and a 20 km section in SMF, as shown in Figure 5.6. In the study, FSO transmission in indoor and outdoor atmospheric environments is taken into account. The metrics used for performance evaluation are the packet error rate (PER) and the carrier-to-noise-ratio (CNR) for the GPON transmission and for CATV signal degradation, respectively.

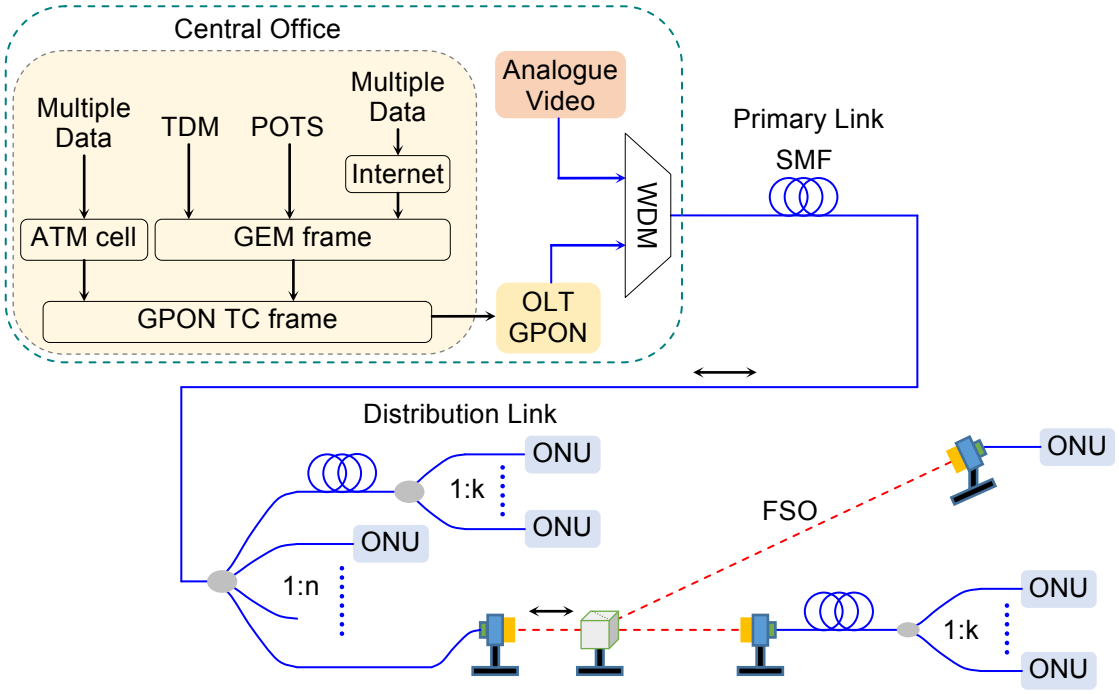

Figure 5.6: GPON traffic structure and the proposed FSO links.

5.3.1 Experimental Setup

In this subsection, the optical link performance is analyzed taking into account the different transmission paths proposed and their combinations. Figure 5.7 illustrates the experimental setup, which comprises FSO sections plus 20 km of SMF. The FSO beam will travel an internal path (InFSO) of 17.5 m if the switch (SW) is in position A, or an external path (OutFSO) of 27.5 m if the SW is in position B. In the assembled configuration, the InFSO section was established within a closed and controlled environment (hallways of a building), while the OutFSO section was established in a turbulent environment, conditioned by atmospheric variations.

The values of the atmospheric parameters recorded during the experiment involving the OutFSO channel were: 91% relative humidity, an average temperature of 12 °C and 5 m/s for the average wind speed. The “IXIA©

Generator and Traffic Analyzer" (IGTA) previously created the data traffic sent by the OLT. The data frames were sent by the OLT downstream to the ONU, using 1490 nm for the wavelength at a binary rate of 630 Mbps. The IGTA is also responsible for producing and distributing user data traffic to the ONU. Subsequently, this traffic is sent from the ONU to the OLT (upstream direction) at 1310 nm using a binary rate of 560 Mbps. Furthermore, IGTA helps to determine the packet error rate (PER) or data packet loss (DPL) of downstream traffic received by the ONU or received upstream by the OLT.

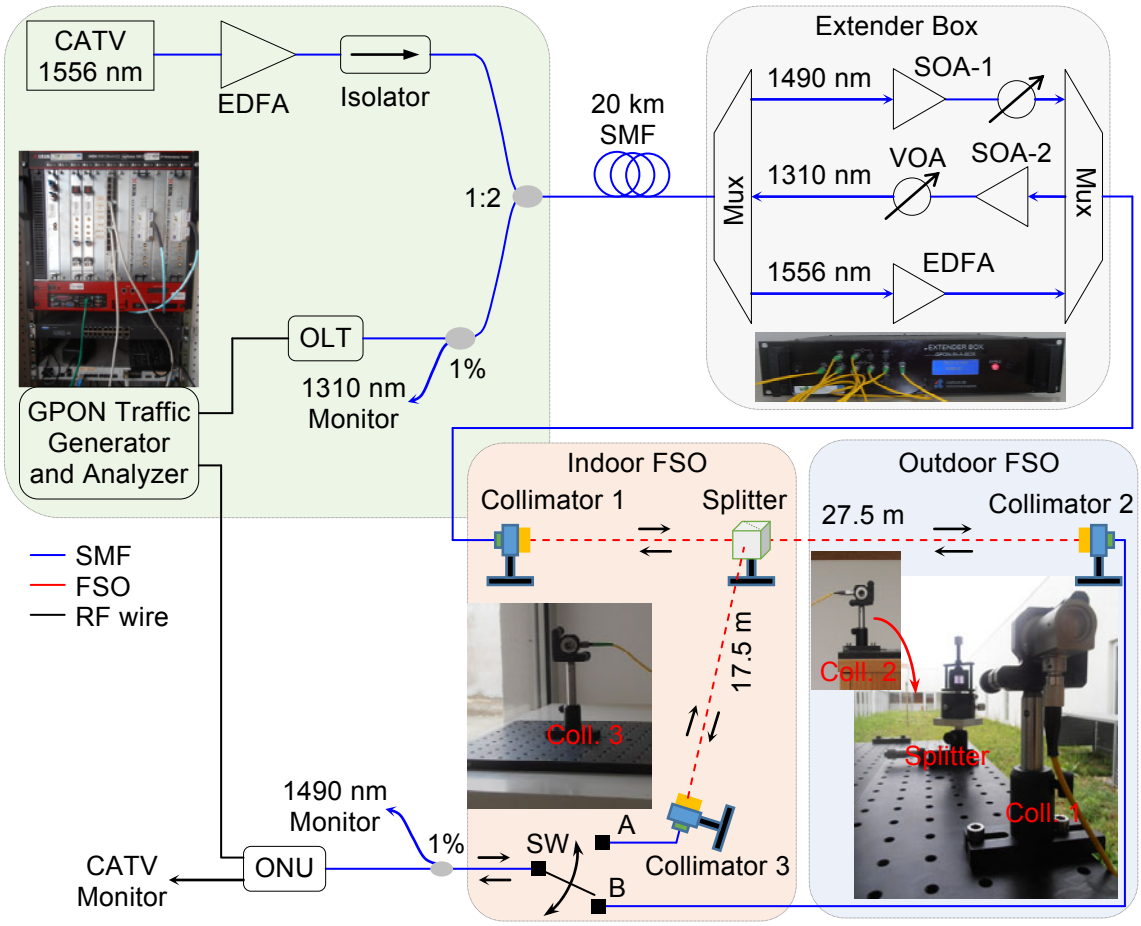

Figure 5.7: Experimental configuration of the GPON and CATV system through the hybrid transmission medium formed by SMF and an atmospheric link in FSO.

According to the ITU recommendations on the video overlay on the GPON system [13], a sample of the CATV signal was obtained from a public telecommunications operator. The captured signal comprised 40 analog channels in the range of 180 to 860 MHz (channel 26 - ITU-100), which modulated the wavelength of 1556.56 nm. The CATV signal started to be amplified by means of an EDFA and placed in the optical network through a 50:50 optical coupler. The signal, after reaching the ONUs, was then distributed to the respective users.

The FSO link in this work was implemented by means of fiber collimators. Through concave mirrors, these collimators capture the optical beam emanated (and divergent) by the SMF, collimate and launch it in free space. This process is necessary to reduce beam scattering and maximize power transfer. Due to the presence of three relatively spaced wavelengths which are present in the GPON + CATV system (i.e., 1310, 1490 and 1556.55 nm), collimators are used in which collimation of the optical beam is performed by reflection on the surface of a mirror. The collimators used allow mechanical adjustment, so that the three wavelengths can be simultaneously adjusted for maximum power transfer and without significant variations between them. It should be noted that collimators in which collimation is made by refraction through lenses have wavelength-dependent focal points, which leads to disproportionate attenuations when dealing with the presence of different wavelengths in the optical beam.

Noted that the FSO transmission, as well as the used collimators in this system, imposes significant losses in optical transmission. An Extender Box (ExB), which assists in the amplification of the optical beam, compensated this excess attenuation. In the ExB, two multiplexers split up the optical signals into three distinct wavelength signals, amplifying them separately by means of semiconductor optical amplifiers (SOA) at the wavelength of 1490 nm (SOA-1), 1310 nm (SOA-2) and an EDFA at 1556.56 nm. It should be noted that Variable Optical Attenuators (VOA), located at wavelengths of 1310 and 1490 nm, are used to optimize GPON link gain for both upstream/downstream directions. This allows the analysis of the PER versus optical beam sensitivity at the input of the OLT as well as the ONU.

5.3.2 Experimental Results and Discussion

DPL analysis in GPON was carried out by using the PER values offered by the IGTA equipment. The power sensitivity at the ONU input was determined with the aid of a VOA, which varies power only at the wavelength of 1490 nm, as well as by means of a coupler (1%). In the same way and upstream, the power sensitivity at the OLT input was evaluated by a VOA, which varies power only at the wavelength of 1310 nm, as well as by means of a coupler (1%). In this way, the results of the optical connection configurations between OLT and ONU were obtained considering this connection in back-to-back (B2B), or with 20 km of SMF or with the InFSO section. In addition, the configuration with the 20 km of SMF plus the InFSO section (SMF + InFSO) and the configuration with the SMF and OutFSO section (SMF + OutFSO) was tested. In previous configurations, SMF + InFSO and SMF + OutFSO, optical amplification using ExB was used. Figure 5.8 shows the PER results measured for the five tested configurations, taking into consideration the optical power at the ONU input, Figure 5.8 *a)*, and at the OLT input, Figure 5.8 *b)*.

The experimental data of the degradation of the sensitivity for the different configurations, considering as reference the B2B configuration and a PER of 10^{-3} %, are given in Table 5.1. When the results of the SMF + InFSO and SMF settings are related, there is an increase in sensitivity degradation of 1.6 dB and 1.3 dB for downstream and upstream, respectively.

Similarly, because of the atmospheric turbulence and scintillation present in the space-free section of the optical path in the SMF + OutFSO link, there is an increase in degradation of 2.8 dB and 4.8 dB respectively downstream and upstream, in relation to the SMF Link. The increased slope and spacing observed in the curves of Figure 5.8 *a)* and the greater degradation of the sensitivity at the ONU input, when compared to the curves of Figure 5.8 *b)*, are due to the lack of sophistication of the optical receiver existing in the ONU compared to that used in the OLT.

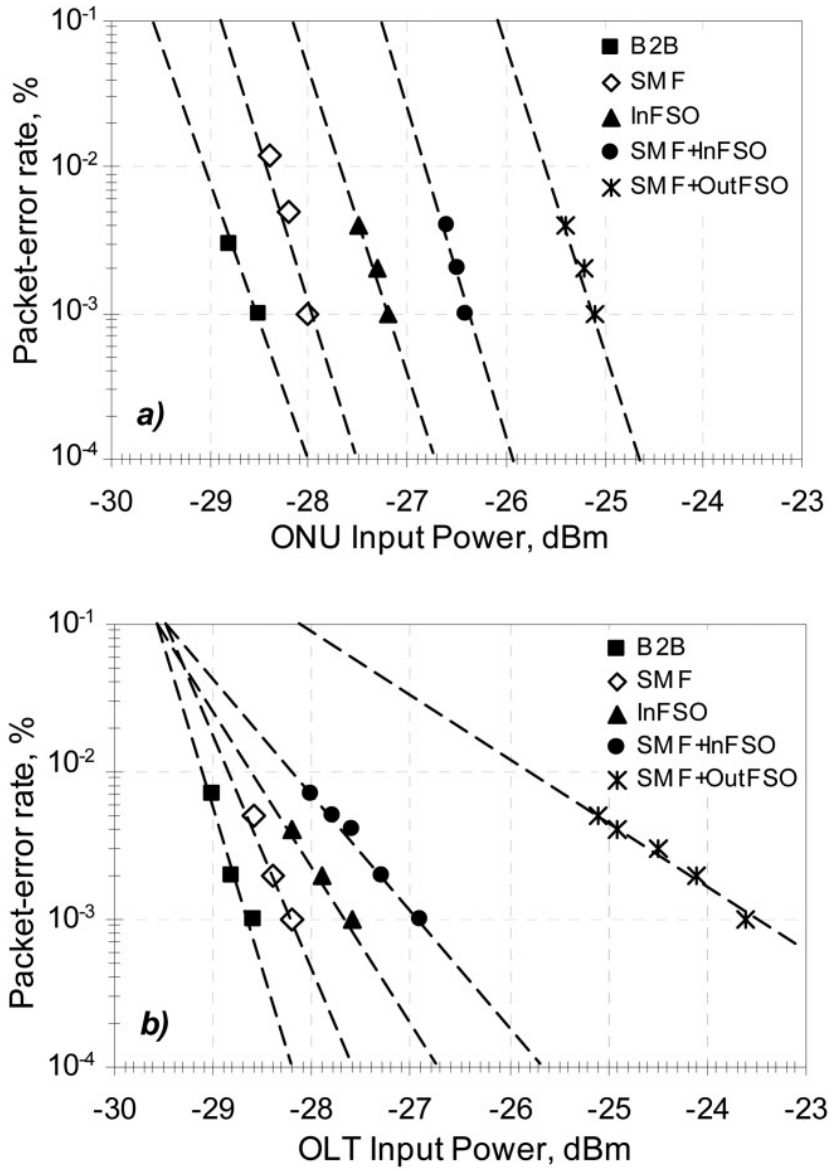

Figure 5.8: Experimental results. *a)* Downstream, 1490 nm and *b)* Upstream, 1310 nm.

It should be noted that another analysis comprising the SMF + OutFSO link results shown in Figure 5.8 *b)* and the upstream data presented in Table 5.1 should be considered. Thus, the high value of the sensitivity degradation (5.3 dB) for the SMF + OutFSO link, compared to the value of the others in Table 5.1, is due to the SOA-2 used in the ExB in Figure 5.7. This circumstance is not

experienced when it is analyzed downstream, Figure 5.8 *a)*. The power fluctuations of ± 0.1 dB and ± 0.7 dB were observed for the optical beam over the InFSO and OutFSO sections, respectively. Therefore, the obtained value of sensitivity degradation for the SMF + OutFSO link shows a relatively higher scintillation of the optical beam. On the other hand, it is well known that the amplification process in SOA is affected by the spontaneous emission of photons with phases and random polarizations. This results in noise, which is one of the degradation factors of the optical signal. It is observable in Figure 5.7 that the transmitted upstream optical signal (1310 nm) is first degraded by the atmospheric turbulence affecting the OutFSO section of the link. Therefore, at SOA-2 input, the optical signal may have small or null random values, with magnitude orders close to the noise values generated internally in SOA, which hinders the fidelity of signal amplification. Consequently, in the upstream SMF + OutFSO configuration, the value of the sensitivity degradation is closely linked to the quality of the SOA (it must be of internal low-noise) as well as the scintillation margin of the link.

Link	Downstream OLT → ONU (dB)	Upstream ONU → OLT (dB)
SMF	0.5	0.4
InFSO	1.3	1.0
SMF + InFSO	2.1	1.8
SMF + OutFSO	3.3	5.3

Table 5.1: Sensitivity Degradation (dB) of GPON Traffic to the B2B Setup and a PER of 10^{-3} %

In addition, the RF spectrum of the CATV signal, when transmitted only by SMF at 1556.56 nm, is illustrated in Figure 5.9 a). Likewise, Figure 5.9 b) shows this CATV transmission through the SMF + OutFSO link.

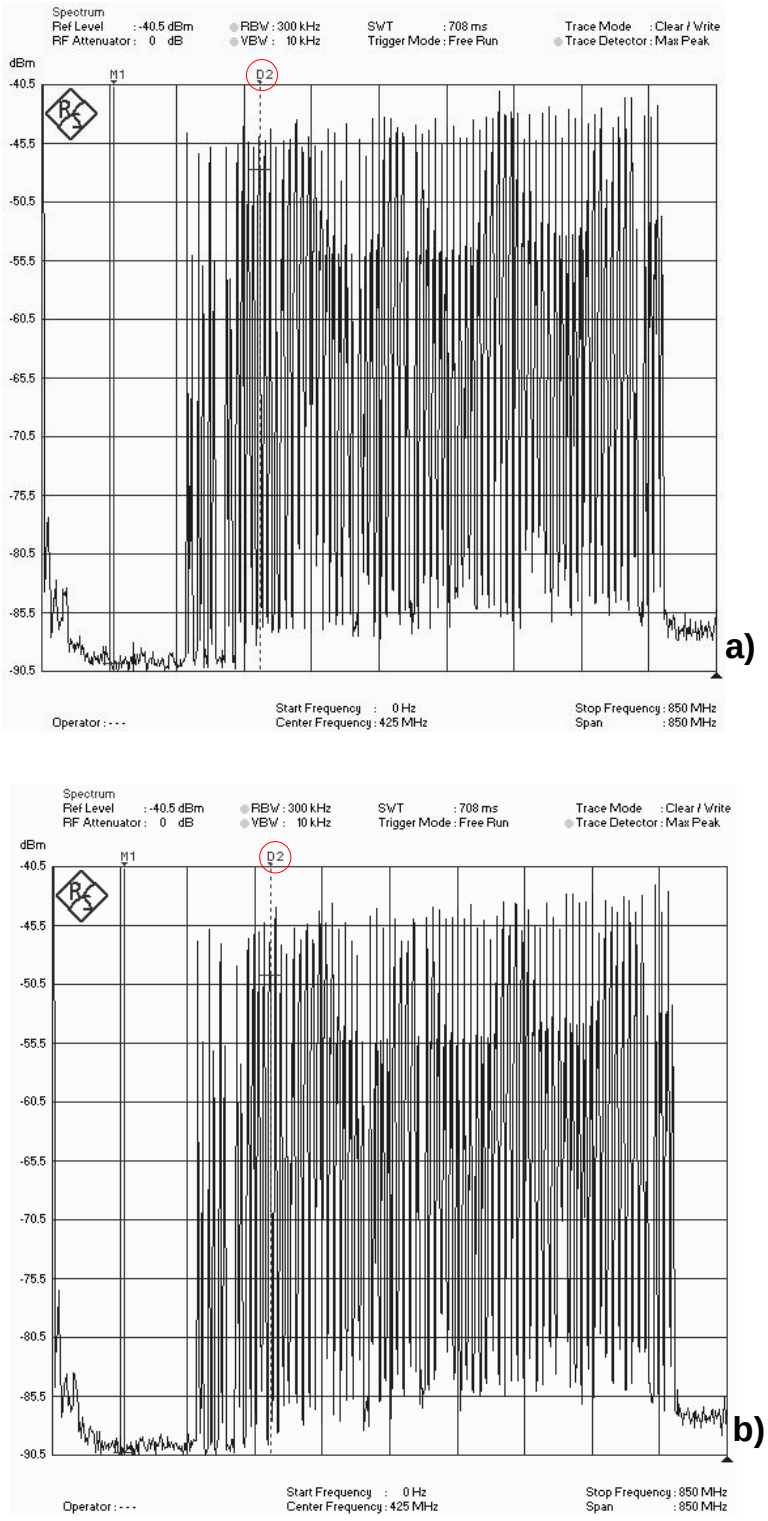

Figure 5.9: RF spectra of an optical transmission at 1556.56 nm through a) 20 km in SMF with 42 dB of CNR and of b) SMF + OutFSO link with 40.6 dB of CNR.

The analysis of the graphs shows a degradation of the CNR by about 1.5 dB, relative to the transmission only by the SMF section. This is highlighted in the figures by the D2 marker, which ranges from ~ -47.5 to ~ -49 dBm because of atmospheric turbulence.

5.4 Research Contributions

The contributions of this chapter focused mainly on the SMF-FSO hybrid system, the performance of GPON data traffic as well as the CATV optical signal transmission. Contributions in these areas and other subjects are discussed in the following subsections.

With reference to manuscript [J4] and the book chapter in [B2], laboratory assemblies integrated into proofs-of-concept are presented, which help to validate the transmission capacities of a hybrid SMF-FSO system. The experiments are relevant in coherent long-range PON systems, validating the FSO application in several areas of the networks where direct/physical connections through only optic fiber cables are impractical. Furthermore, in [J5], the possibility of using FSO interfaces between SMF and PF-POF couplings is presented.

In [J1, C1], apart from the transmission capabilities of a coherent UDWDM-PON and outdoor FSO systems, which were experimentally demonstrated, the implementation of an indoor FSO link was also experimentally validated in [C1]. From the experimental results, it was shown that the UDWDM-PON is an attractive scheme in the implantation of the future access network involving different scenarios.

In [C2, C3], a bi-directional 12 × 10 Gb/s PON based on a hybrid ODN, consisting of sections in SMF and FSO, is experimentally demonstrated. A power budged of 30.5 dB was observed for an extension of 80 km in the optical distribution network (ODN) and hybrid division based on beam dividers. In addition, a shifted TWDM signal was introduced to examine the effects of the heterogeneous coexistence solution on the system.

It was experimentally demonstrated a GPON plus CATV system in [J2]. The configuration was based on a bidirectional transmission over 20 km of SMF or/and FSO section. The feasibility of the proposed system was studied by measuring the data packets loss and the carrier-to-noise ratio value for the video signal degradation.

Another contribution of this chapter is based on the optimization of power parameters per channel in both direction and band separation involving hybrid point-to-multipoint ODN in [C3]. In the carried-out work, it was considered the coexistence of UDWDM with video overlay, as well as their corresponding impacts on the system operation. High aggregated capacity and high spectral efficiency were achieved. This is a result of the reduced effects of stimulated Raman scattering (SRS), as well as cross-phase modulation (XPM) with optimal band-guard employed between the RF-video and the UDWDM channels.

5.5 Conclusions

In this chapter, an experiment was presented for the proof-of-concept of a coherent UDWDM-PON and hybrid system containing SMF plus FSO media with long-reach and gigabit-capable. The experiment is based on DP signals, with the proposed architecture being able to support different applications over a shared fiber infrastructure. In addition, OLT/ONU transceivers have been validated with real-time reconfigurable DSPs emulated by commercial FPGAs for DP-QPSK signals over SMF, as well as, for the first time, over FSO links. The MBH network analyzed in this work is based on 20 x 625 Mbaud and DP-QPSK channels with 2.5 GHz spacing. Moreover, the obtained results indicate the feasibility of coherent, flexible and dual-polarized PON supported by software-defined transceivers. In addition, the feasibility of a bidirectional GPON + CATV system has been experimentally demonstrated. In this work, the possibility of employing a FSO path as an alternative and/or complementary solution for the bidirectional GPON + CATV systems was validated.

References

[1] I. Alimi, A. Shahpari, V. Ribeiro, N. Kumar, P. Monteiro, and A. Teixeira, “Optical wireless communication for future broadband access networks”, in *2016 21st European Conference on Networks and Optical Communications (NOC)*, June 2016, pp. 124–128.

[2] M. A. Khalighi and M. Uysal, “Survey on free space optical communication: A communication theory perspective”, *IEEE Communications Surveys & Tutorials*, vol. 16, no. 4, pp. 2231–2258, Fourthquarter 2014.

[3] I. A. Alimi, A. M. Abdalla, J. Rodriguez, P. P. Monteiro, and A. L. Teixeira, “Spatial interpolated lookup tables (LUTs) models for ergodic capacity of MIMO FSO systems”, *IEEE Photonics Technology Letters*, vol. 29, no. 7, pp. 583–586, April 2017, DOI: 10.1109/LPT.2017.2669337

[4] H. Dahrouj, A. Douik, F. Rayal, T. Y. Al-Naffouri, and M. S. Alouini, “Cost-effective hybrid RF/FSO backhaul solution for next generation wireless systems”, *IEEE Wireless Communications*, vol. 22, no. 5, pp. 98–104, October 2015.

[5] G. Parca, A. Shahpari, V. Carrozzo, G. M. Tosi Beleffi, and A. L. J. Teixeira, “Optical wireless transmission at 1.6-Tbit/s (16 × 100 Gbit/s) for next-generation convergent urban infrastructures”, *Optical Engineering*, vol. 52, no. 11, pp. 116102-1 – 116102-5, 2013, DOI: 10.1117/1.OE.52.11.116102

[6] A. Sheth, “Internet of things to smart IoT through semantic, cognitive, and perceptual computing”, *IEEE Intelligent Systems*, vol. 31, no. 2, pp. 108–112, March 2016.

[7] J. Prat, I. N. Cano, M. Presi, I. Tomkos, D. Klonidis, G. Vall-llosera, R. Brenot, R. Pous, G. Papastergiou, A. Rafel, and E. Ciaramella, “Technologies for cost-effective UDWDM-PONs”, *Journal of Lightwave Technology*, vol. 34, no. 2, pp. 783-791, Jan 2016.

[8] D. Hillerkuss and J. Leuthold, “Software-defined transceivers in dynamic access networks”, *Journal of Lightwave Technology*, vol. 34, no. 2, pp. 792–797, Jan 2016.

[9] D. Lavery, M. Ionescu, S. Makovejs, E. Torrengo, and S. J. Savory, “A long-reach ultra-dense 10 Gbit/s WDM-PON using a digital coherent receiver”, *Opt. Express*, vol. 18, no. 25, pp. 25 855–25 860, Dec 2010, DOI: 10.1364/OE.18.025855, [Online]. http://www.opticsexpress.org/abstract.cfm?URI=oe-18-25-25855

[10] A. Shahpari, R. M. Ferreira, R. S. Luis, Z. Vujicic, F. P. Guiomar, J. D. Reis, and A. L. Teixeira, “Coherent access: A review”, *Journal of Lightwave Technology*, vol. 35, no. 4, pp. 1050–1058, Feb 2017, DOI: 10.1109/JLT.2016.2623793

[11] I. N. Cano, A. Lerin, V. Polo, and J. Prat, “Direct Phase Modulation DFBs for Cost-Effective ONU transmitter in UDWDM PONs”, *IEEE Photonics Technology Letters*, vol. 26, no. 10, pp. 973–975, May 2014, DOI: 10.1109/LPT.2014.2309852

[12] R. M. Ferreira, A. Shahpari, J. D. Reis, and A. L. Teixeira, “Coherent UDWDM-PON with dual-polarization transceivers in real-time”, *IEEE Photonics Technology Letters*, vol. 29, no. 11, pp. 909–912, June 2017, DOI: 10.1109/LPT.2017.2693419

[13] *Gigabit-capable Passive Optical Networks (G-PON): Transmission convergence layer specification*, ITU-T, February 2004, recommendation, G.984.3, [Online]. https://www.itu.int/rec/T-REC-G.984.3-200402-S/en

Chapter 6

Conclusions and Future Works

This chapter presents the results obtained through research, simulation and experimental works involving the alternative optical transmission media, namely those obtained through [J2, J4, J5]. In addition, a perspective on possible guidelines for future work is given.

6.1 Conclusions

The PF-POF and atmospheric FSO were studied as alternative media of optical transmission in relation to SMFs and short-distance RF transmission. In addition to the GPON network, WDM networks defined by the ITU-T G989.1 standard were analyzed, namely DWDM networks and PtP-WDM networks, which seek to provide one λ per client (UDWDM).

In Chapter 2, a bidirectional dual-polarized QPSK system with a total capacity of 400 Gbps in each direction is exposed [J5]. Optically transparent and diverse media such as silica and polymer performed the transmission. It was found that the option of using fiber collimator pairs in the optical beam coupling between SMF and PF-POF fibers with different cores and NA allowed uniform bidirectional attenuation at the connections. The 50 m length of the PF-POF is longer than the

coupling length (Lc) assigned to this type of optical fiber, placing it in a high coupling modal regime, making its impulse response independent of polarization. However, it was observed in the transmission through PF-POF, in both polarizations, that the spectrum received at the input of coherent receivers presents phase dispersion distortion due to the irregular variation of fiber refractive index. This work established a new benchmark for PF-POF transmission, regarding the speed and spectral response received in the transmission range around 1550 nm.

UDWDM has been shown to be an attractive solution for improving network flexibility and spectral efficiency (SE) considering the use of digital signal processing (DSP) implemented by software-defined transceivers. Chapter 5 introduces a UDWDM-PON hybrid system using SMF+FSO as transmission media. The system comprises 20 DP-QPSK channels spaced at 2.5 GHz, with a symbol rate of 20×625 Mbaud and the ability to support multiple applications on the same fiber frame, considering MBH networks [J4]. Interference between 2.5 GHz narrowly spaced UDWDM channels, as well as optical beam fluctuation due to turbulence in the FSO channel, affects the received signal. The experimental performance of the system was estimated in terms of receiver sensitivity, considering 1, 4 and 20 channels. In this system, the application of reconfigurable real-time OLT/ONU DSP-based transceivers, emulated by a commercial FPGA, has been shown in the recovery of DP-QPSK signals over SMF and FSO links.

Chapter 5 describes a two-way GPON+CATV system consisting of three wavelengths propagating through an optical channel, formed by SMF and turbulent outdoor or indoor FSO section, as first announced in publication [J2]. A lens-refracted beam angle is a wavelength function that differently affects the wavelength amplitudes received by the ONUs. Thus, reflection-based collimators (mirrors) were used, which allowed adjusting the three wavelengths equally, even occupying distinct bands. Optical transparency was ensured in the bidirectional propagation of the signal through different optical transmission

media, with a clear advantage in preserving bandwidth. In FSO transmission, signal fluctuation by atmospheric turbulence and phase dispersion distortion associated with random refractive index fluctuation were challenges regarding the feasibility of CATV signal propagation as RF-based video overlay. The CATV signal was found to be satisfactorily received, with 1.4 dB CNR degradation across 54 m of a external FSO link.

6.2 Future Work

In the course of the researches and experiments presented in this thesis, questions were observed that may pave the way for further studies in this field. Below are listed some of the possible research topics.

In the various laboratory implementations involving optical transmission in free space, it was necessary to construct an optical channel assembly in open space subject to real atmospheric conditions, therefore, not controllable. Thus, atmospheric phenomena such as wind, rain, haze, snow, hail, dust, artificial smoke or industrial gases could not be applied to the channel at the appropriate time and with reasonable parameter control. In the future, to optimize the study of a free space transmission, it will be pertinent to construct an optical channel within a tunnel in which it is possible, in a controlled way, to simulate the various atmospheric conditions of interest.

The connection between optical guided media with different core diameters such as silica SMF and PF-POF creates modes coupling problems and energy transfer. This is most pronounced when there is bidirectional and multiband transmission (eg GPON + video overlay) through a lens, leading to distinct attenuations for different wavelengths. A future study evaluating the relative attenuation losses due to the use of mirrors and lenses in the adaptation between different fiber cores is pertinent.

Esta Tese foi defendida na
Universidade de Aveiro em
17 de Setembro de 2020,
tendo obtida a classificação de:
Aprovada por Unanimidade dos
votos do Júri.